APPENDIX

Appendix A

Chapter 3A

Figure A-1 to **A-3:** IR, ^{1}H-NMR, and ^{13}C-NMR spectra of **L1a**

Figure A-4 to **A-6:** IR, ^{1}H-NMR, and ^{13}C-NMR spectra of **L1b**

Figure A-7 to **A-9:** IR, ^{1}H-NMR, and ^{13}C-NMR spectra of **L2a**

Figure A-10 to **A-12:** IR, ^{1}H-NMR, and ^{13}C-NMR spectra of **L2b**

Figure A-13 to **A-15:** IR, ^{1}H-NMR, and ^{13}C-NMR spectra of **L3a**

Figure A-16 to **A-18:** IR, ^{1}H-NMR, and ^{13}C-NMR spectra of **L3b**

Figure A-19 to **A-21:** IR, ^{1}H-NMR, and ^{13}C-NMR spectra of **L4a**

Figure A-22 to **A-24:** IR, ^{1}H-NMR, and ^{13}C-NMR spectra of **L4b**

Figure A-25: Experimental PXRD of **L2a**, **L3a**, **L3b**, **L4a** and **L4b**

Figure A-26: The emission spectra for table 2 in chapter 3A

Table A-1: The comparison of λ_{max}

Table A-2: Molar Extinction Coefficient of UV-Vis spectra of **L2b**, **L3a**, **L3b**, **L4a** and **L4b** in λ near 300nm

Figure A-27: Merged of absorption and emission spectra (λ_{ex} 300nm) of **L3a**, **L3b**, **L4a** and L4b

Figure A-28 to **A-33**: TCSPC decay profiles of **L2a**, **L3a**, **L3b**, **L4a** and **L4b** in different concentration in MeOH

Figure A-1: Merged of absorption and emission spectra (excitation 300nm) of **L3a**, **L3b**, **L4a** and **L4b**

Figure A-2: TCSPC decay profiles of **L2a, L3a, L3b, L4a and L4b** in different concentration in MeOH

Table A-3: Fluorescence lifetime data for **L2a**, **L2b**, **L3a**, **L3b**, **L4a** and **4b**

Figure A-34: ^{1}H NMR spectra of **L2b** in $CDCl_3$ by changing the concentration of compound

Figure A-35: ^{1}H NMR spectra of **L2d** in $CDCl_3$ by changing the concentration of compound

Chapter 3B

Figure A-36 to A-37: IR and ^{1}H-NMR spectra of **L5a**

Figure A-38 to A-40: IR, ^{1}H-NMR, and ^{13}C-NMR spectra of **L6a**

Figure A-41 to A-42: IR and ^{1}H-NMR spectra of **L7a**

Figure A-43 to A-45: IR, ^{1}H-NMR, and mass spectra of **L8a**

Figure A-46 to A-49: IR, ^{1}H-NMR, ^{13}C-NMR, and mass spectra of **L9a**

Figuire A-50 : Three sharp absorption peaks in pyrene monomer

Chapter 3C

Figure A-51 to A-53: IR, ^{1}H-NMR, and ^{13}C-NMR spectra of **L10**

Figure A-54 to A-56: IR, ^{1}H-NMR, and ^{13}C-NMR spectra of **L11**

Figure A-57 to A-60: IR, ^{1}H-NMR, ^{13}C-NMR, and mass spectra of **L12**

Chapter 4A

Figure A-61 to A-64: IR, ^{1}H-NMR, ^{13}C-NMR, and mass spectra of **L3c**

Figure A-65 to A-68: IR, ^{1}H-NMR, ^{13}C-NMR, and mass spectra of **L2′c**

Figure A-69 to A-72: IR, ^{1}H-NMR, ^{13}C-NMR, and mass spectra of **L4c**

Figure A-73 to A-75: IR, ^{1}H-NMR, and ^{13}C-NMR, of **L13c**

Figure A-102: (a) Titration UV-Visible spectra of Fe^{+2} with **L2c** and (b) Linear fit of Absorbance (~595nm) *Vs* Concentration of Fe (II) in 1×10^{-5} M of **L2c**

Figure A-103: (a) UV-Visible spectra for interfering metal ion test, (b) UV-Visible spectra of pH study

Table A-8: Theoretical Data Table

Table A-8a: Comparison with other reported sensors

Chapter 5

Figure A-104 to A-106: IR, ^{1}H-NMR, and ^{13}C-NMR spectra of **L15b**

Figure A-107 to A-109: IR, CHN analysis, and PXRD of **CP1** and **CP2**

Figure A-110 to 119: IR, PXRD and TGA analysis of **CP1***, **CP2***, **I_2@CP1** and **I_2@CP2**

Figure A-120 to 121: IR and PXRD of **CP1-BT**

Figure A-122 to **A-125**: ORTEP diagram and TGA analysis of **CP1** and **CP2**

Figure A-126 to **A-127**: Dye degradation of **CP1** and **CP2** under **CFL** light

Figure A-128: Dye degradation of **CP1** under **UV** light

Figure A-129: Rate constants for the photodegradation of MO, RB, and MB in presence of **CP2** under UV light

Figure A-130: PXRD of recovered samples after photocatalysis (under UV light)

Figure A-131 to **A-132**: PXRD of **I_2@CP1** and **I_2@CP2.**

Figure A-133: Plot of ***ln[I_2]*** Vs. **Time** to study the kinetics of Iodine adsorption

Chapter 6

Figure A-134 to A-135: IR and ^{1}H-NMR spectra of **L14c**

Figure A-136: IR spectra of **Zn-MOF**

Figure A-137 to **A-145**: ^{1}H-NMR spectra of;

2-benzylidenemalononitrile,

2-(4-nitrobenzylidene)malononitrile,

2-(2-nitrobenzylidene)malononitrile,

2-(3-nitrobenzylidene)malononitrile,

2-(4-chlorobenzylidene)malononitrile,

2-(3-chlorobenzylidene)malononitrile,

2-(4-methoxybenzylidene)malononitrile

2-(3,4-dimethoxybenzylidene)malononitrile

2-(naphthalen-1-ylmethylene)malononitrile

Figure A-146: PXRD spectra of **Zn(II)-MOF** before and after catalysis

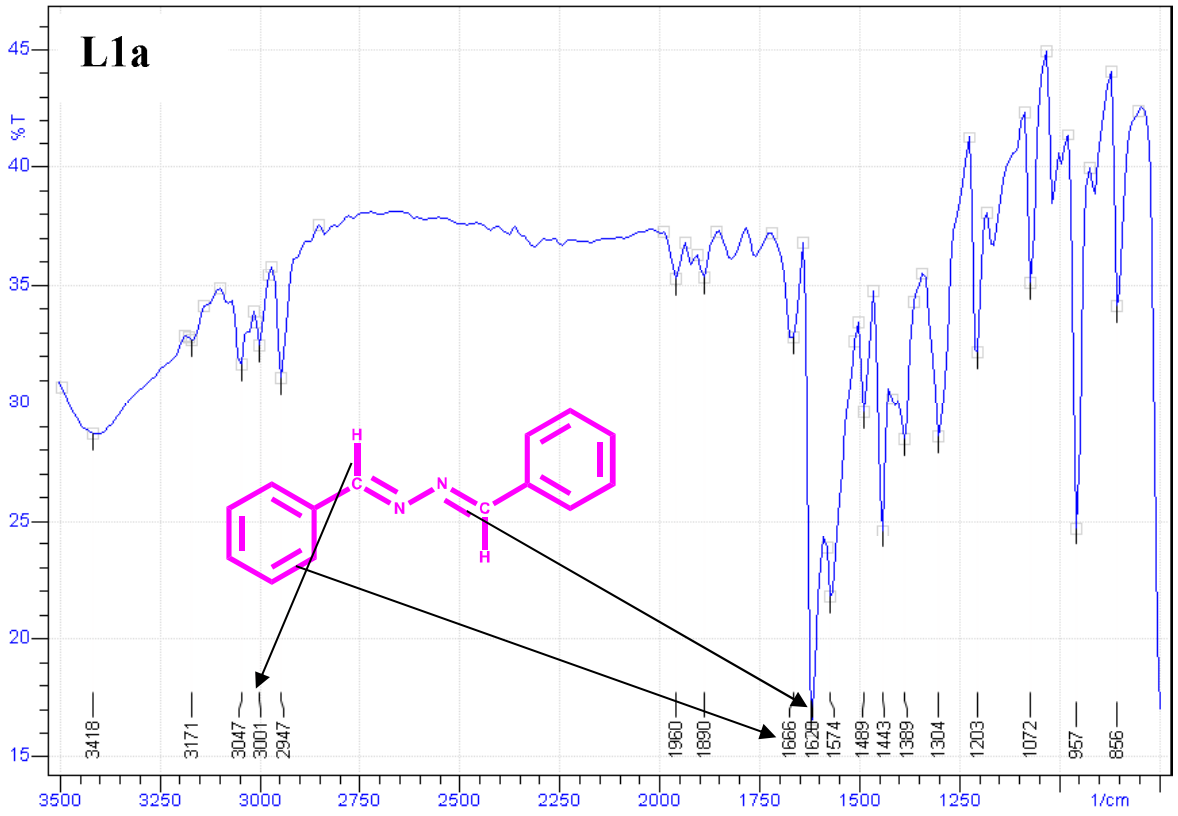

Figure A-1: IR spectra of **L1a:** (cm^{-1} KBr pellet) 3418(w), 3171(w),3047(w),3001(w),2947(m), 1666(m), 1628(vs),1574(w), 1489(w),1443(m), 1304(w),1203(w),957(m),856(w).

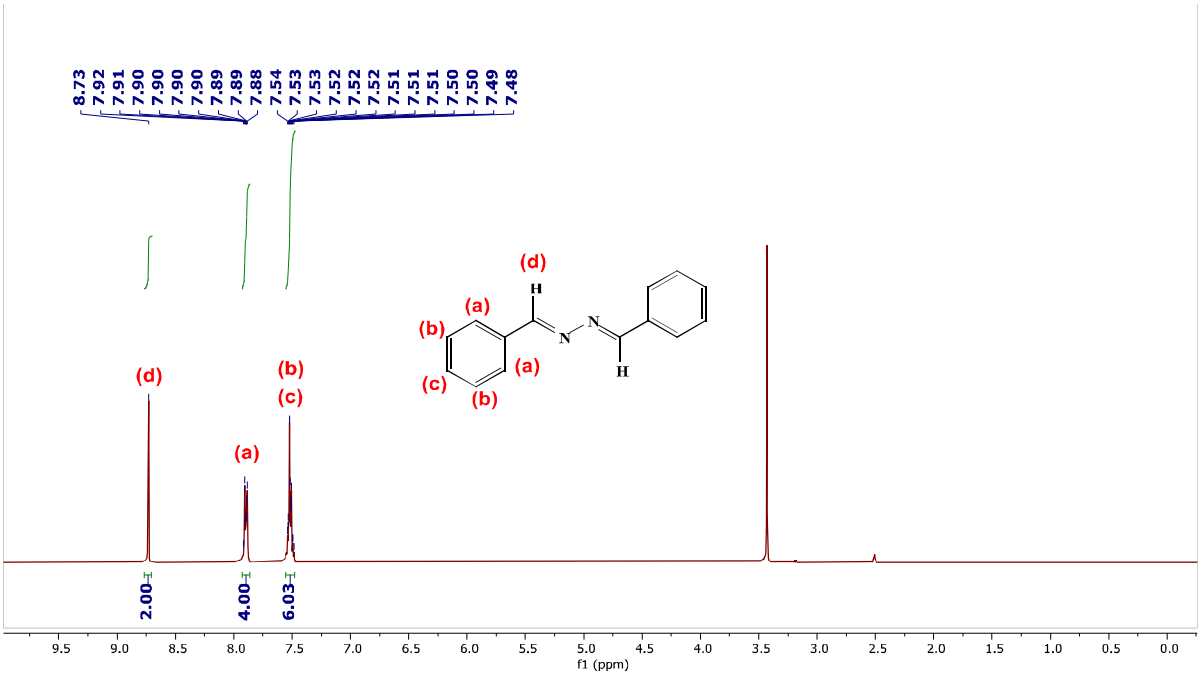

Figure A-2: ^{1}H NMR spectra of **L1a**

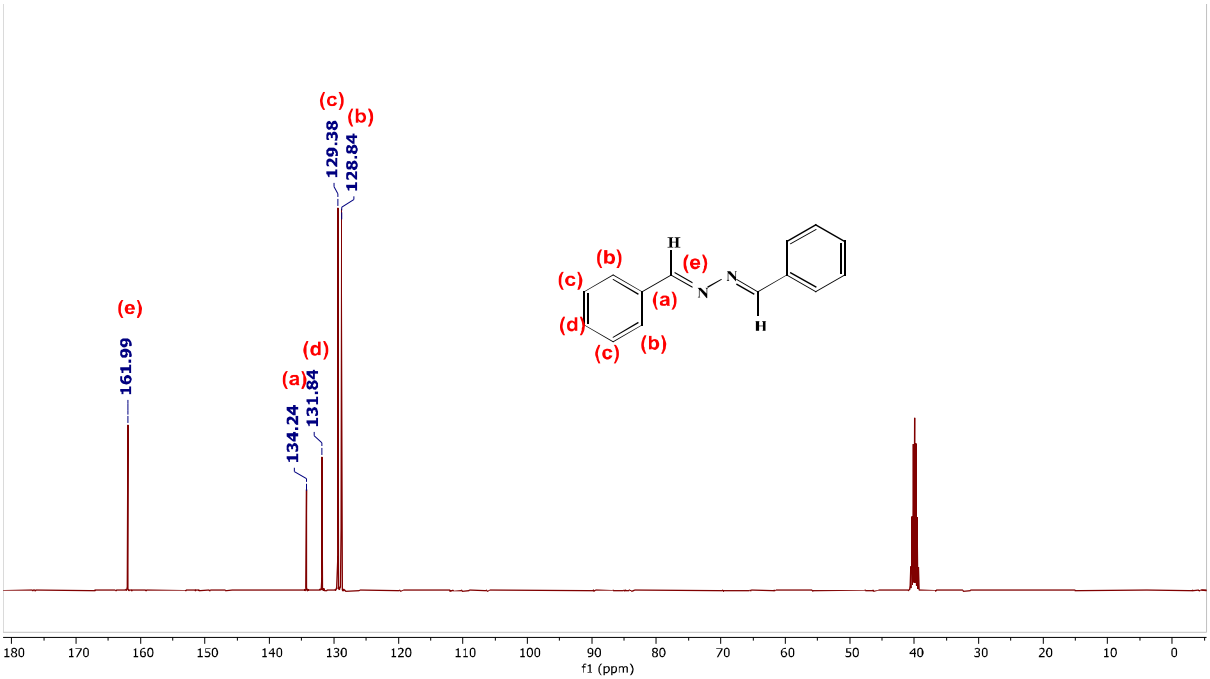

Figure A-3: ^{13}C NMR spectra of **L1a**

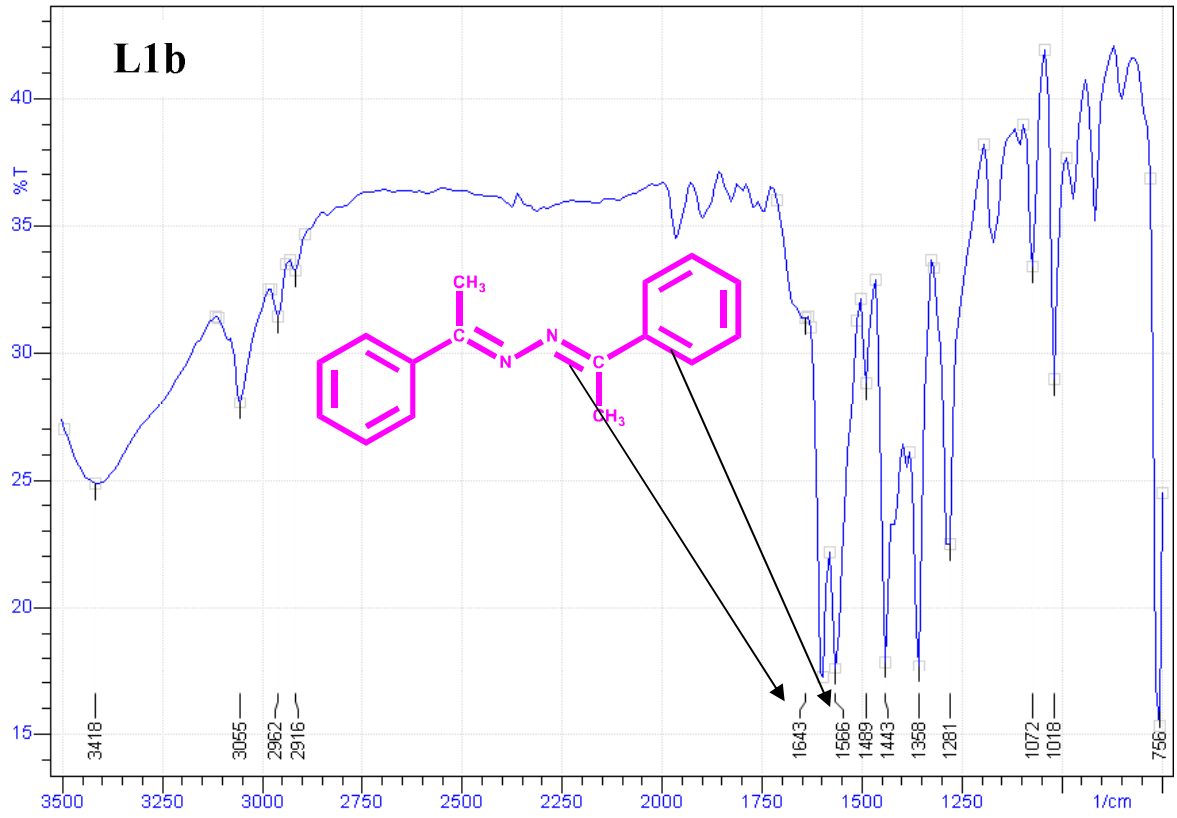

Figure A-4: IR spectra of **L1b:** (cm^{-1} KBr pellet): 3418(m), 3055(m), 2962(m), 2916(w), 1643(vs), 1566(vs), 1489(w), 1443(vs), 1358(vs), 1281(s), 1072(m), 1018(m), 756(vs).

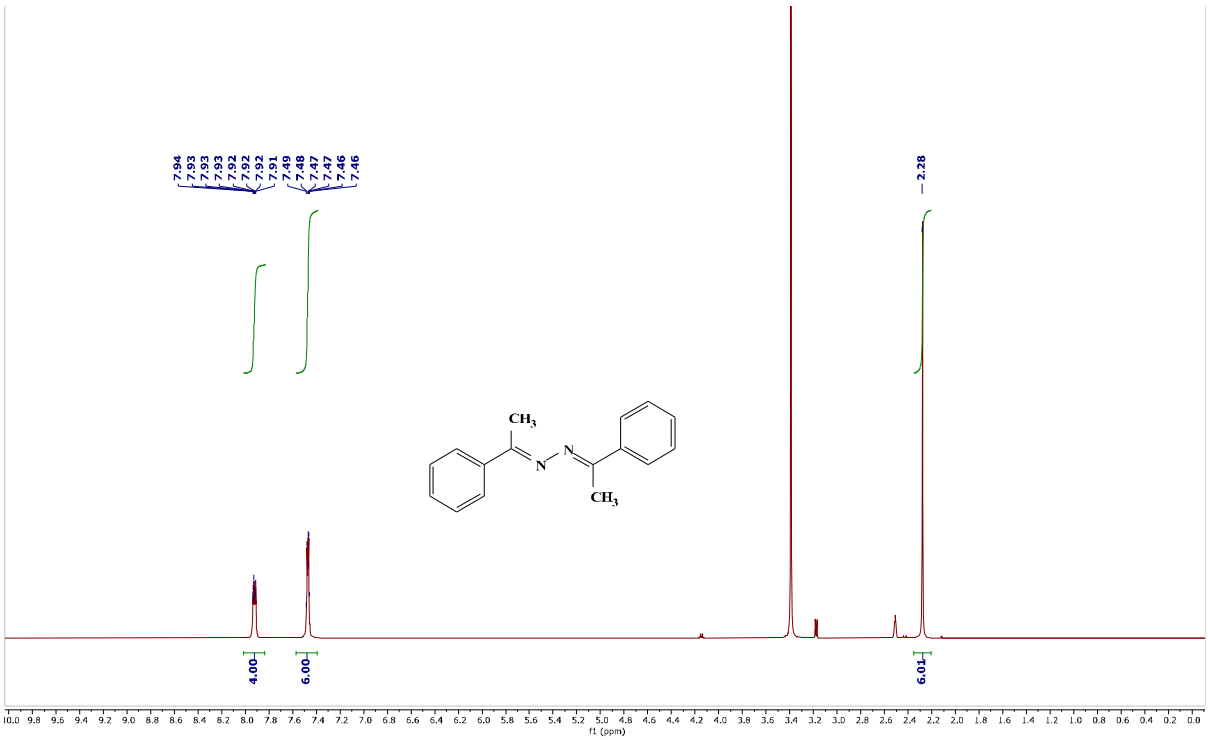

Figure A-5: ^{1}H NMR spectra of **L1b**

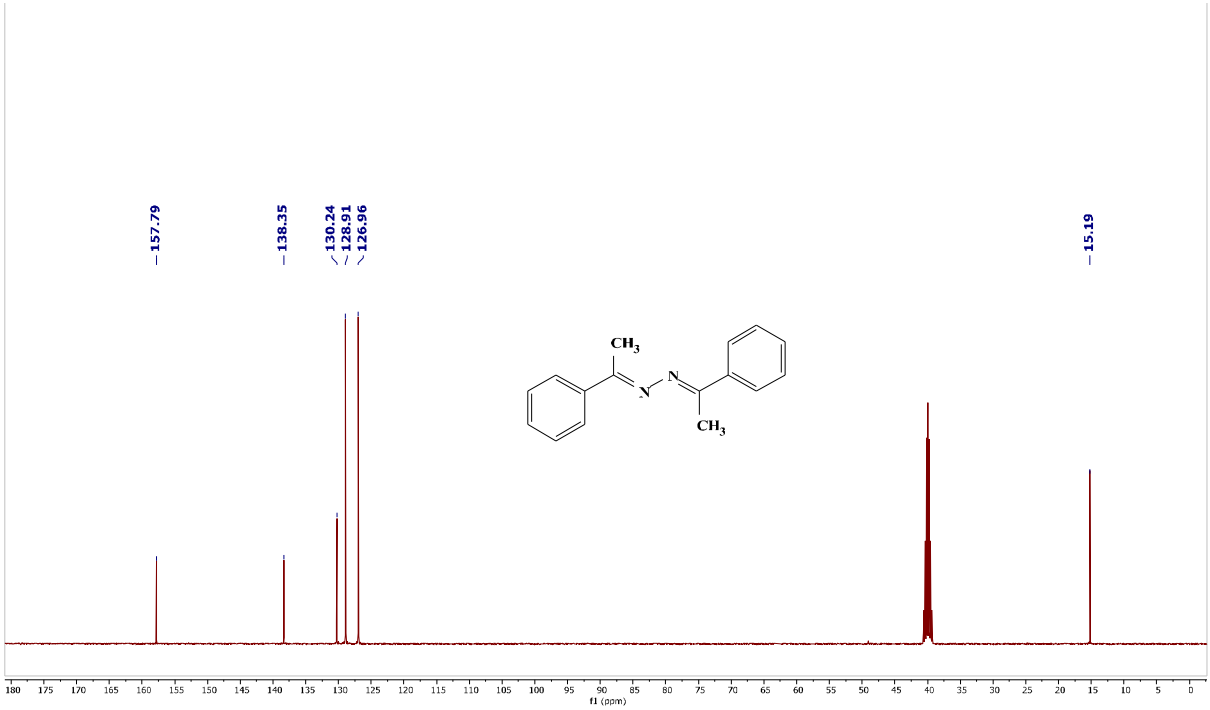

Figure A-6: ^{13}C NMR spectra of **L1b**

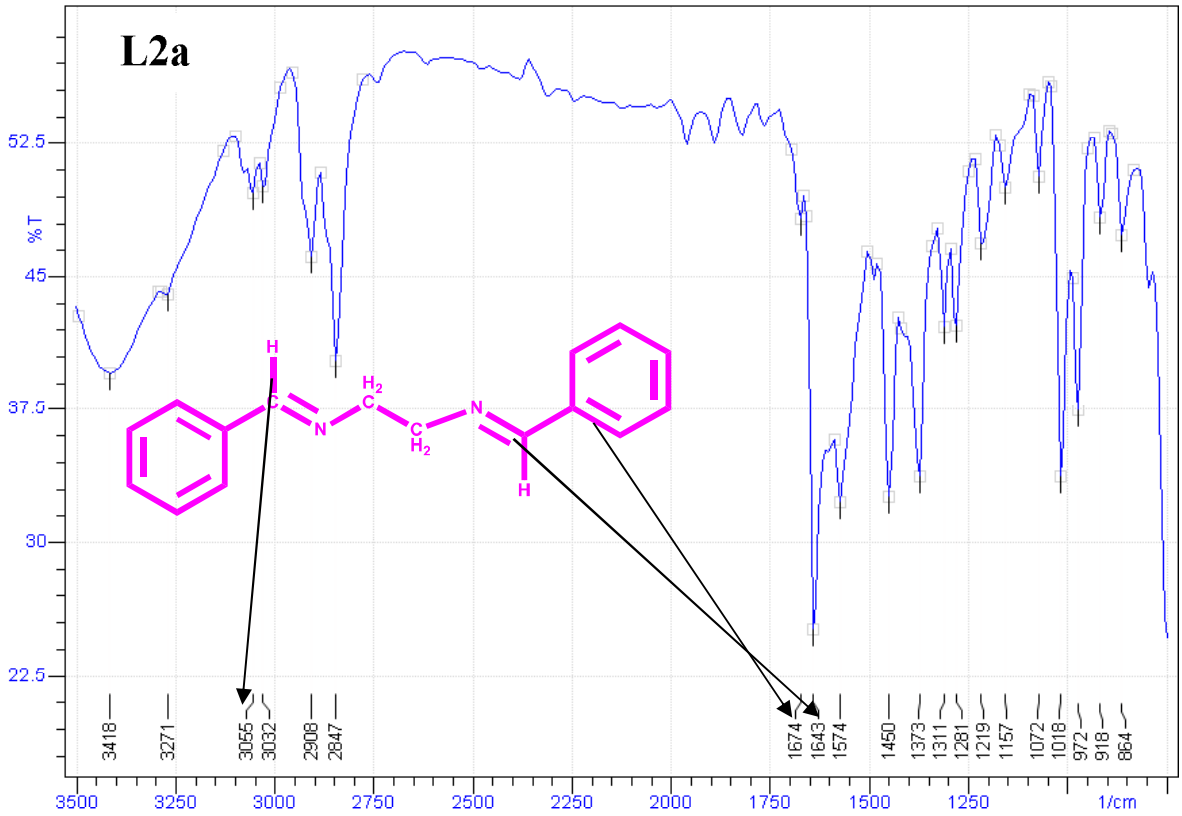

Figure A-7: IR spectra of **L2a (**cm^{-1} KBr pellet) **:**3418(m), 3271(w), 3055(w), 3032(w), 2908(w), 2843(m),1674(w), 1643(vs), 1574(w),1450(m), 1373(m), 1281(w), 157(w), 1018(s), 972(w), 918(w).

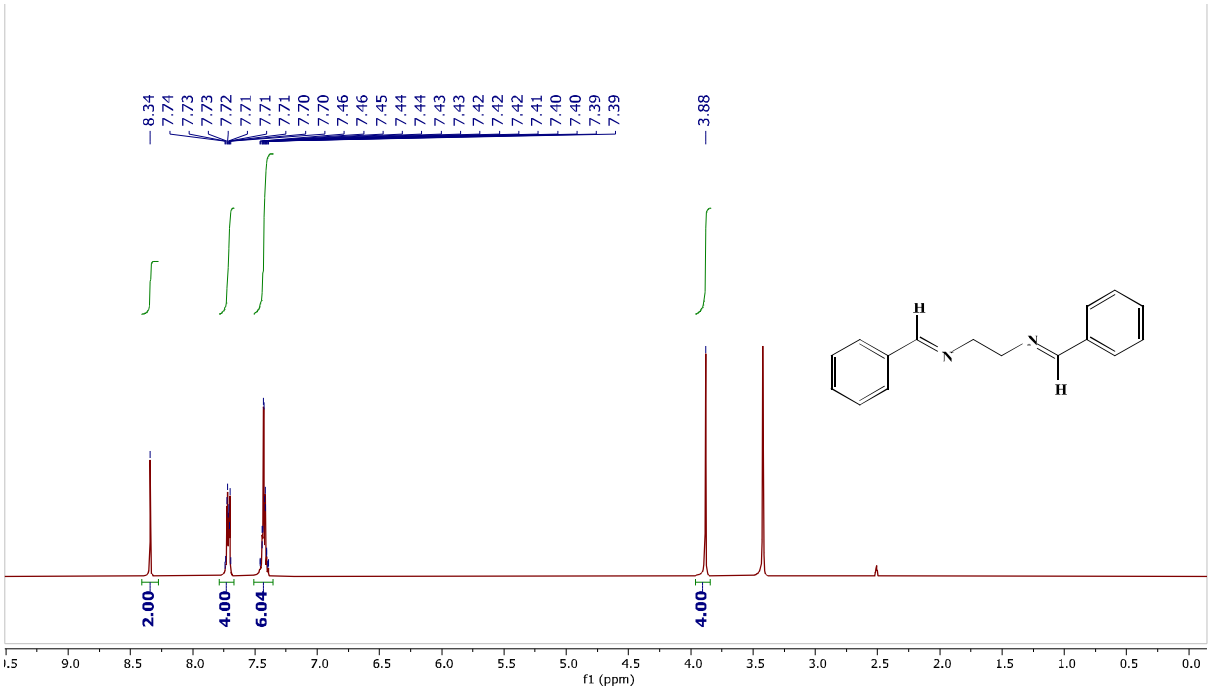

Figure A-8: ^{1}H NMR of **L2a**

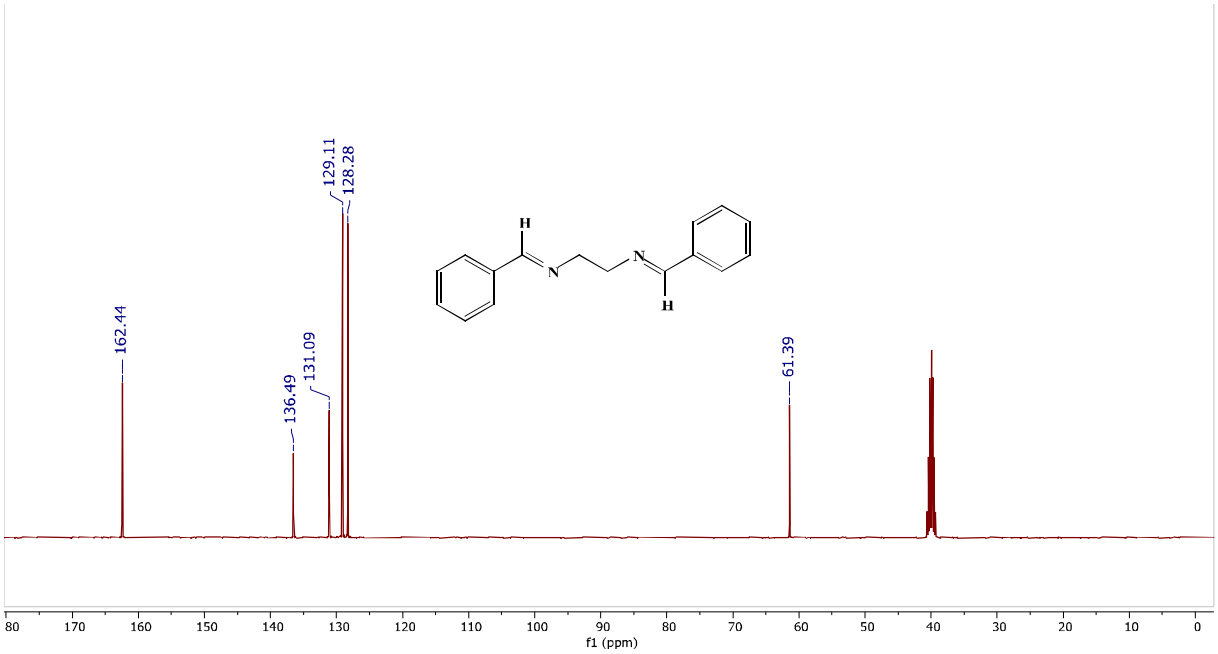

Figure A-9: ^{13}C NMR of **L2a**

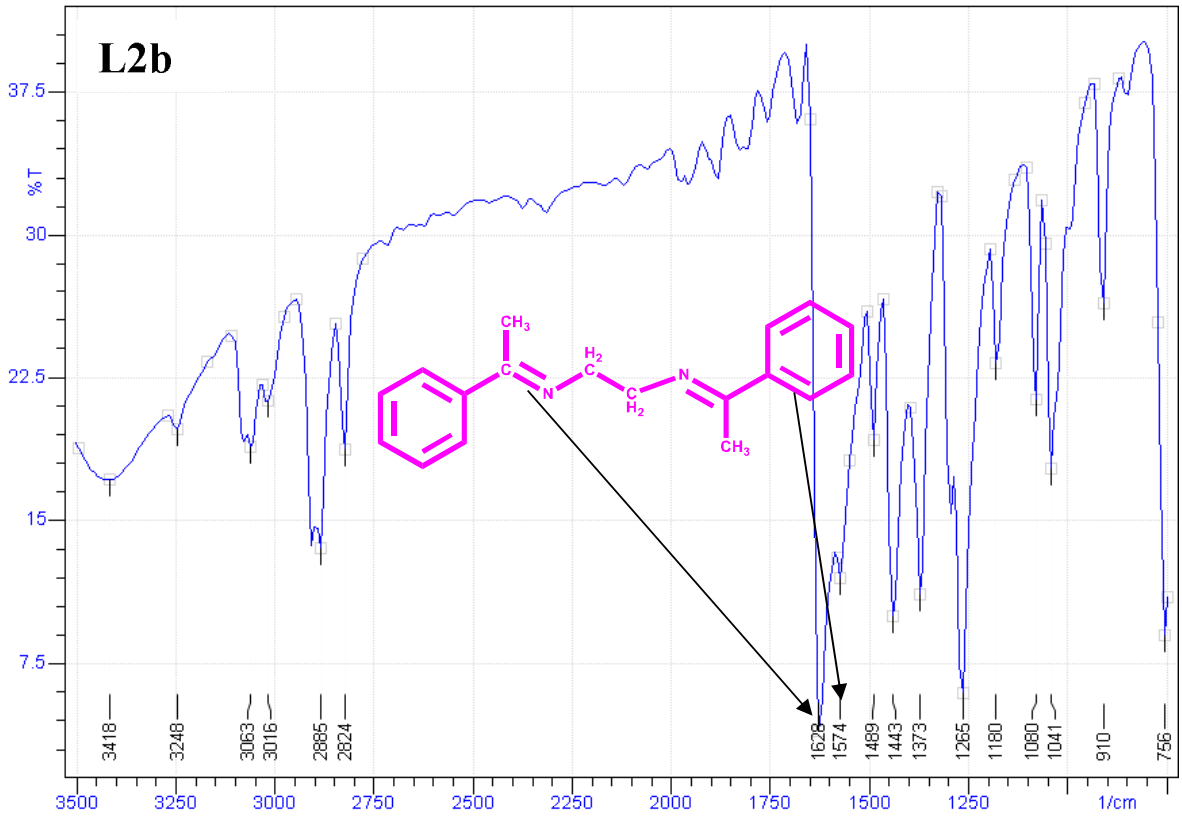

Figure A-10: IR spectra of **L2b (**cm^{-1} KBr pellet):3418(m), 3248(w), 3063(w), 3016(w), 2885(m), 2824(m), 1628(vs), 1574(w), 1489(w), 1443(m), 1373(m), 1265(vs), 1180(w), 1080(m), 1041(m), 910(m),756(vs).

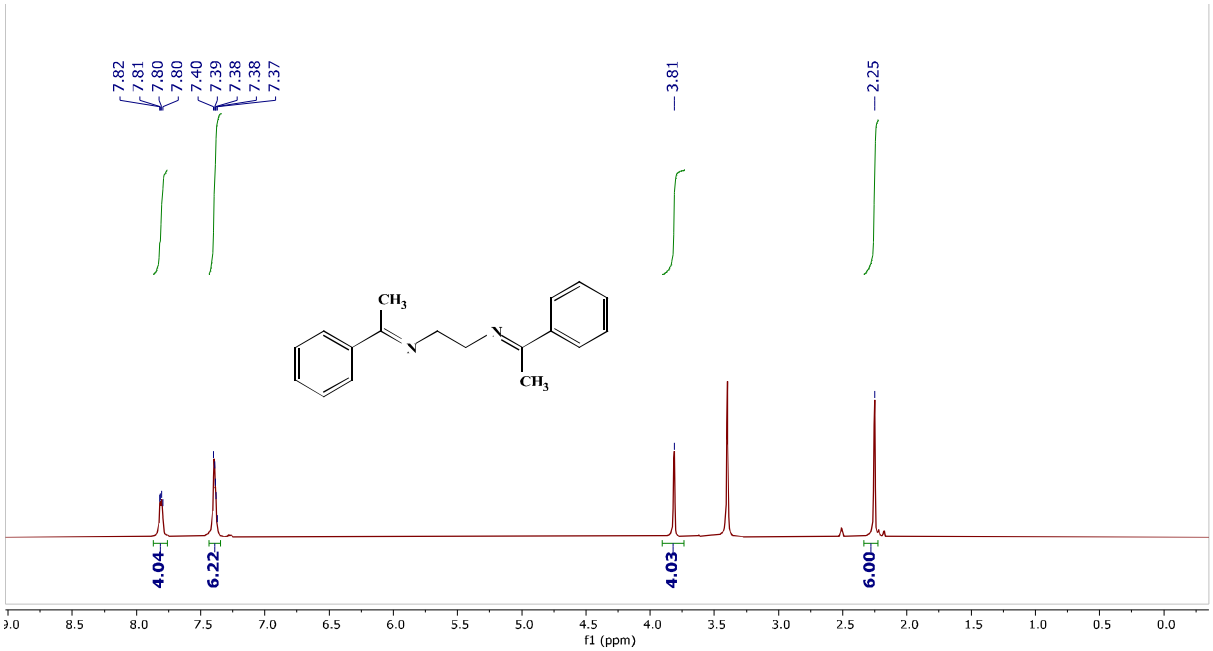

Figure A-11: ^{1}H NMR of **L2b**

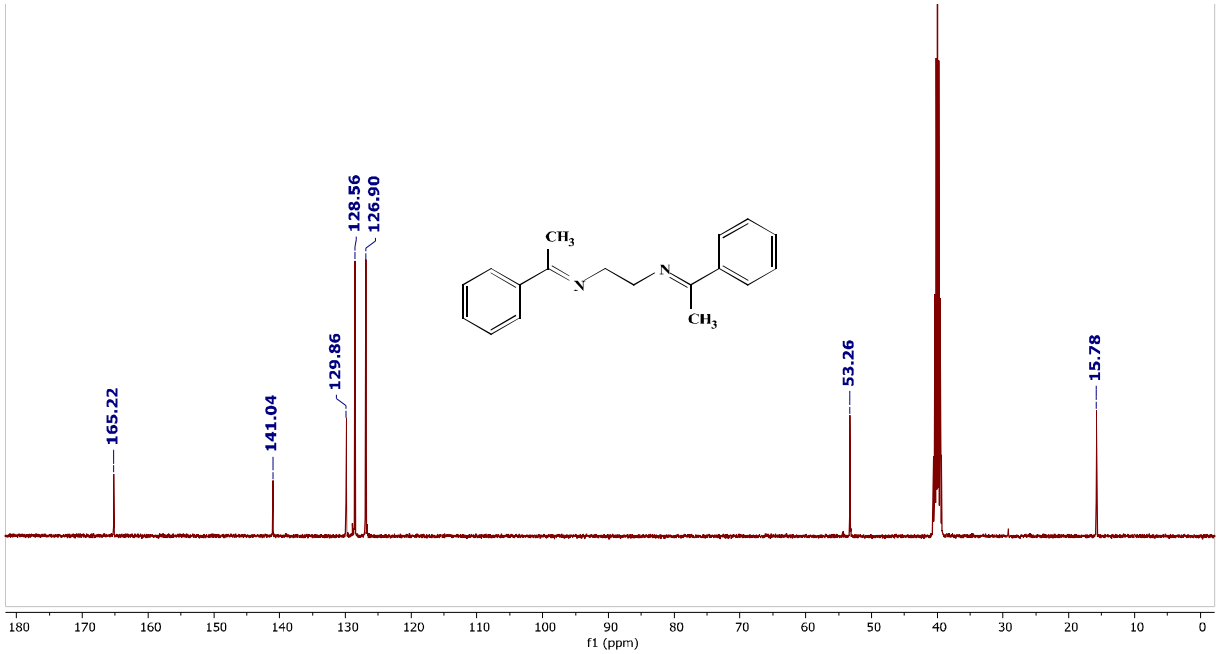

Figure A-12: ^{13}C NMR of **L2b**

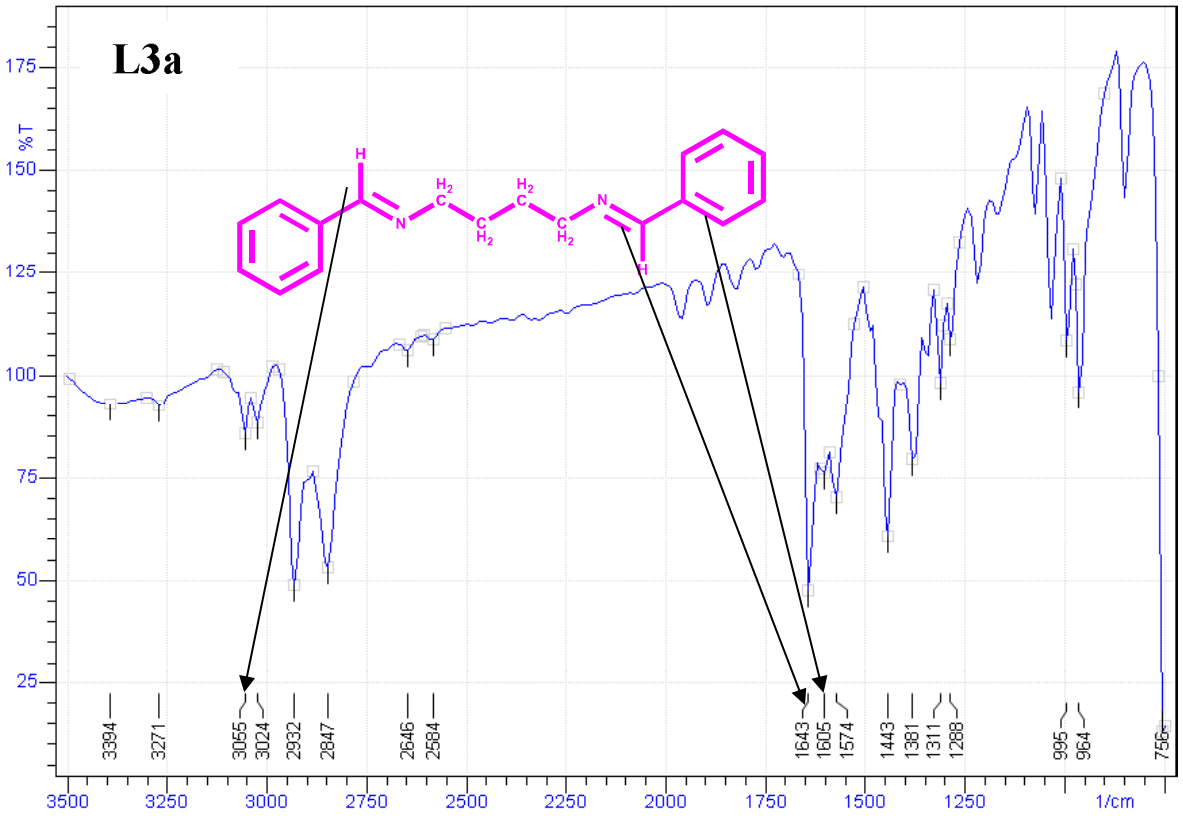

Figure A-13: IR spectra of **L3a**(cm^{-1} KBr pellet): 3394(w), 3271(w), 3055(w), 3024(w),2932(m), 2847(m),2646(w), 1643(vs), 1605(w), 1574(w), 1443(s), 1381(w), 1288(w), 965(w),756(vs).

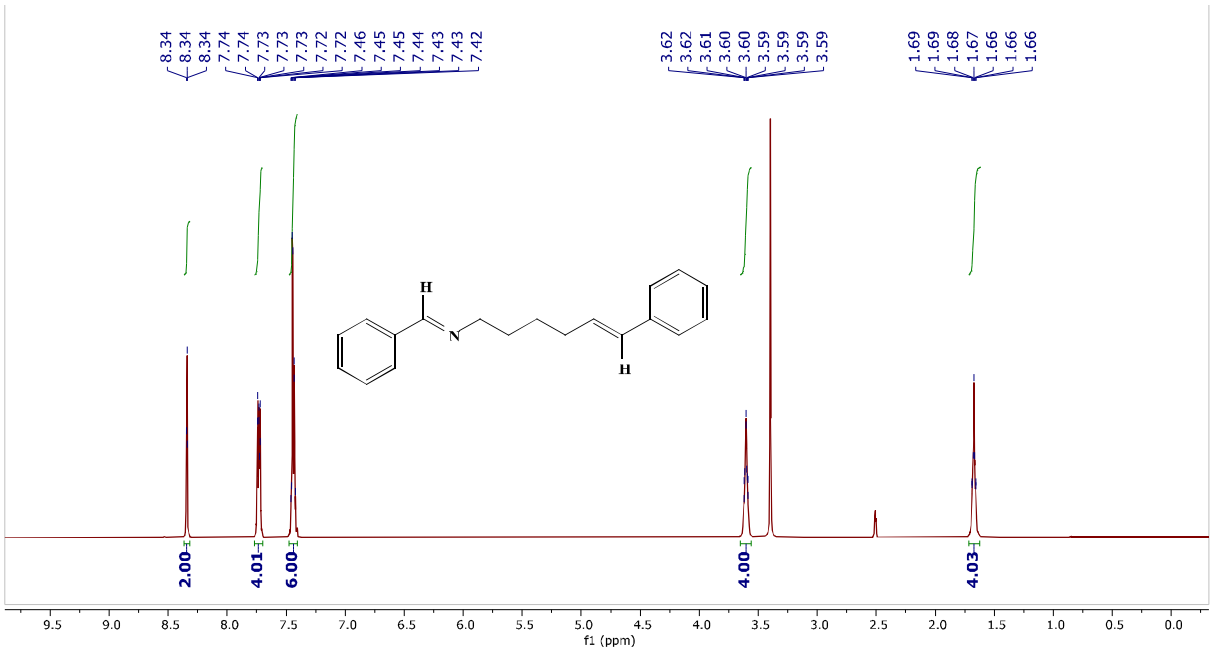

Figure A-14: ^{1}H NMR of **L3a**

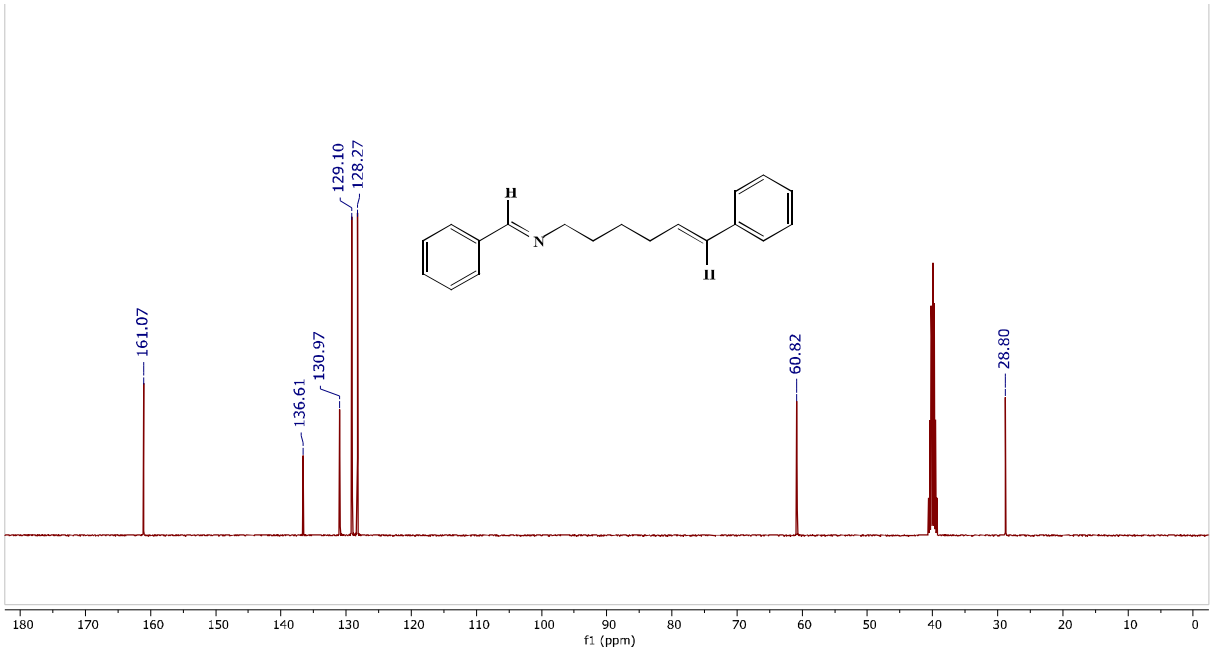

Figure A-15: ^{13}C NMR of **L3a**

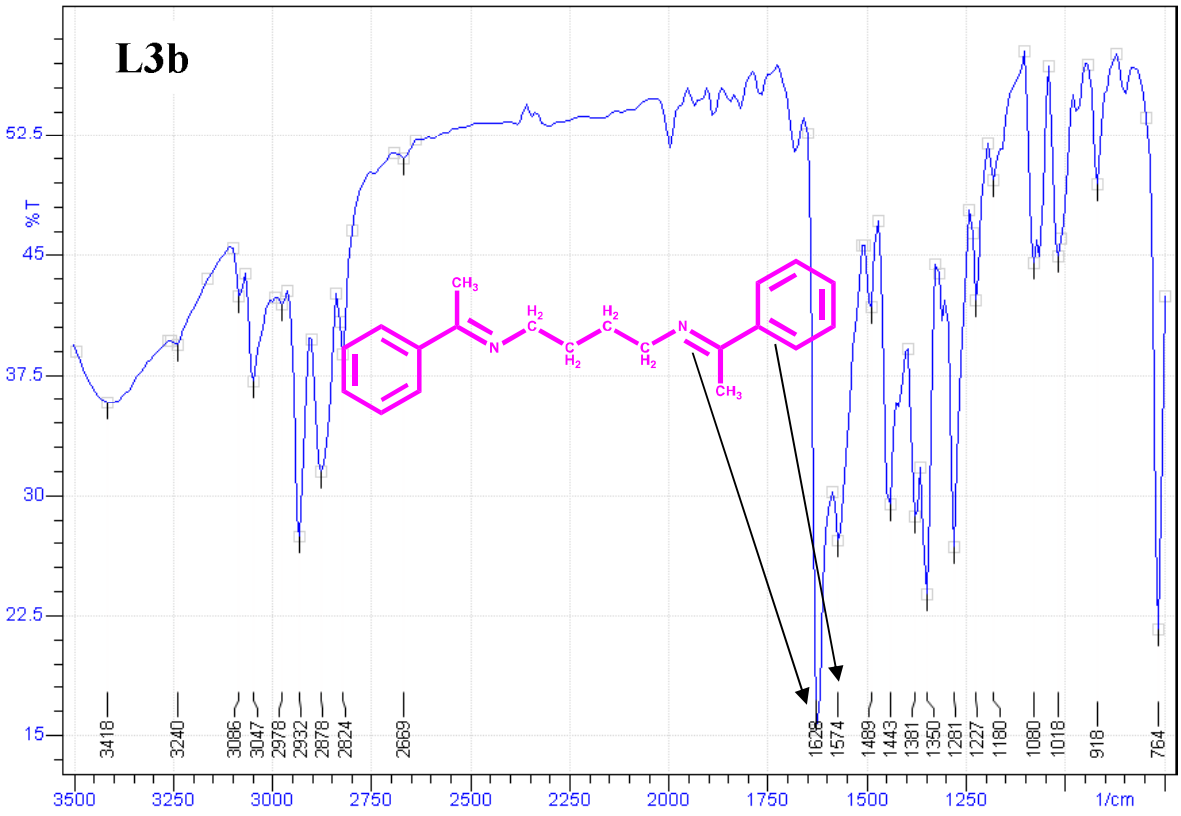

Figure A-16: IR spectra of **L3b** (cm^{-1} KBr pellet): 3418(m), 3240(w), 3086(w),3047(w), 2932(m), 2878(m), 1628(vs), 1574(w), 1489(w), 1443(w), 1350(m), 1281(m), 1180(w), 1080(w), 918(w),764(vs).

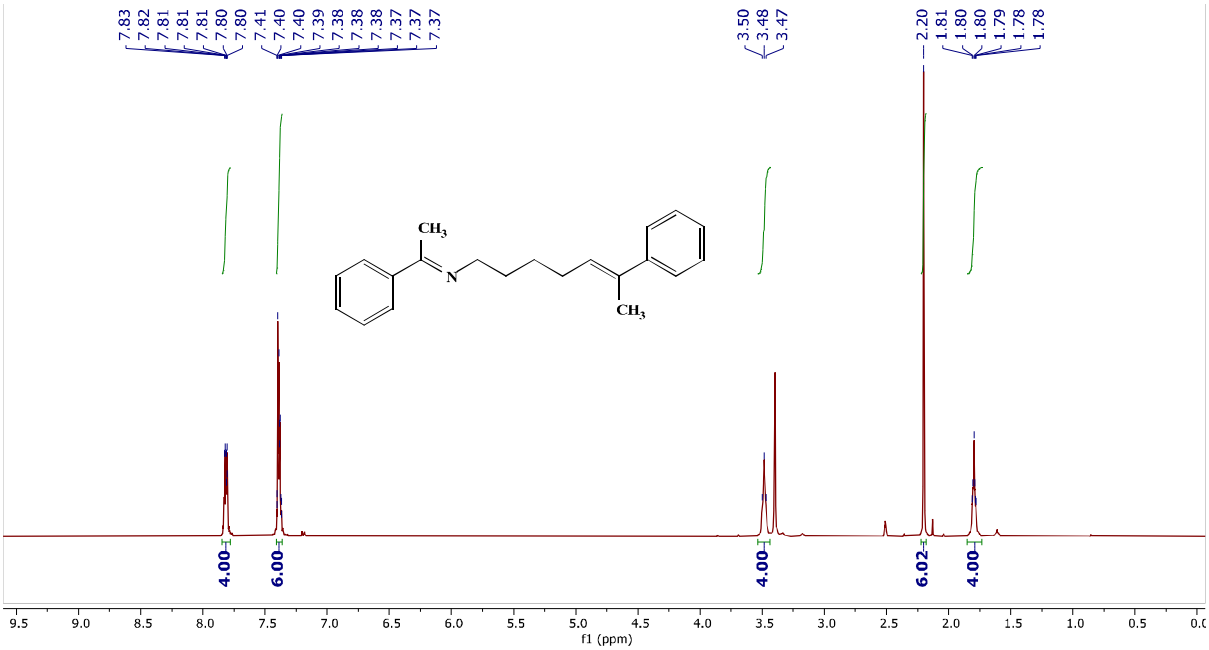

Figure A-17: ^{1}H NMR of **L3b**

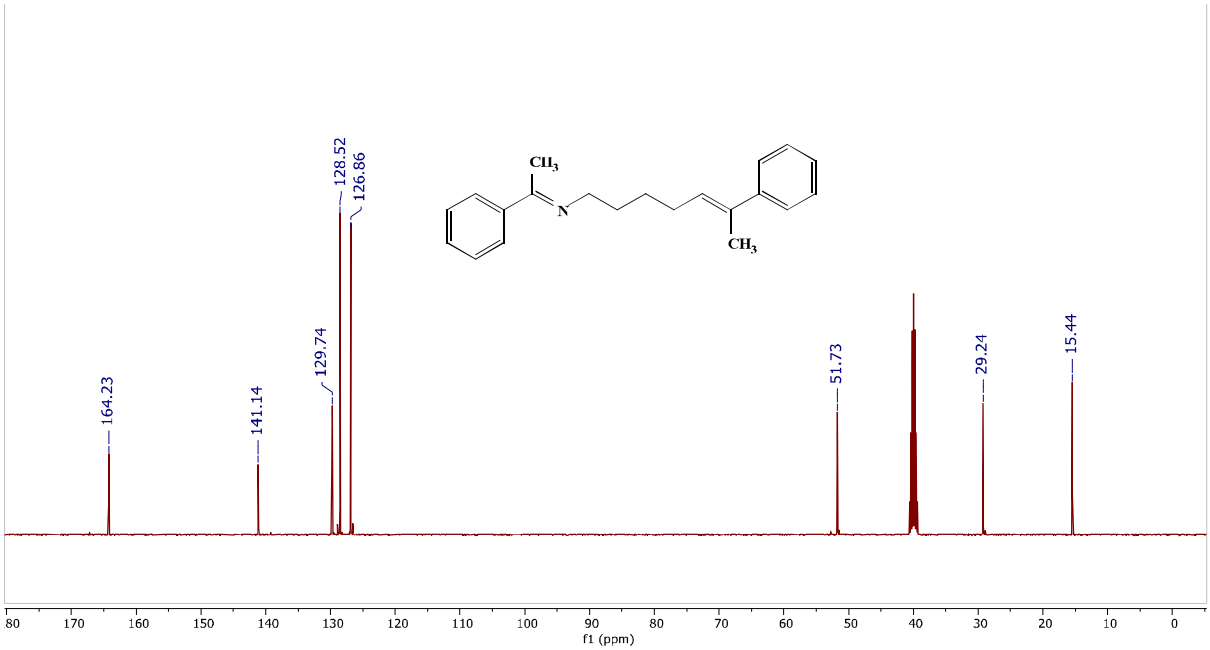

Figure A-18: ^{13}C NMR of **L3b**

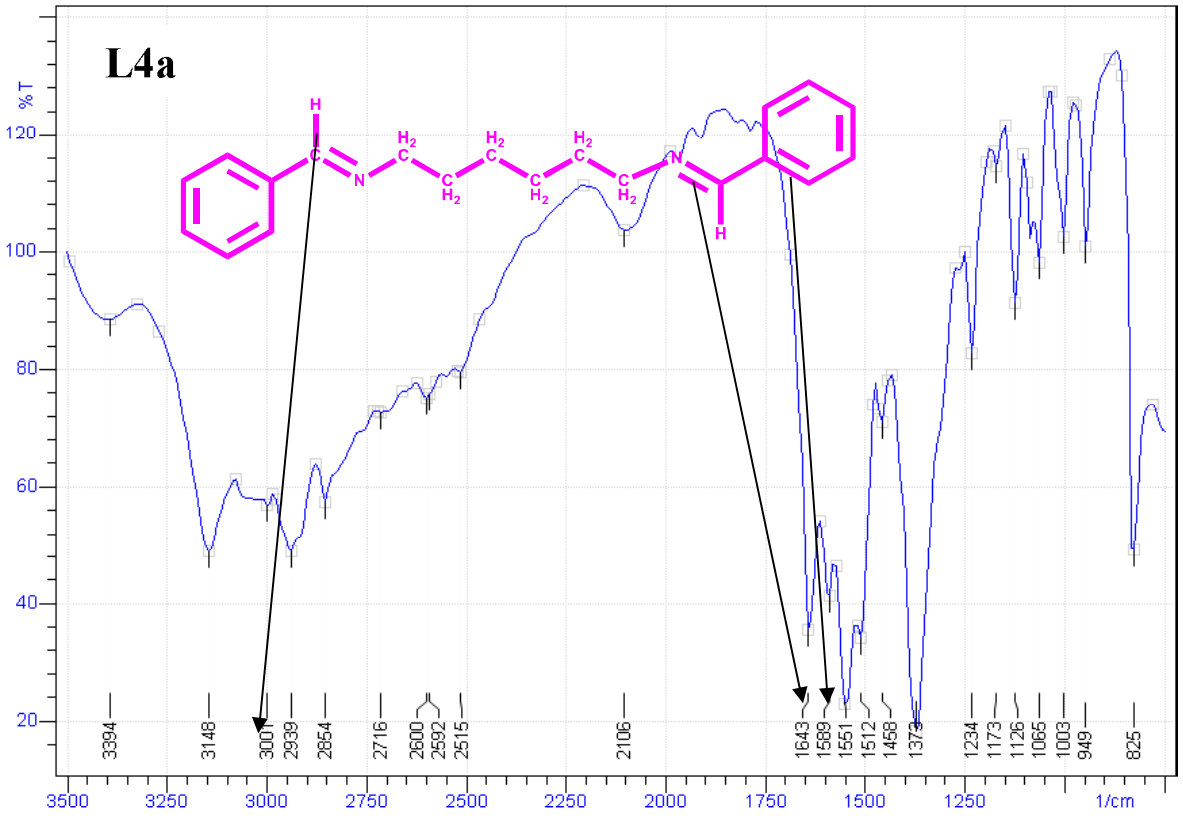

Figure A-19: IR spectra of **L4a (**cm^{-1} KBr pellet): 3394(w),3148(m), 3001(w), 2939(w), 2854(w), 2716(w), 2106(w),1643(s),1589(w), 1551(vs), 1379(vs), 1234(w), 1173(w), 1065(w), 949(w),825(s).

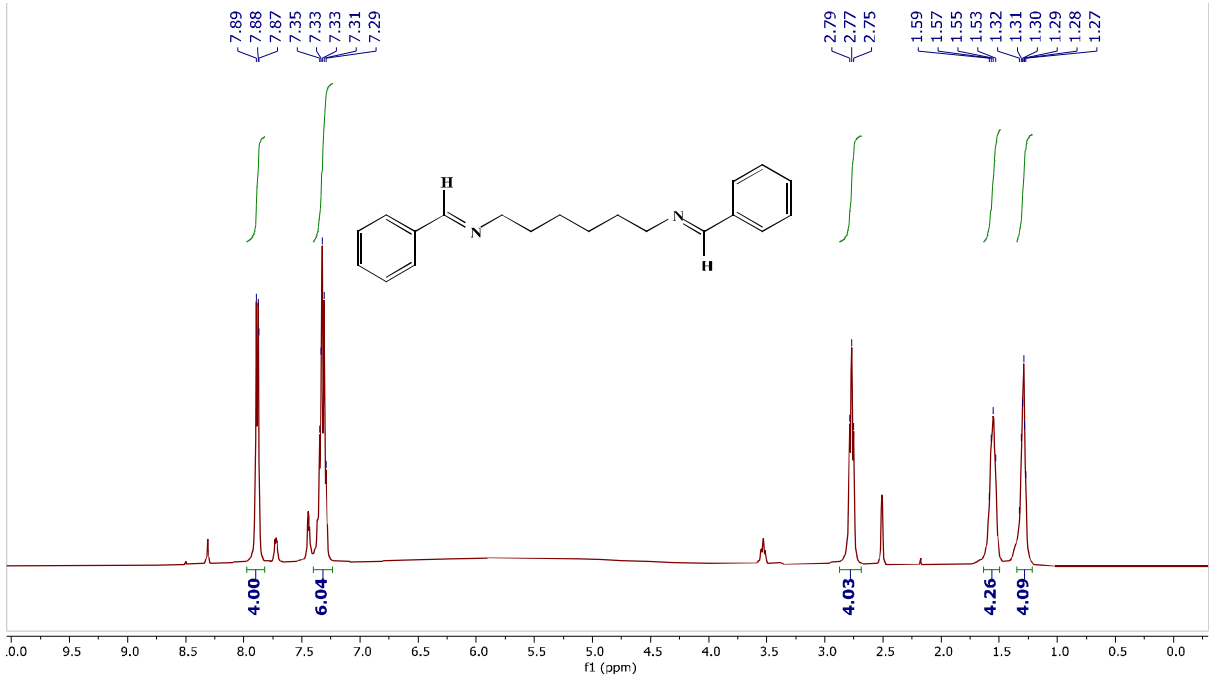

Figure A-20: ^{1}H NMR of **L4a**

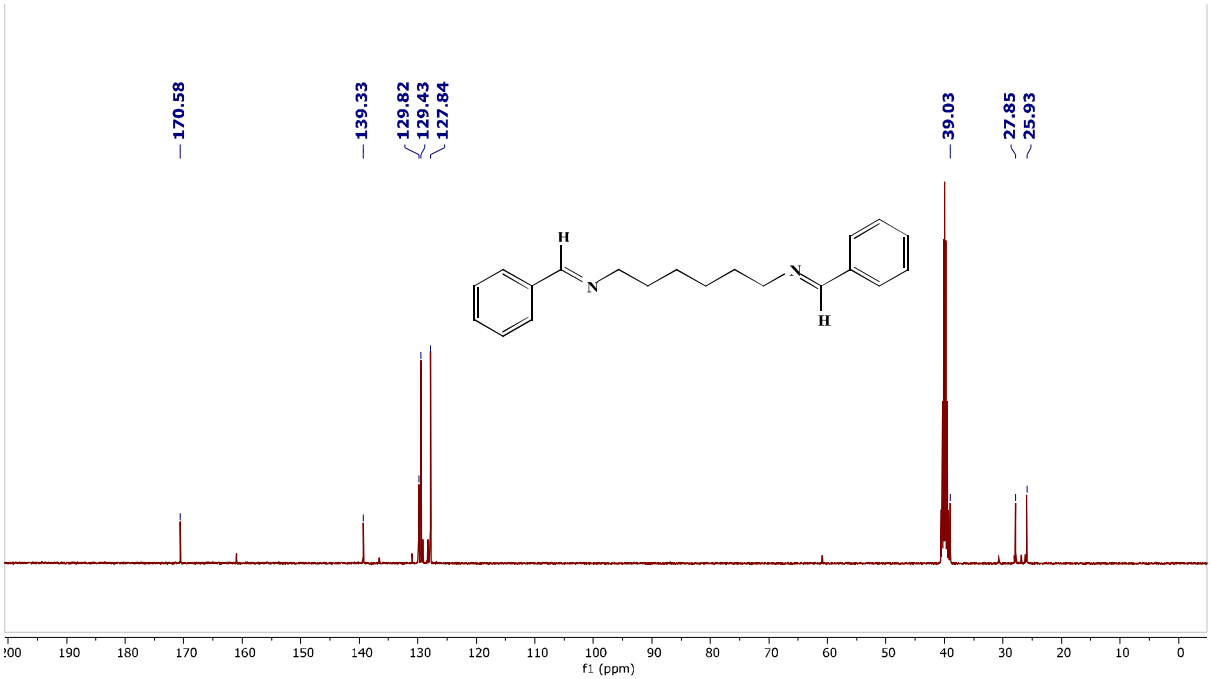

Figure A-21: ^{13}C NMR of **L4a**

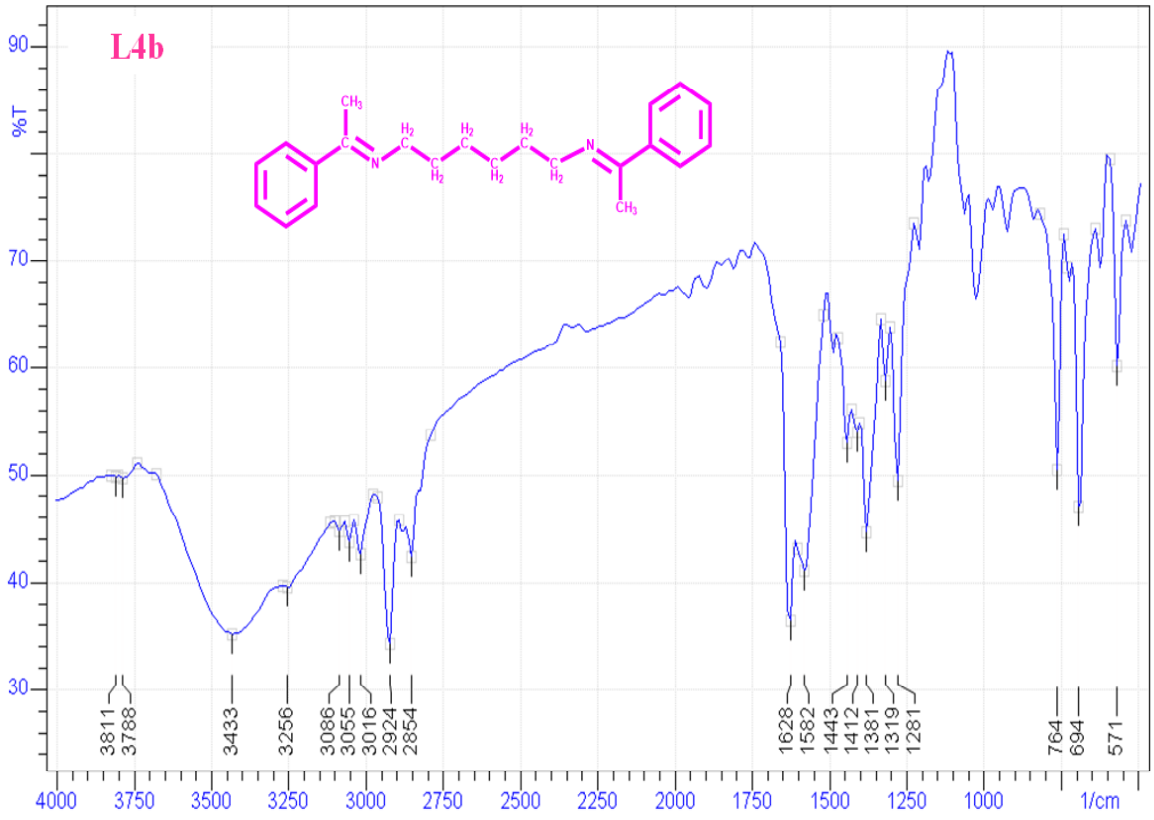

Figure A-22: IR spectra of **L4b**(cm^{-1} KBr pellet): 3811(w), 3433(m), 3256(w), 3055(w), 2924(m), 2854(w), 1628(vs), 1582(w), 1443(w), 1412(m), 1381(m), 1281(w), 794(m), 694(s),571(w).

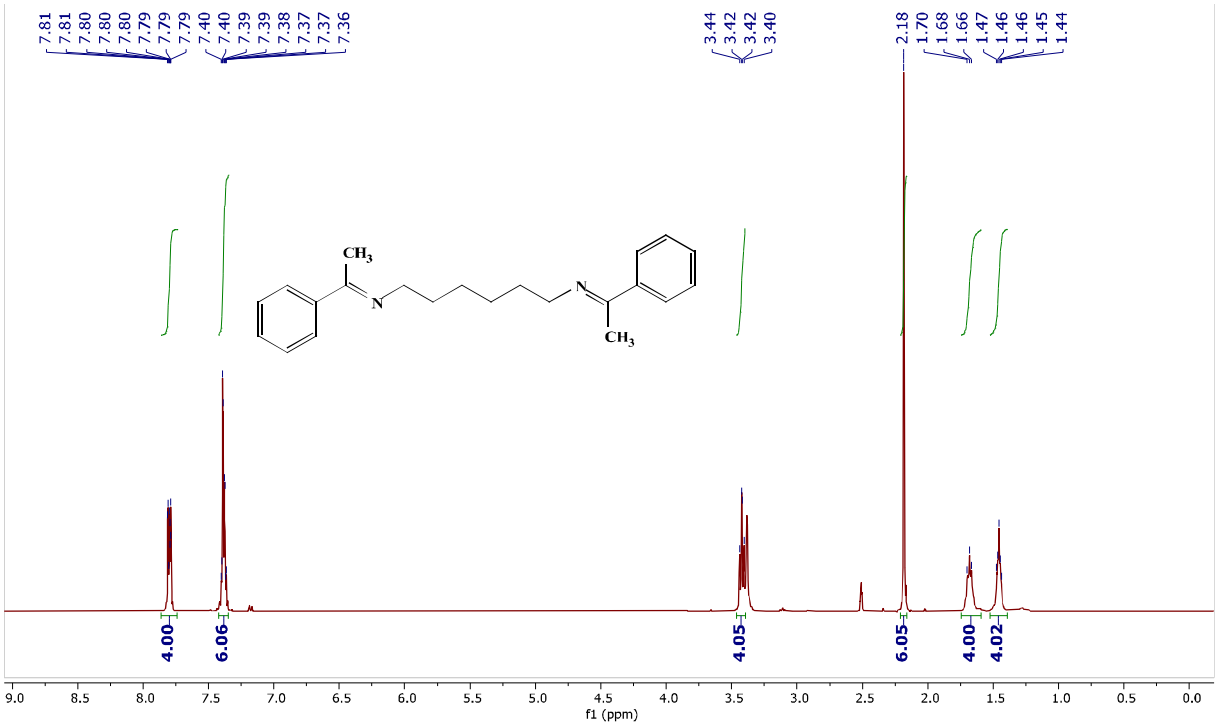

Figure A-23: ^{1}H NMR of **L4b**

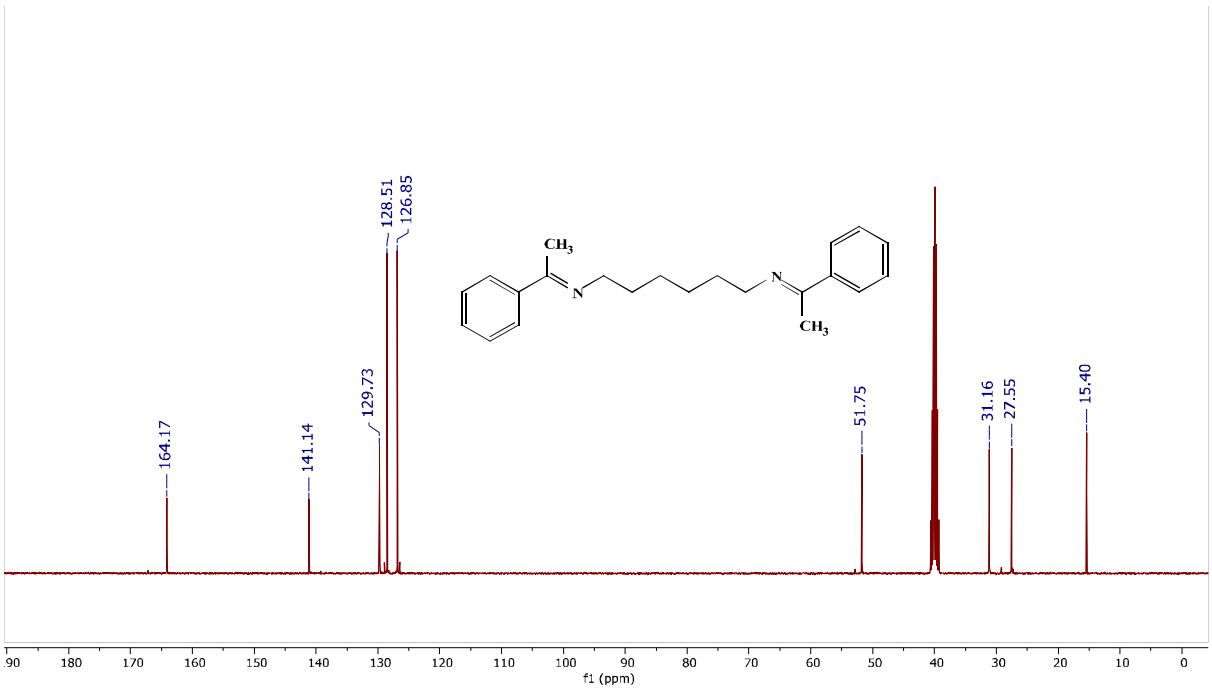

Figure A-24: ^{13}C NMR of **L4b**

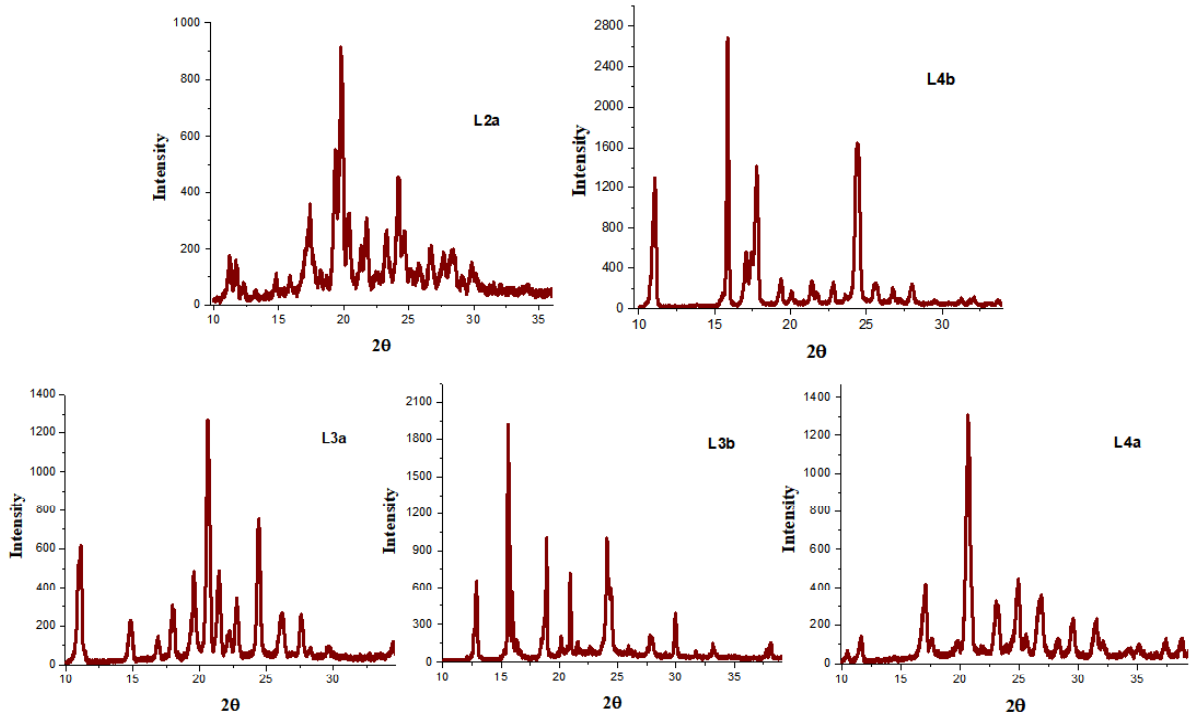

Figure A-25: Experimental PXRD of **L2a**, **L3a**, **L3b**, **L4a** and **L4b**

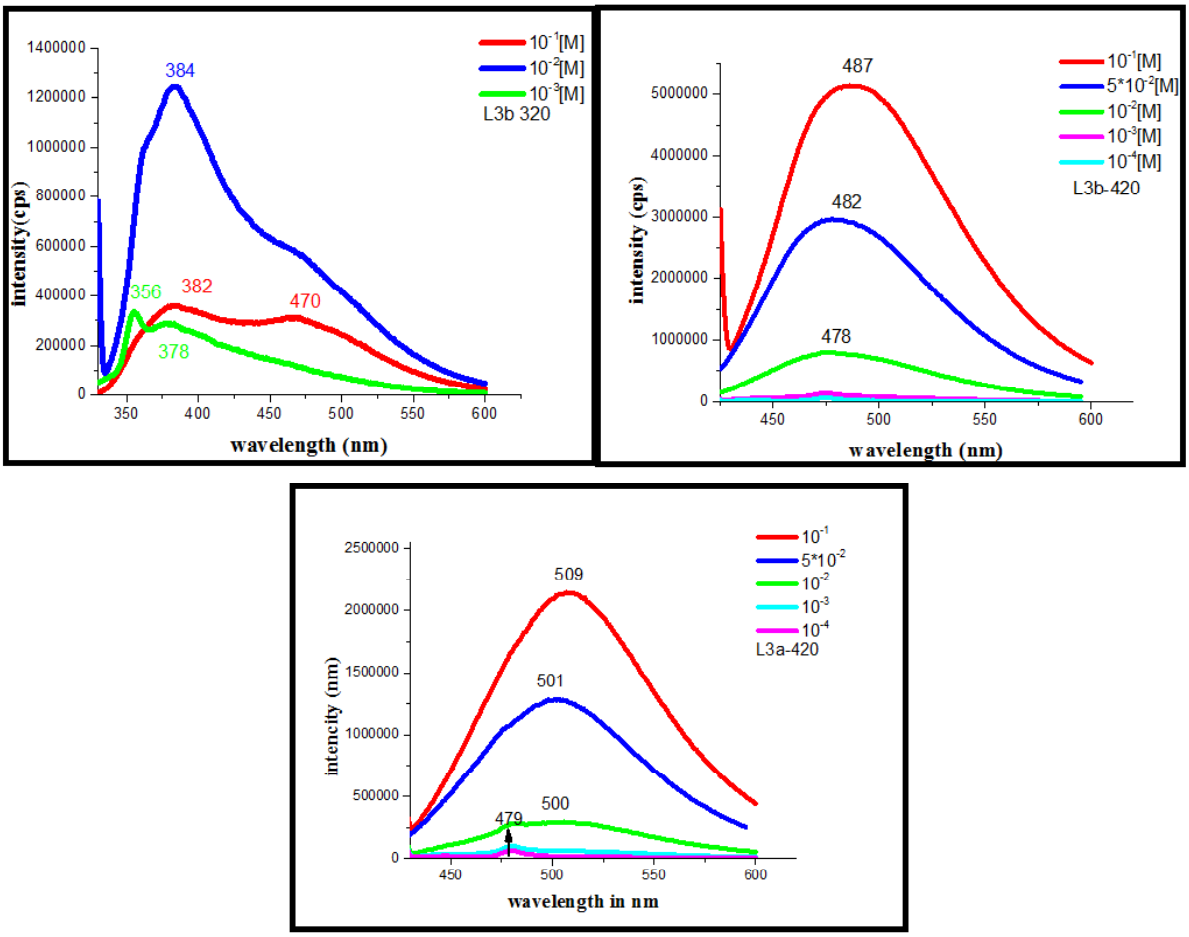

Figure A-26: The emission spectra for table 2 in chapter 3A

Table A-1: The comparison of λ_{max}

λ_{ex}	300 nm		350 nm		400 nm		450 nm	
	Conc. (M)	λ_{em} (nm)	Conc. (M)	λ_{em} (nm)	Conc. (M)	λ_{em} (nm)	Conc.(M)	λ_{em} (nm)
L2a	0.1	439	0.1	435	0.1	474	0.1	518
	0.01	358,428	0.01	432	0.01	466	0.01	517
	0.001	359,426	0.001	431	0.001	453	0.001	517
	0.0001	330,364	0.0001	391,429	0.0001	452	0.0001	518
L2b	0.1	464	0.1	440	0.1	466	0.1	500
	0.01	365,431	0.01	435	0.01	459	0.01	490
	0.001	359,424	0.001	433	0.001	454	0.001	489
	0.0001	330,364	0.0001	391,429	0.0001	453	0.0001	489
λ_{ex}	320 nm		380 nm		420 nm		430 nm	
L3a	0.1	463	0.1	463	0.1	509	0.1	511
	0.05	459	0.05	461	0.05	501	0.05	504
	0.01	391,449	0.01	428,458	0.01	500	0.01	497
	0.001	353,386	0.001	428,460	0.001	479	0.0001	493
λ_{ex}	320 nm		350 nm		400 nm		450 nm	
L3b	0.1	382,470	0.1	469	0.1	477	0.1	508
	0.01	384	0.05	466	0.05	475	0.05	504
	0.001	356,378	0.01	392,463	0.01	473	0.01	503
			0.001	391,454	0.0001	453		
			0.0001	390,430				
λ_{ex}	280 nm		320 nm		380 nm		450 nm	
L4a	0.1	514	0.1	394	0.1	464	0.1	519
	0.05	406	0.05	386	0.05	462	0.05	518
	0.01	383	0.01	383	0.01	460	0.01	517
	0.001	304,373	0.001	380	0.001	460	0.001	517
	0.0001	306,370					0.0001	517
λ_{ex}	320 nm		380 nm		400 nm		420 nm	
L4b	0.1	465	0.1	469	0.1	481	0.1	493
	0.01	356,430	0.05	468	0.05	479	0.05	493
	0.001	353,420	0.01	464	0.01	474	0.01	490
			0.001	429,461	0.001	453	0.001	480
			0.0001	428	0.0001	453	0.0001	484

Table A-2: Molar Extinction Coefficient of UV-Vis spectra of **L2b**, **L3a**, **L3b**, **L4a** and **L4b** in wavelengths near 300nm

Compounds		Molar Extinction coefficient (ϵ) ($M^{-1}cm^{-1}$)	Wavelength in nm
L2b	10^{-4}M	521	349
		607	330
		2796	284
	10^{-5}M	930	330
		23170	241
		45310	202
L3a	10^{-3}M	126.7	299
	10^{-4}M	259	345
		375	300
		1760	269
		1338	277
	10^{-5}M	-136570	345
		10250	223
		12600	201
L3b	10^{-4}M	693	349
		2255	275
	10^{-5}M	1620	349
		20370	238
		48380	202
L4a	10^{-4}M	493	347
		1361	277
		1842	269
	10^{-5}M	540	349
		16720	223
		26650	201
L4b	10^{-4}M	774	348
		2365	278
	10^{-5}M	1710	348
		29620	237
		64060	202

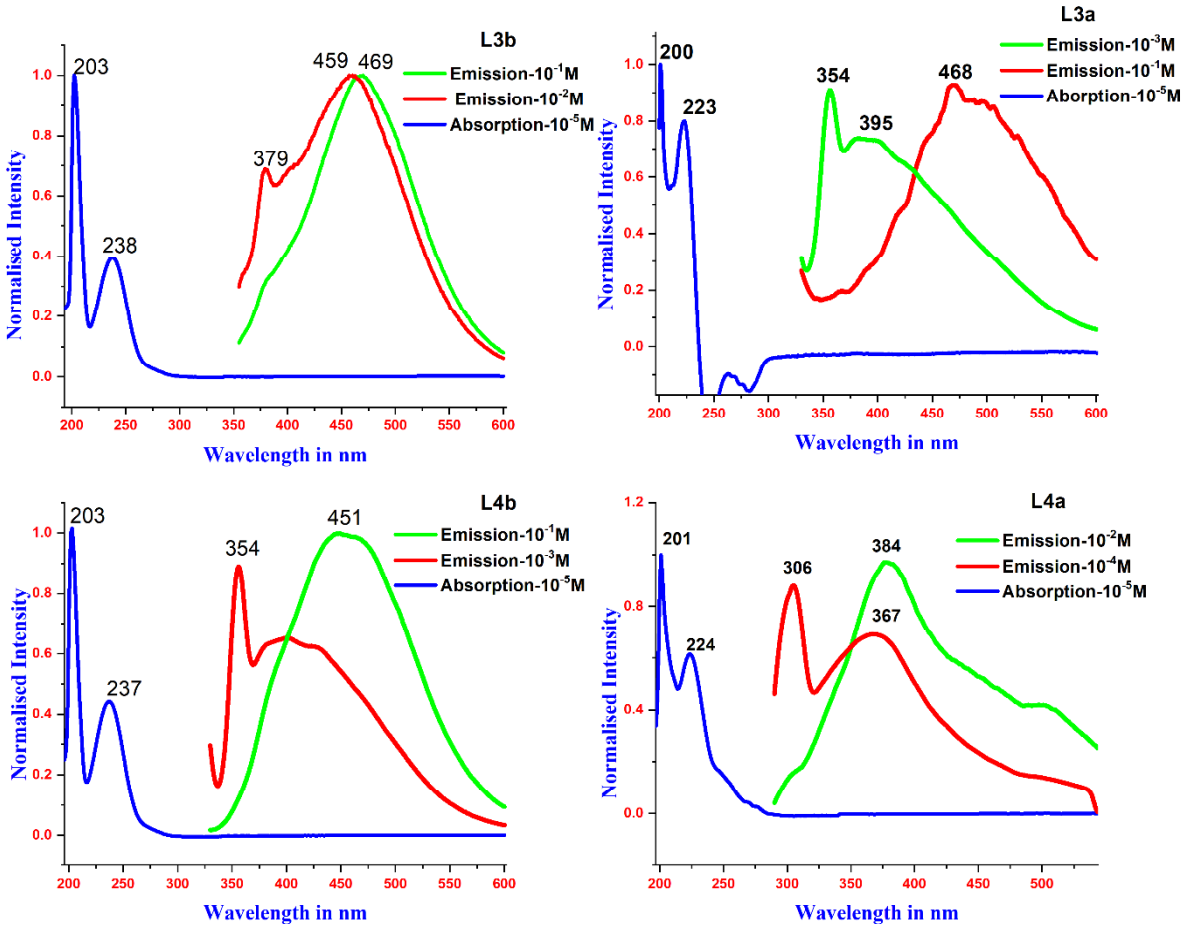

Figure A-27: Merged of absorption and emission spectra (excitation 300nm) of **L3a**, **L3b**, **L4a** and L4b

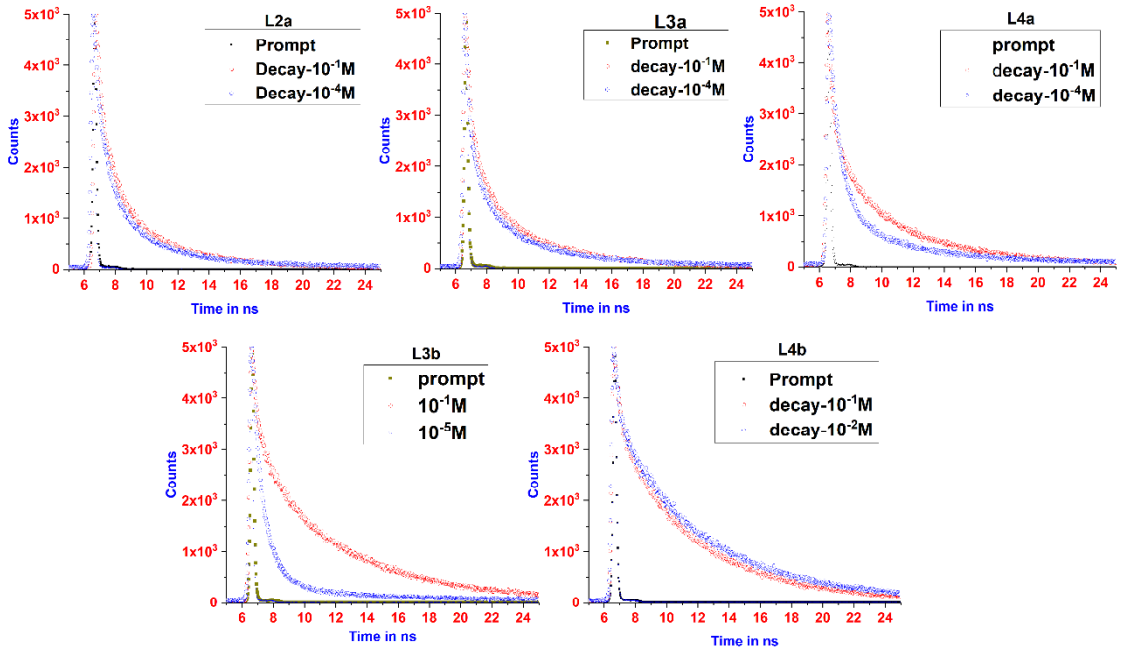

Figure A-28: TCSPC decay profiles of **L2a**, **L3a**, **L3b**, **L4a** and **L4b** in different concentration in MeOH

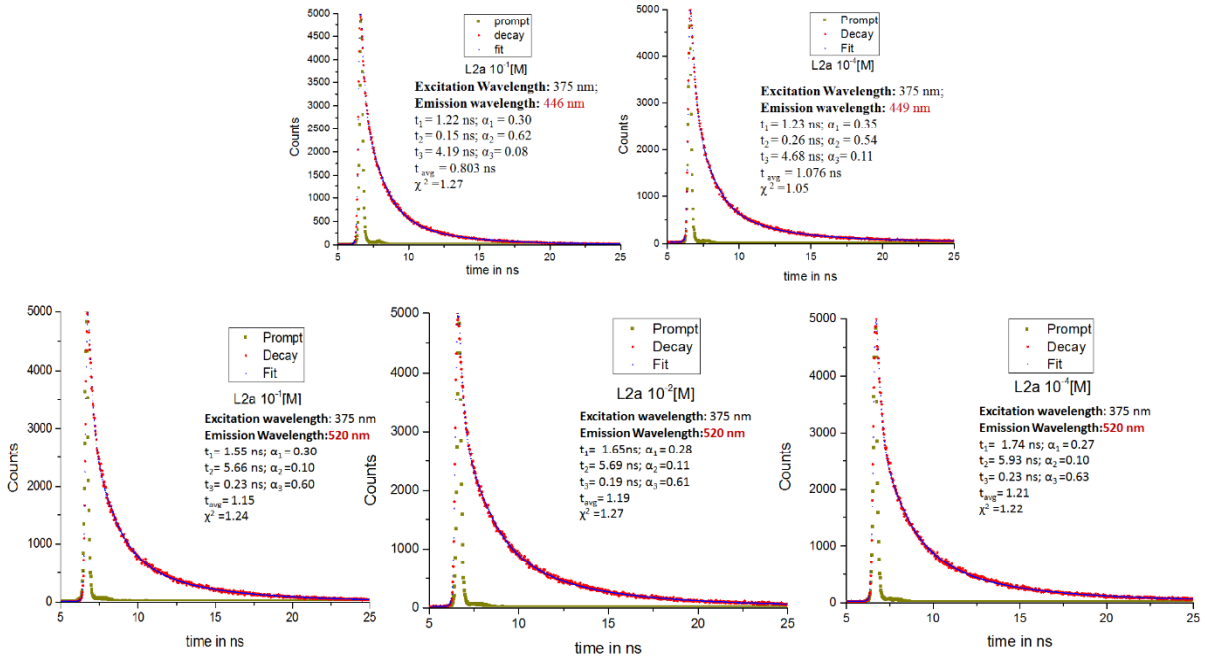

Figure A-29: TCSPC decay profiles of **L2a** in different concentration in MeOH with excitation at 375 nm

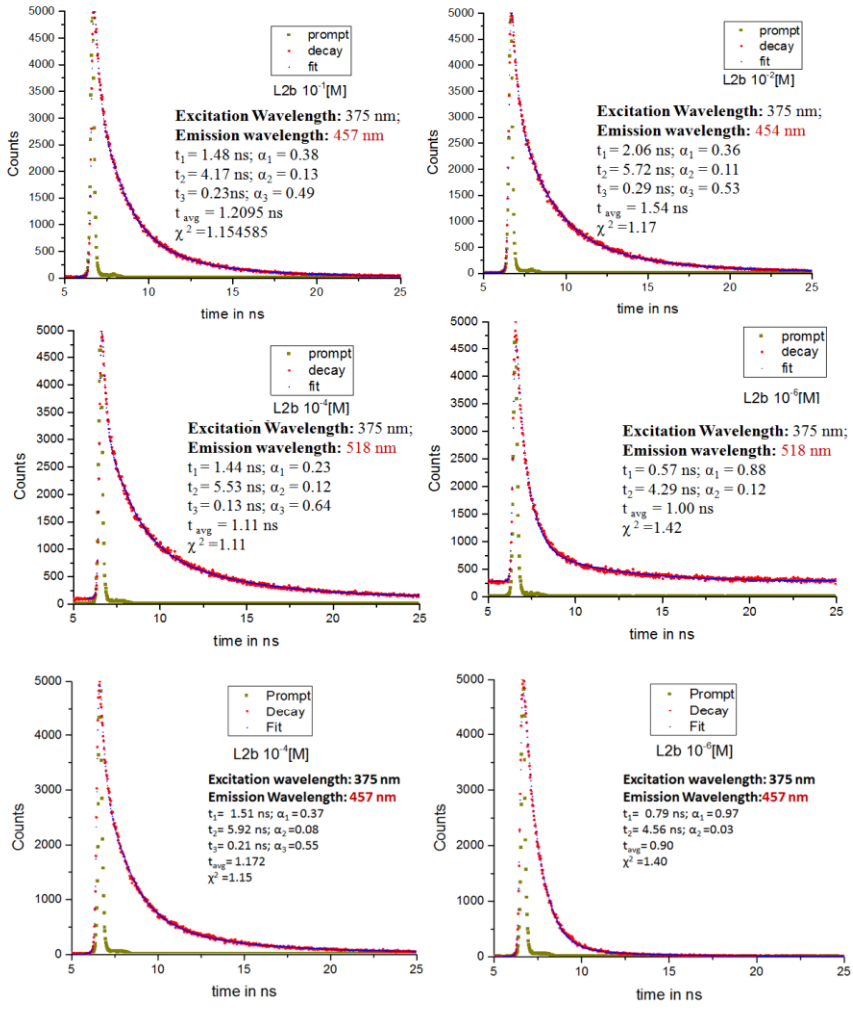

Figure A-30: TCSPC decay profiles of **L2b** in different concentration in MeOH with excitation at 375 nm

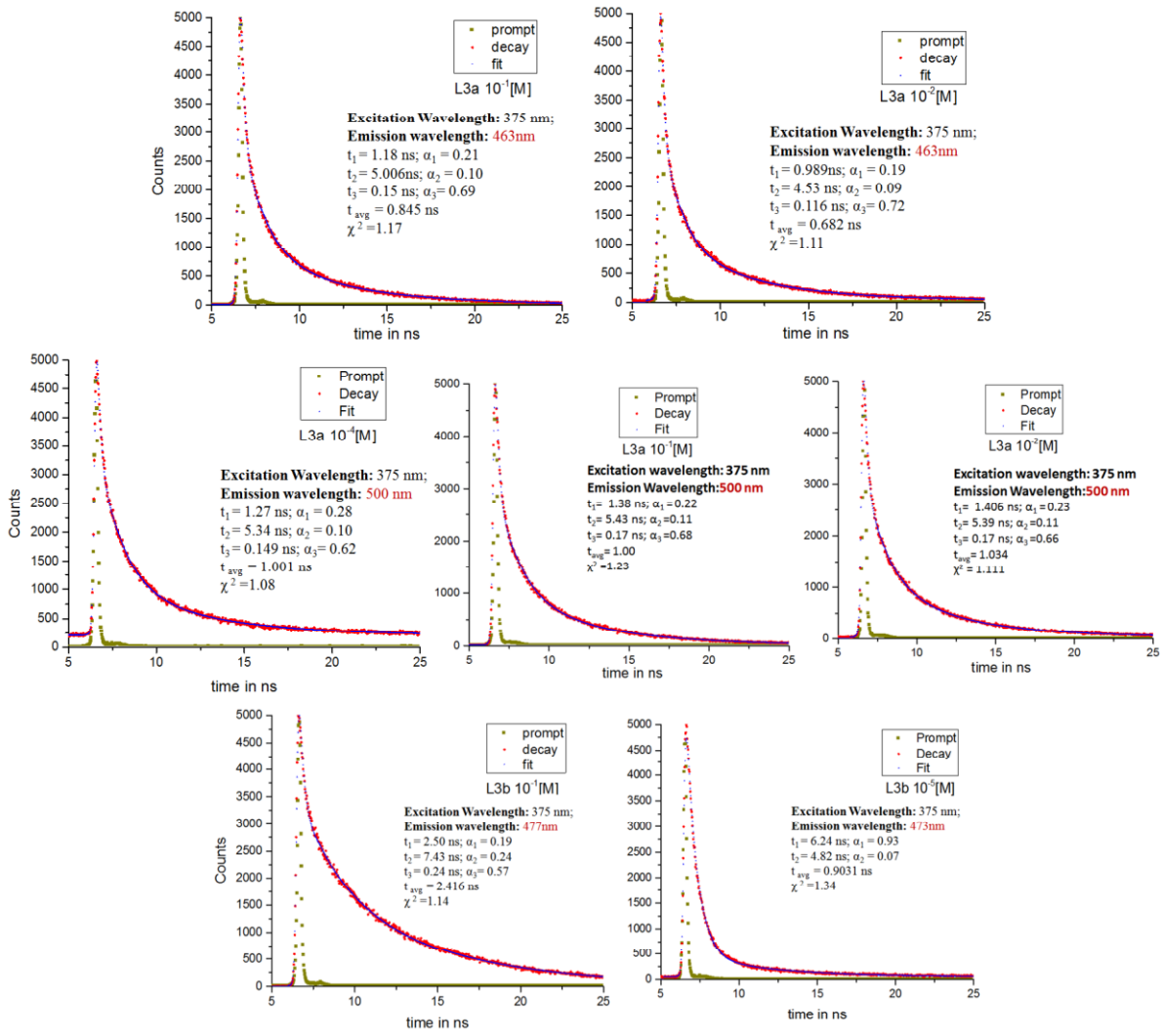

Figure A-31: TCSPC decay profiles of **L3a** and **L3b** in different concentration in MeOH with excitation at 375 nm

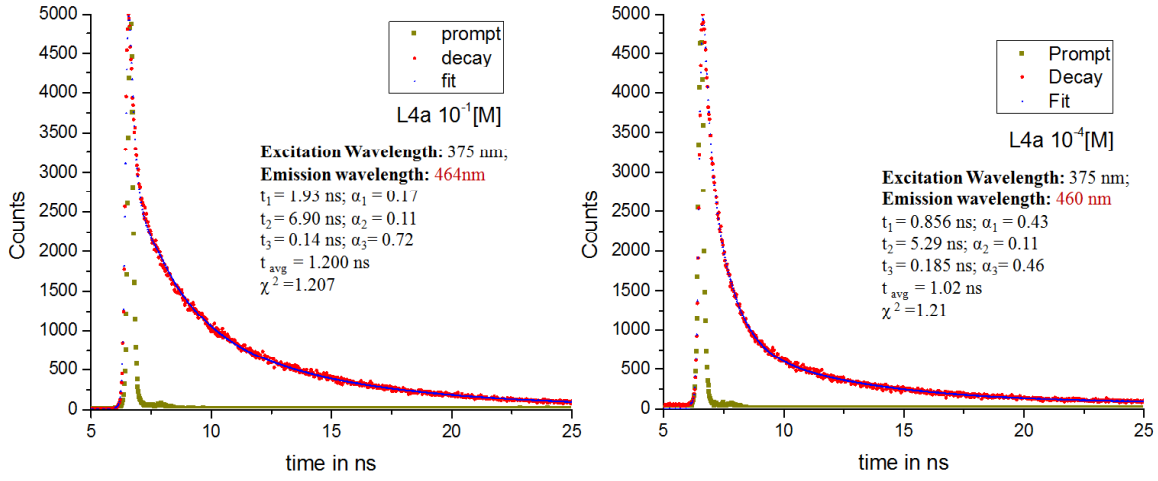

Figure A-32: TCSPC decay profiles of **L4a** in different concentration in MeOH with excitation at 375 nm

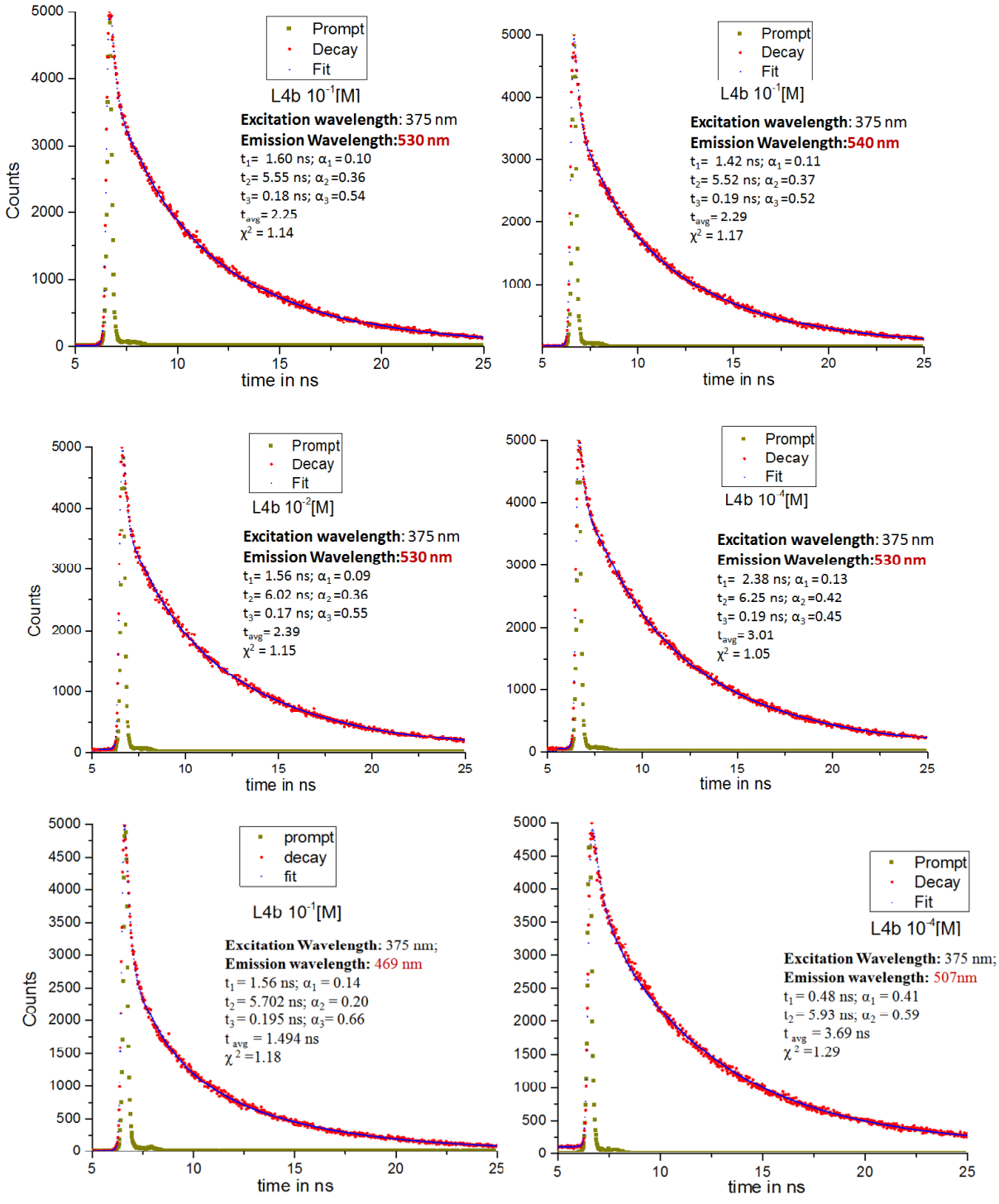

Figure A-33: TCSPC decay profiles of **L4b** in different concentration in MeOH with excitation at 375

Table A-3: Fluorescence lifetime data for **L2a**, **L2b**, **L3a**, **L3b**, **L4a** and **4b**

Excitation Wavelength = 375nm	**τ_1 (ns)**	**τ_2 (ns)**	**τ_3 (ns)**	**τ_{avg} (ns)**
L2a				
10^{-1} M; $\lambda_{Emission}$ 520nm	1.55 (α_1 0.30)	5.66 (α_2 0.10)	0.23 (α_3 0.60)	1.15 (χ^2 1.24)
10^{-1} M; $\lambda_{Emission}$ 446nm	1.22 (α_1 0.30)	0.15 (α_2 0.62)	4.19 (α_3 0.08)	0.803 (χ^2 1.27)
10^{-2}M; $\lambda_{Emission}$ 520nm	1.65 (α_1 0.28)	5.69 (α_2 0.11)	0.19 (α_3 0.61)	1.19 (χ^2 1.27)
10^{-4}M; $\lambda_{Emission}$520nm	1.74 (α_1 0.27)	5.93 (α_2 0.10)	0.23 (α_3 0.63)	1.21 (χ^2 1.22)
10^{-4}M; $\lambda_{Emission}$449nm	1.23 (α_1 0.35)	0.26 (α_2 0.54)	4.69 (α_3 0.11)	1.076 (χ^2 1.05)
L2b				
10^{-1}M; $\lambda_{Emission}$457nm	1.48 (α_1 0.38)	4.17 (α_2 0.13)	0.23 (α_3 0.49)	1.209 (χ^2 1.15)
10^{-2} M; $\lambda_{Emission}$454nm	2.06 (α_1 0.36)	5.72 (α_2 0.11)	0.29 (α_3 0.53)	1.540 (χ^2 1.17)
10^{-4} M; $\lambda_{Emission}$518nm	1.45 (α_1 0.23)	5.53 (α_2 0.12)	0.13 (α_3 0.64)	1.110 (χ^2 1.11)
10^{-4} M; $\lambda_{Emission}$457nm	1.51 (α_1 0.37)	5.92 (α_2 0.08)	0.21 (α_3 0.55)	1.172 ($\chi^2$1.15)
10^{-6} M; $\lambda_{Emission}$518nm	0.57 (α_1 0.88)	4.29 (α_2 0.12)	----	1.001 (χ^2 1.42)
10^{-6} M; $\lambda_{Emission}$457nm	0.79 (α_1 0.97)	4.56 (α_2 0.03)	----	0.90 (χ^2 1.40)
10^{-6} M; $\lambda_{Emission}$457nm	0.33 (α_1 0.38)	0.95 (α_2 0.61)	5.87 (α_3 0.01)	0.79 (χ^2 1.15)
L3a				
10^{-1}M; $\lambda_{Emission}$500nm	1.38 (α_1 0.22)	5.43 (α_2 0.11)	0.17 (α_3 0.68)	1.00 (χ^2 1.23)
10^{-1}M; $\lambda_{Emission}$463nm	1.19 (α_1 0.21)	5.01 (α_2 0.10)	0.15 (α_3 0.69)	0.845 (χ^2 1.17)
10^{-2}M; $\lambda_{Emission}$500nm	1.406 (α_1 0.23)	5.39 (α_2 0.11)	0.17 (α_3 0.66)	1.034 (χ^2 1.111)
10^{-2}M; $\lambda_{Emission}$463nm	0.99 (α_1 0.19)	4.53 (α_2 0.09)	0.12 (α_3 0.72)	0.682 (χ^2 1.11)
10^{-4}M; $\lambda_{Emission}$500nm	1.28 (α_1 0.28)	5.34 (α_2 0.10)	0.15 (α_3 0.62)	1.001 (χ^2 1.08)
L3b				
10^{-1}M; $\lambda_{Emission}$477nm	2.50 (α_1 0.19)	7.43 (α_2 0.24)	0.24 (α_3 0.57)	2.416 (χ^2 1.14)
10^{-5}M; $\lambda_{Emission}$473nm	6.24 (α_1 0.93)	4.83 (α_2 0.07)	----	0.903 (χ^2 1.34)
L4a				
10^{-1}M; $\lambda_{Emission}$464nm	1.93 (α_1 0.17)	6.90 (α_2 0.11)	0.15 (α_3 0.72)	1.201 (χ^2 1.20)
10^{-4}M; $\lambda_{Emission}$460nm	0.86 (α_1 0.43)	5.29 (α_2 0.11)	0.19 (α_3 0.46)	1.021 (χ^2 1.21)
L4b				
10^{-1}M; $\lambda_{Emission}$540nm	1.42 ($\alpha_1$0.11)	5.52 (α_2 0.37)	0.19 (α_3 0.52)	2.29 (χ^2 1.17)
10^{-1}M; $\lambda_{Emission}$469nm	1.57 (α_1 0.14)	5.70 (α_2 0.20)	0.19 (α_3 0.66)	1.495 (χ^2 1.18)
10^{-1}M; $\lambda_{Emission}$530nm	1.60 ($\alpha_1$0.10)	5.55 (α_2 0.36)	0.18 (α_3 0.54)	2.25 (χ^2 1.14)
10^{-2}M; $\lambda_{Emission}$530nm	1.56 (α_1 0.09)	6.02 (α_2 0.36)	0.17 (α_3 0.55)	2.39 (χ^2 1.15)
10^{-2}M; $\lambda_{Emission}$530nm	0.32 (α_1 0.53)	5.8 (α_2 0.47)	----	2.90 (χ^2 1.33)
10^{-4}M; $\lambda_{Emission}$530nm	2.38 (α_1 0.13)	6.25 (α_2 0.42)	0.19 (α_3 0.45)	3.01 (χ^2 1.05)
10^{-4}M; $\lambda_{Emission}$530nm	0.432 (α_1 0.41)	5.84 (α_2 0.59)	----	3.61 (χ^2 1.33)
10^{-4}M; $\lambda_{Emission}$507nm	0.49 (α_1 0.41)	5.94 (α_2 0.59)	----	3.692 (χ^2 1.29)

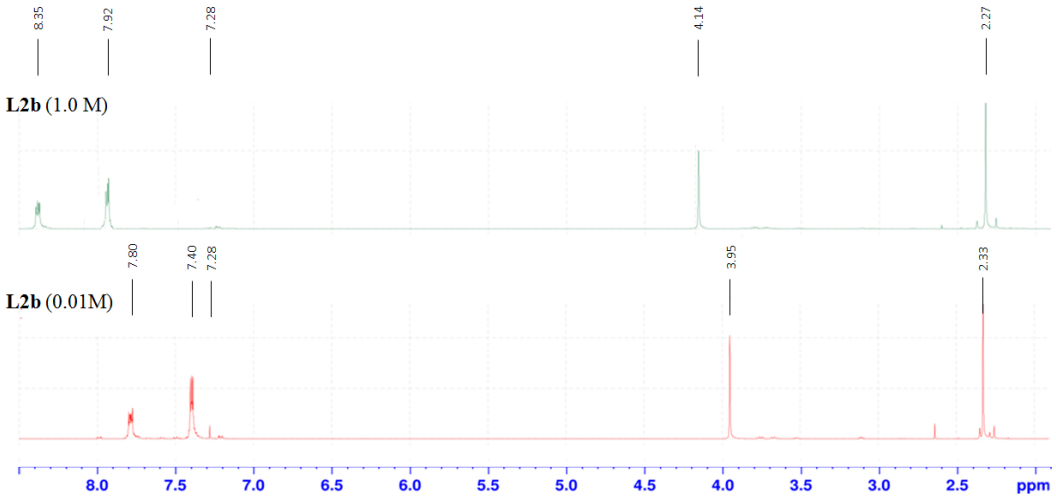

Figure A-34: ^{1}H NMR spectra of **L2b** in $CDCl_3$ by changing the concentration of compound

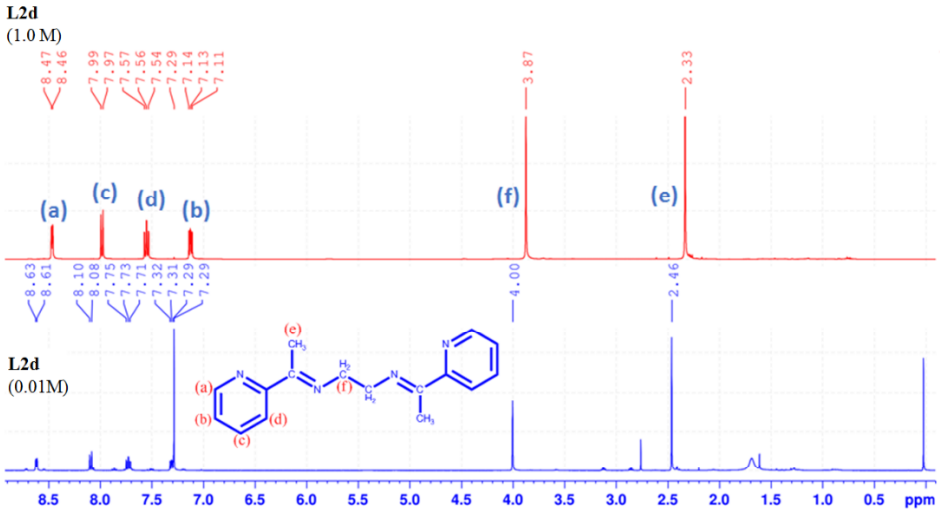

Figure A-35: ^{1}H NMR spectra of **L2d** in $CDCl_3$ by changing the concentration of compound

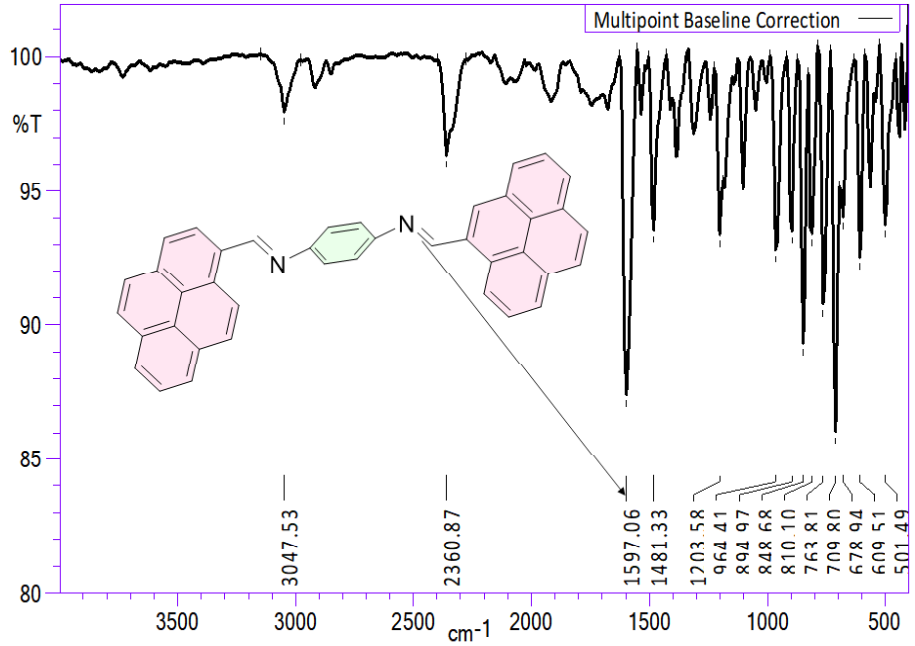

Figure A-36: IR spectra of **L5a**

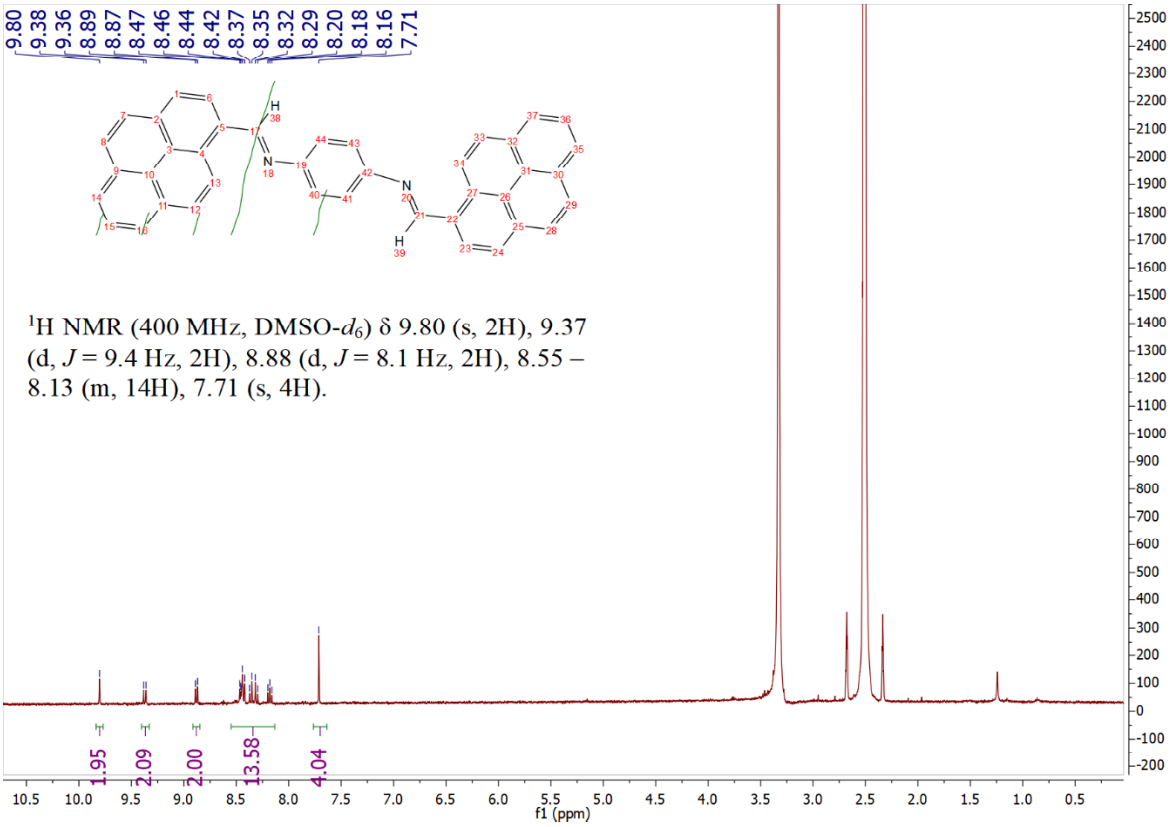

Figure A-37: ^{1}H-NMR spectra of **L5a**

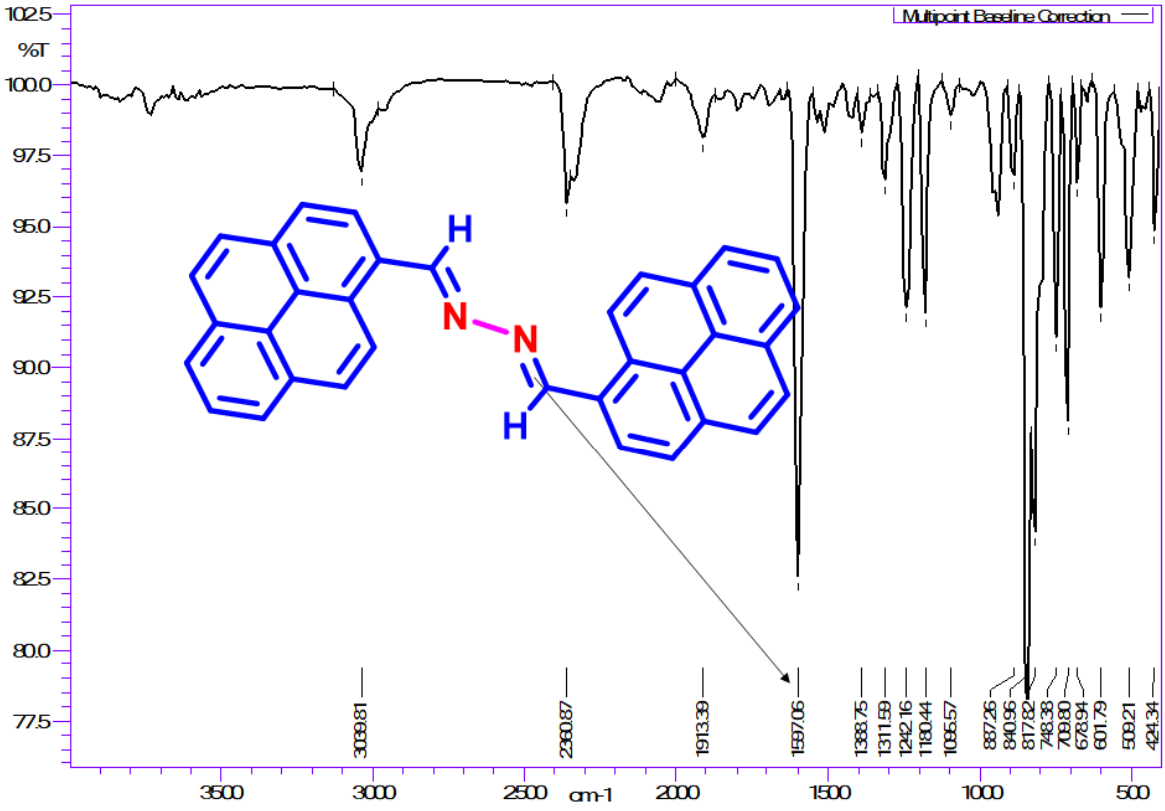

Figure A-38: IR spectra of **L6a**

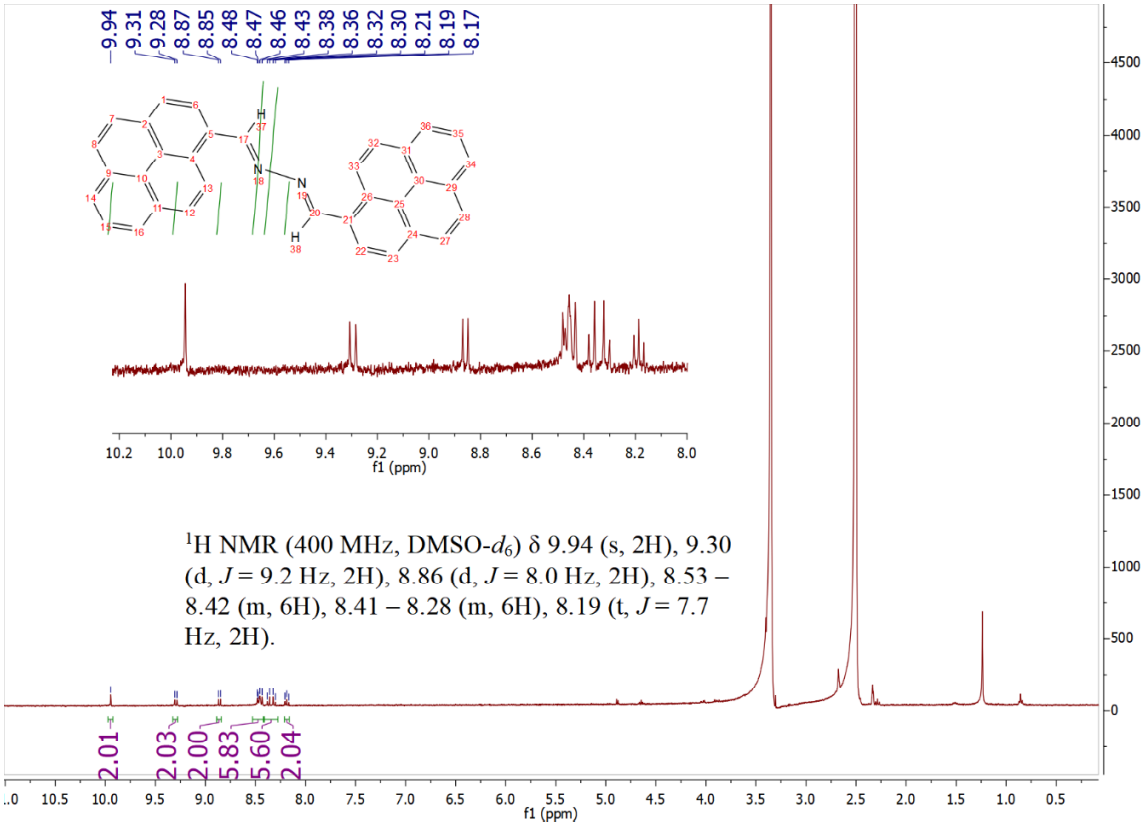

Figure A-39: ^{1}H-NMR spectra of **L6a**

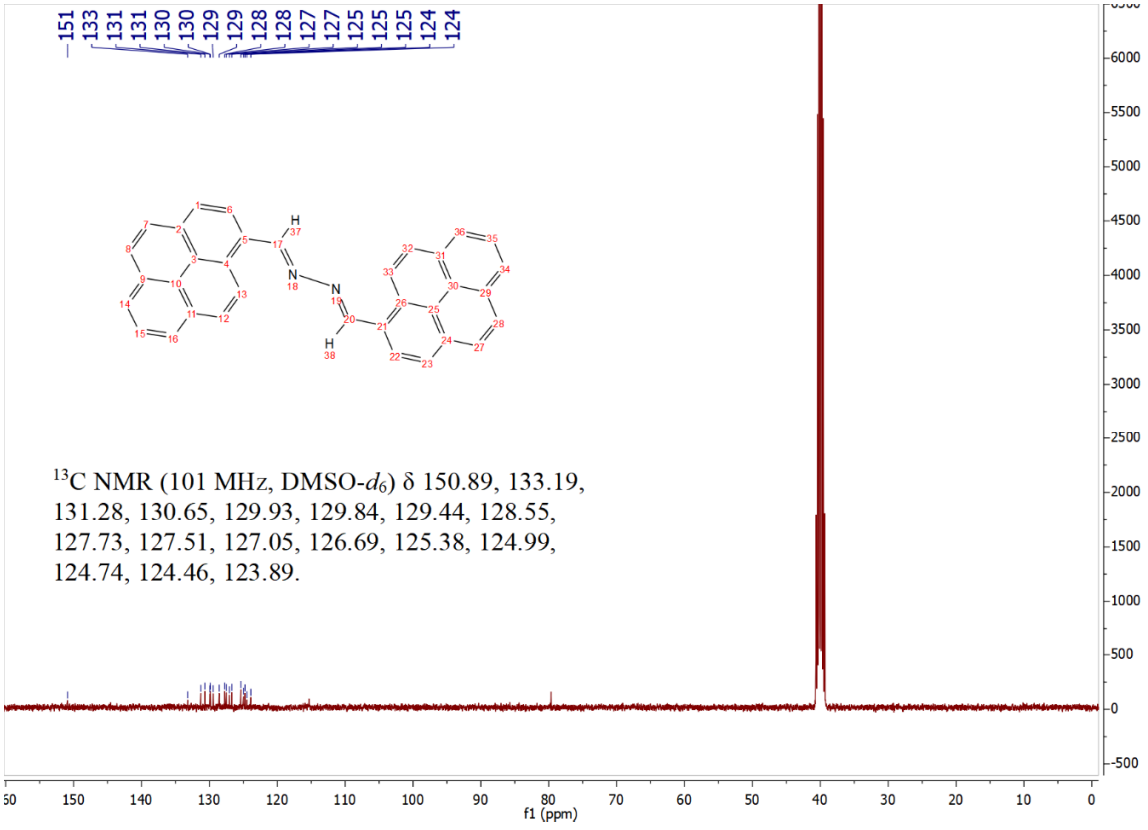

Figure A-40: ^{13}C-NMR spectra of **L6a**

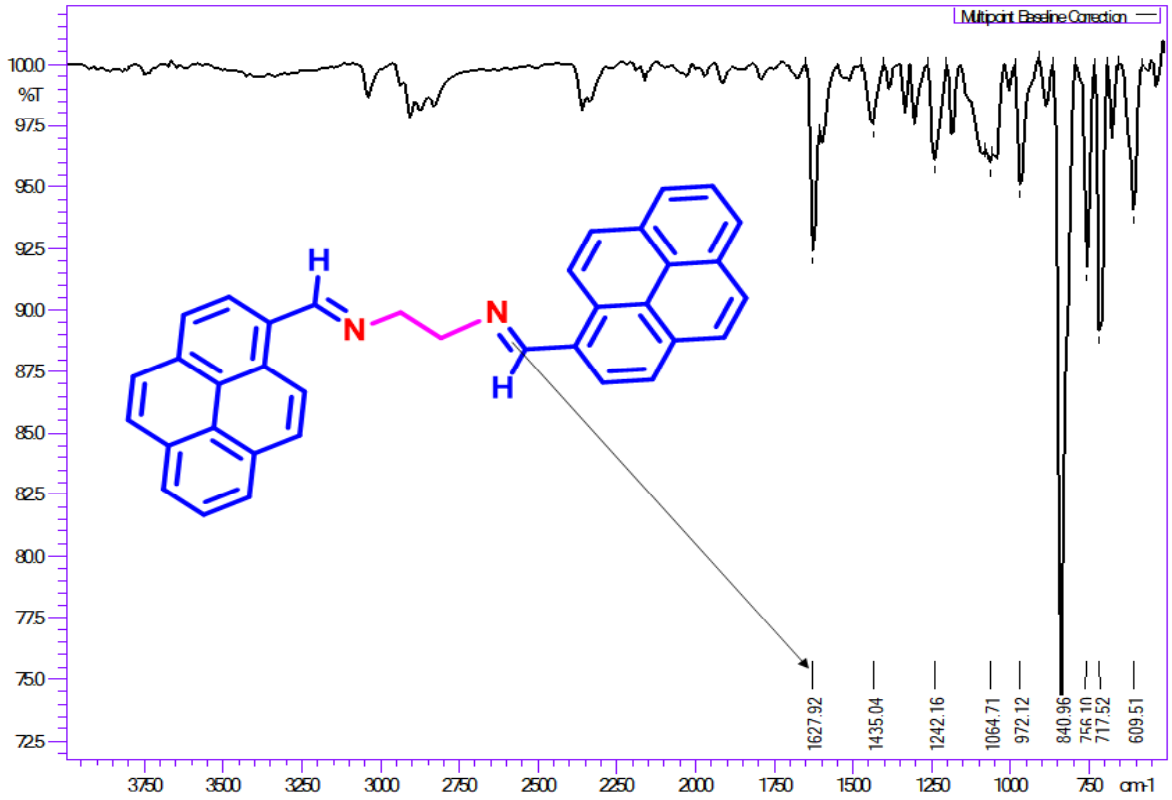

Figure A-41: IR spectra of **L7a**

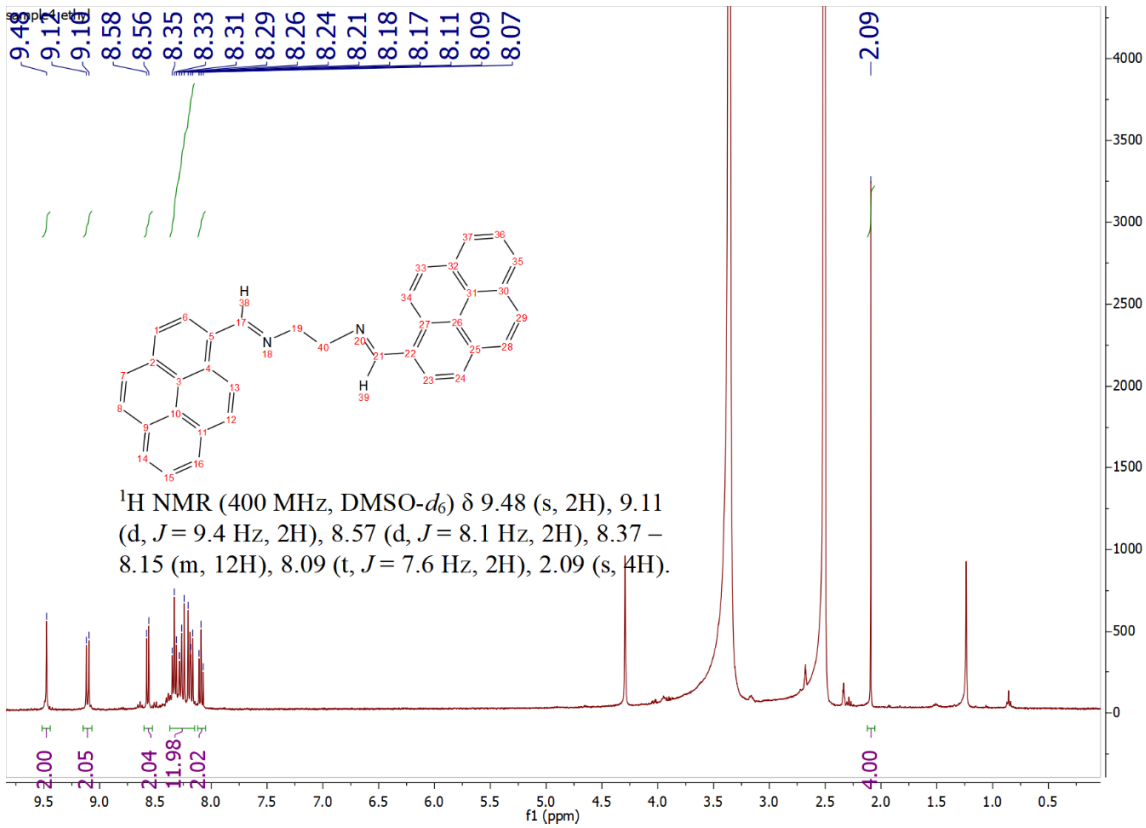

Figure A-42: ^{1}H-NMR spectra of **L7a**

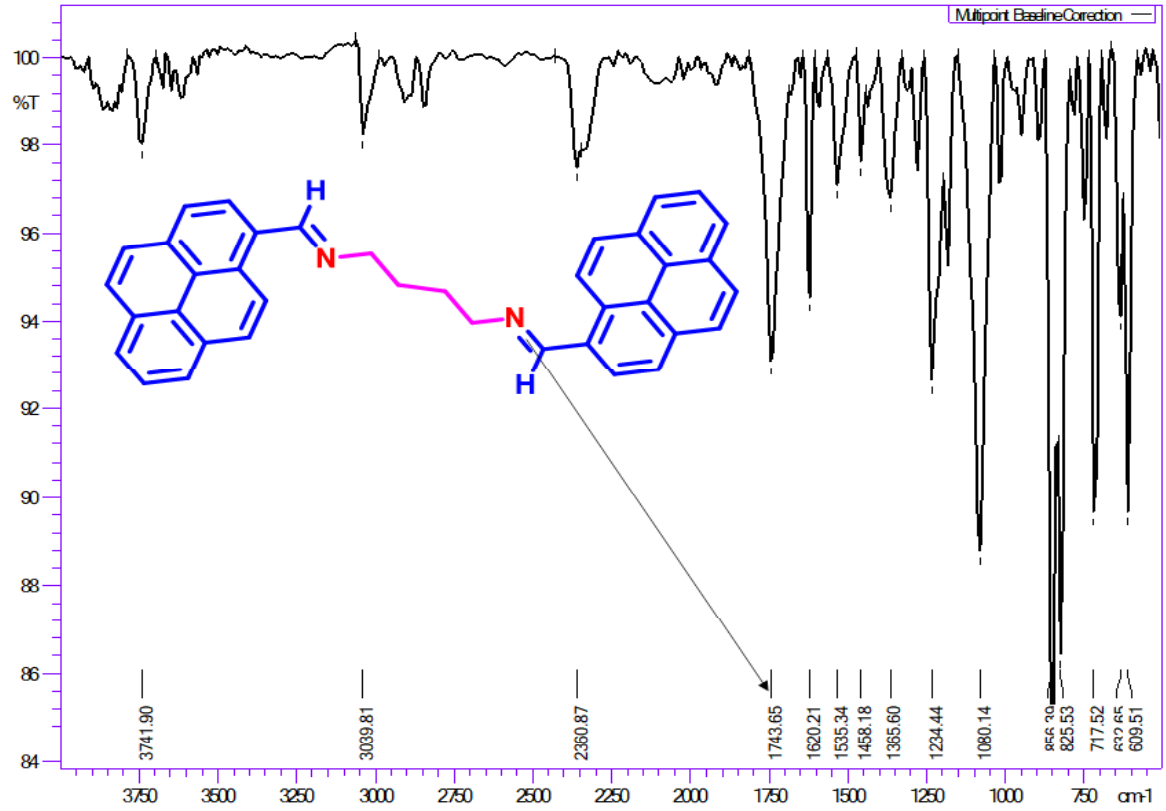

Figure A-43: IR spectra of **L8a**

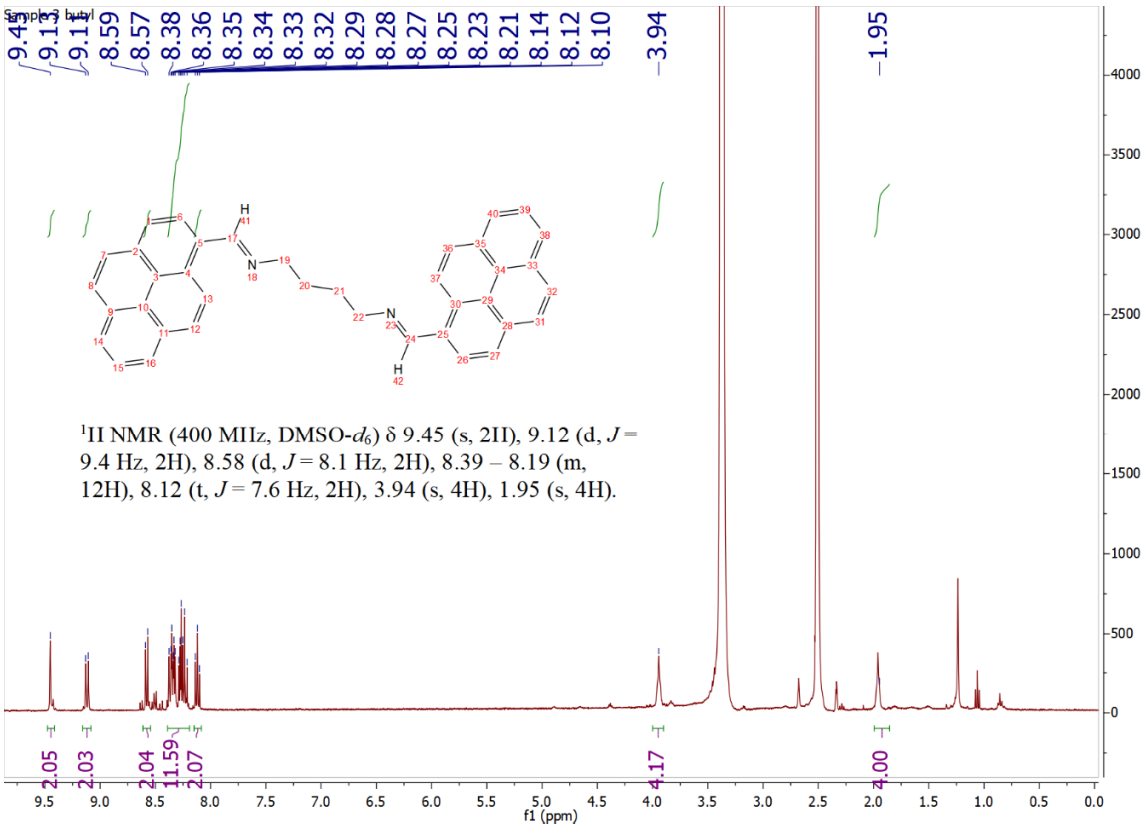

Figure A-44: [1]H-NMR spectra of **L8a**

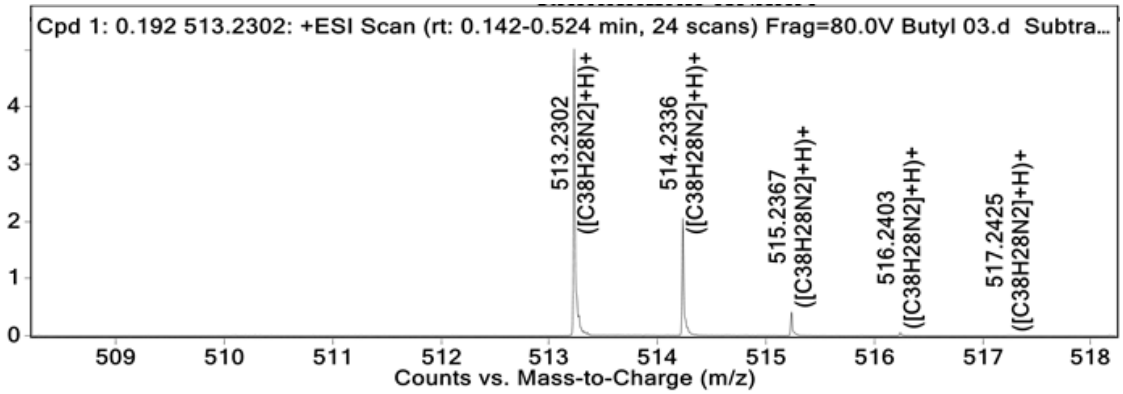

Figure A-45: Mass spectra of **L8a**

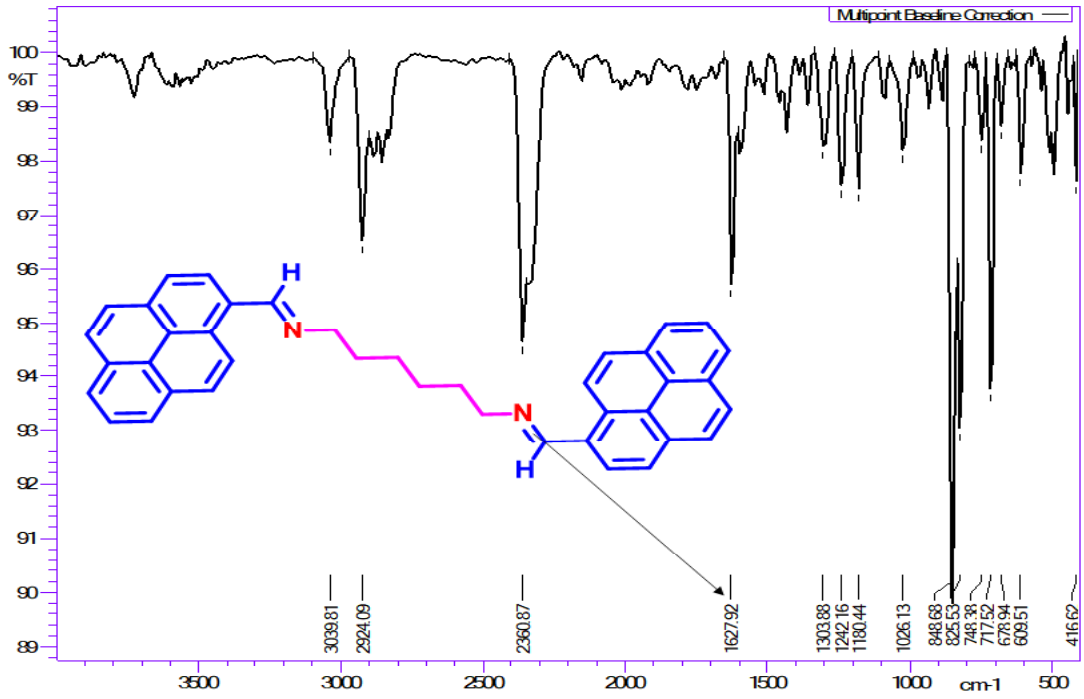

Figure A-46: IR spectra of **L9a**

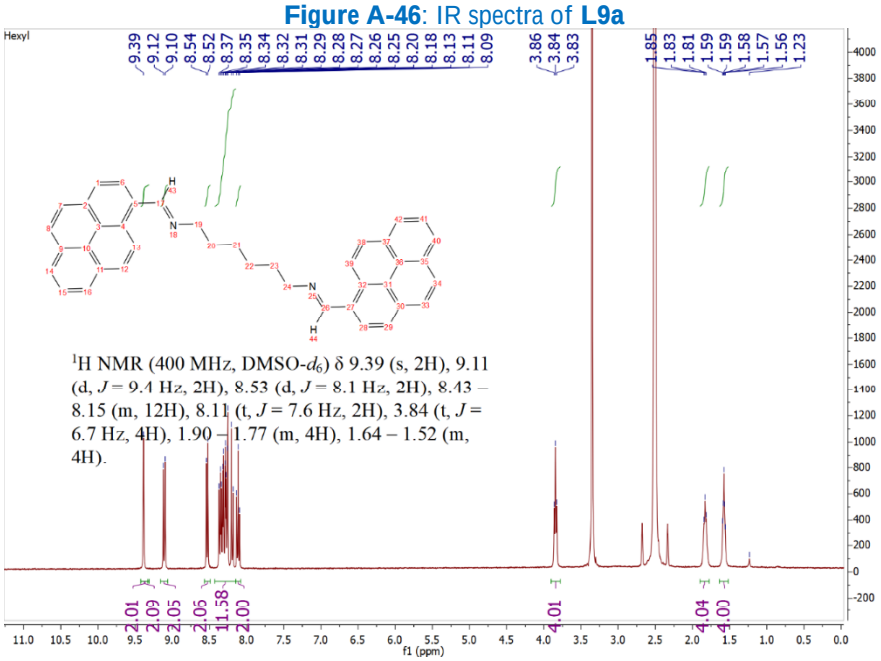

Figure A-47: ^{1}H-NMR spectra of **L9a**

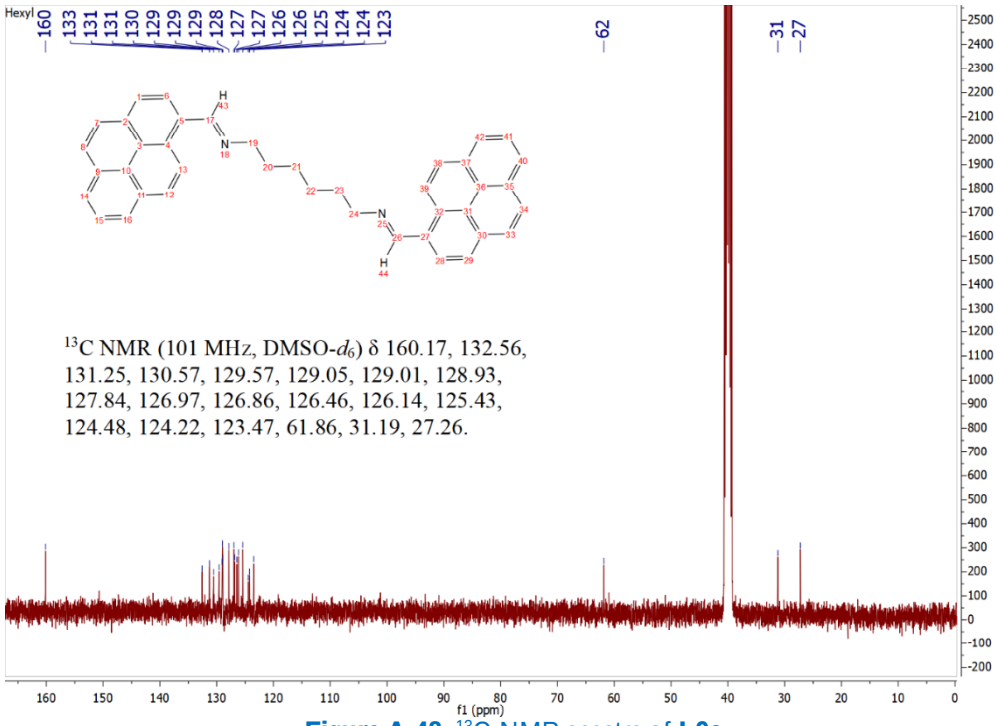

Figure A-48: ^{13}C-NMR spectra of **L9a**

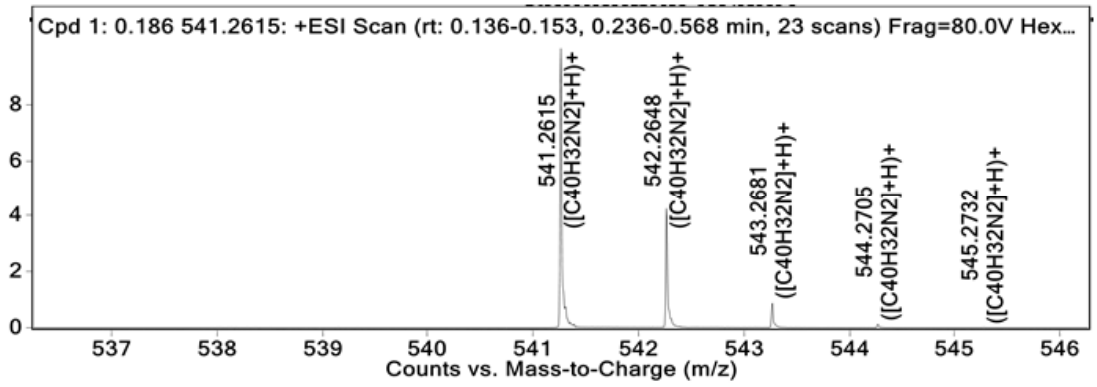

Figure A-49: Mass spectra of **L8a**

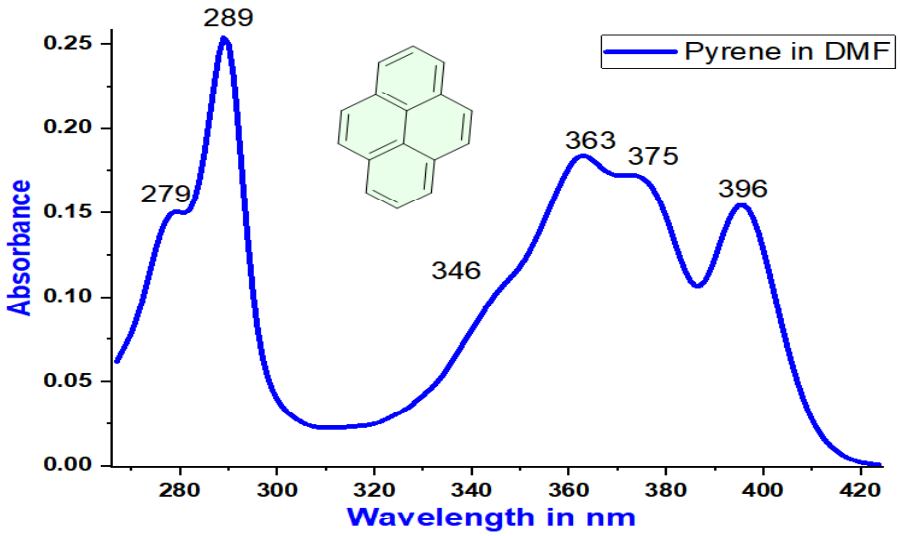

Figure A-50 : The Pyrene monomer has shown three sharp absorption peaks

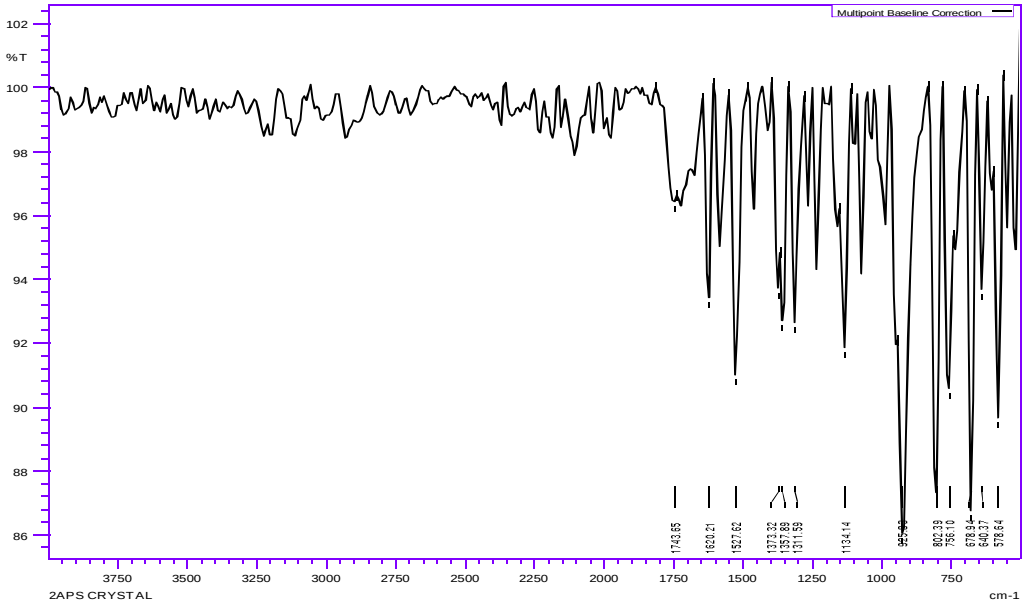

Figure A-51: IR spectra of **L10b**

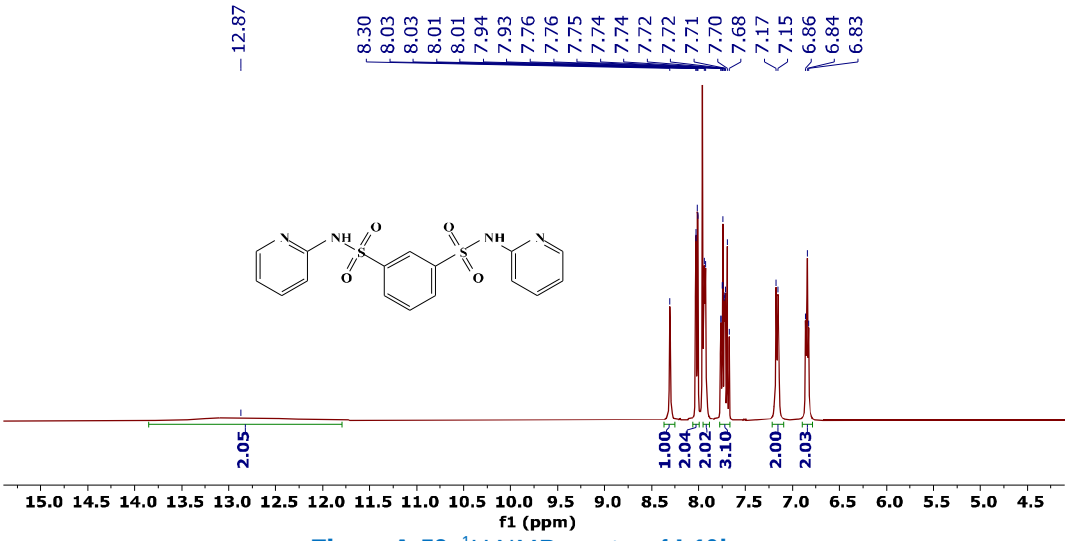

Figure A-52: ^{1}H NMR spectra of **L10b**

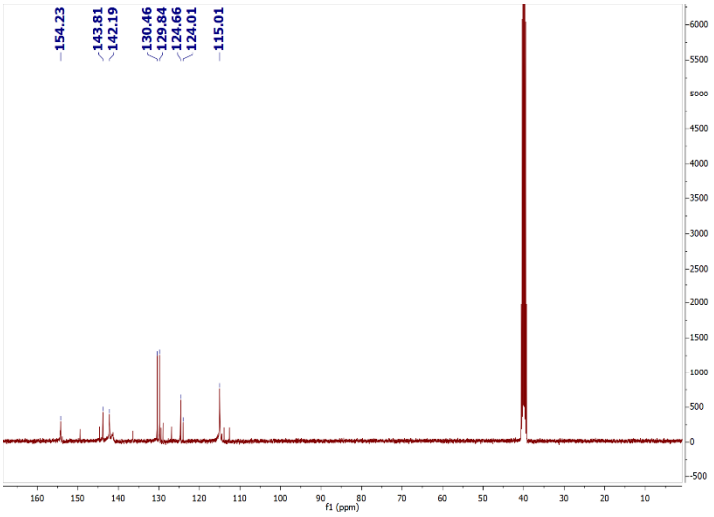

Figure A-53: ^{13}C NMR spectra of **L10b**

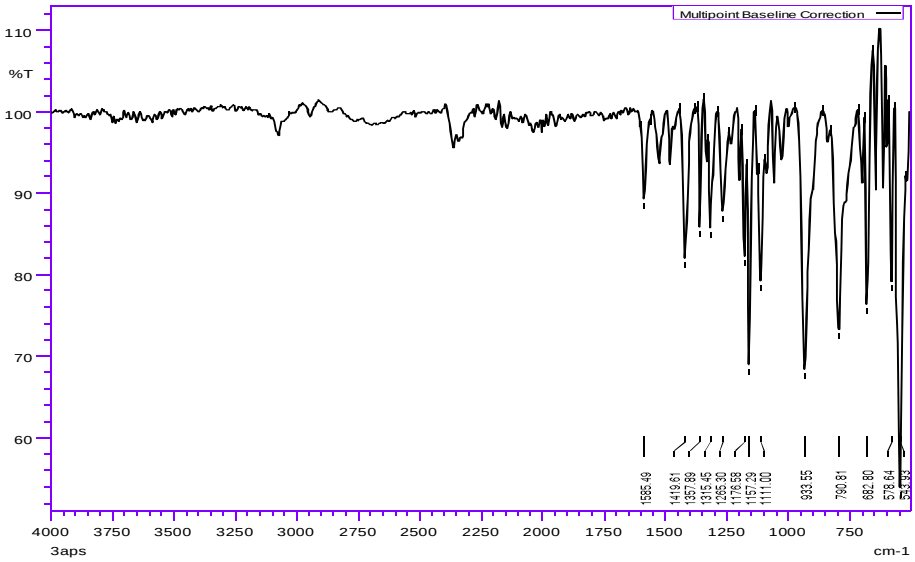

Figure A-54: IR spectra of **L11b**

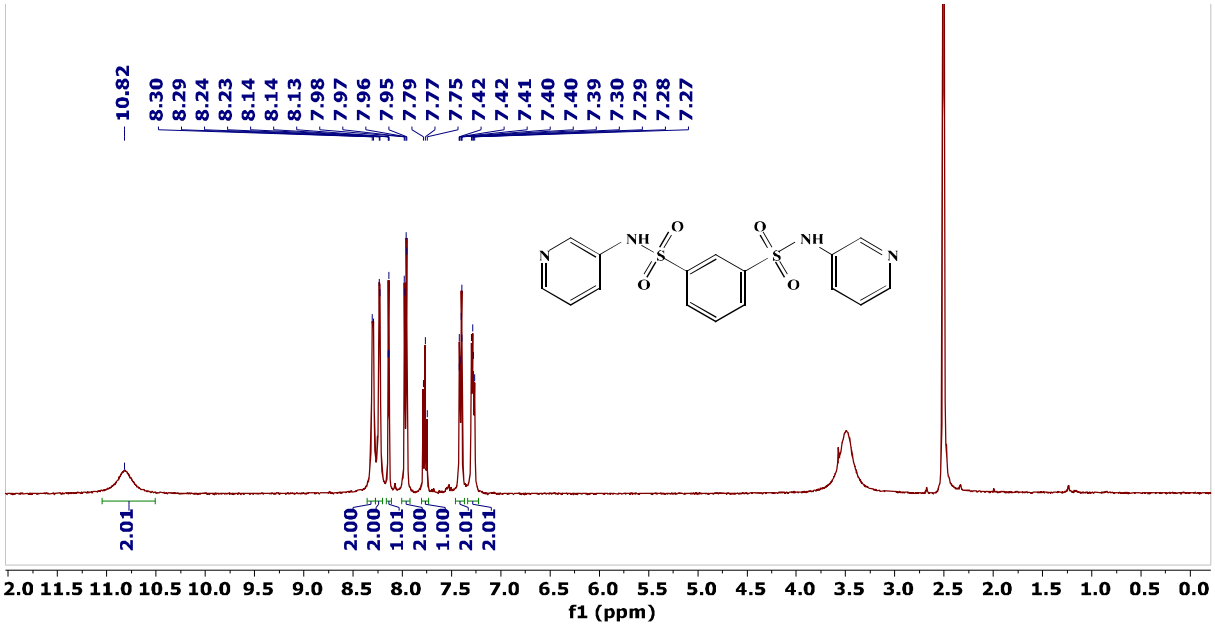

Figure A-55: ^{1}H NMR spectra of **L11b**

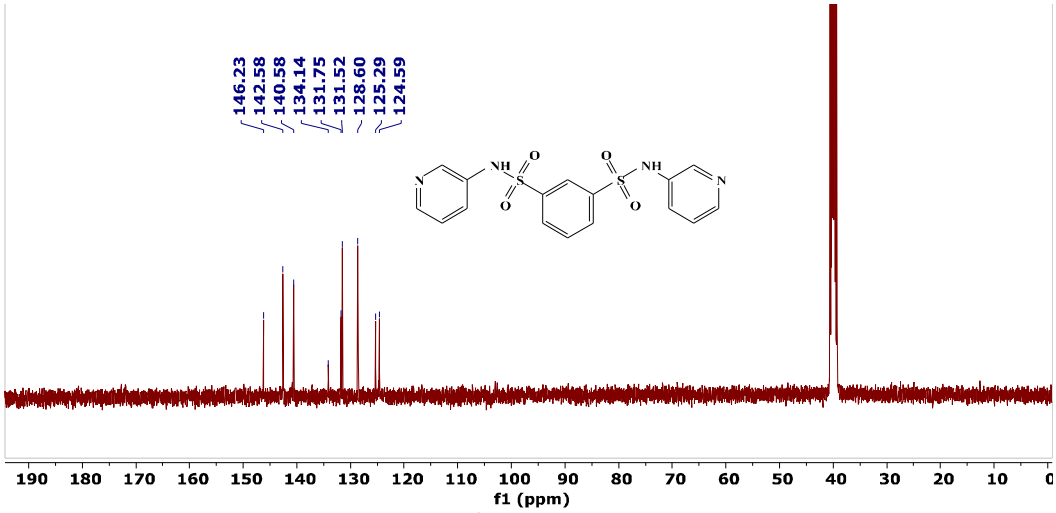

Figure A-56: ^{13}C NMR spectra of **L11b**

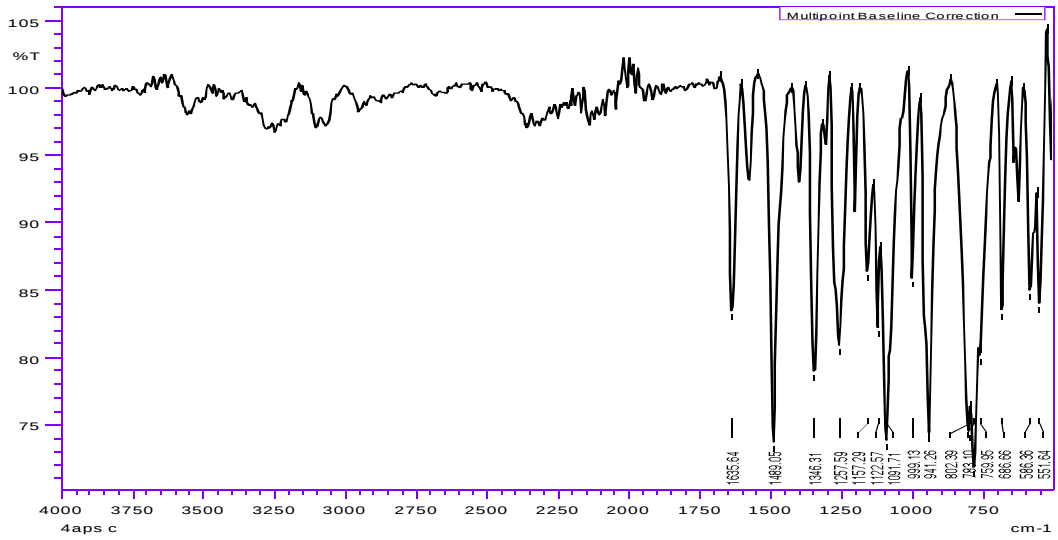

Figure A-57: IR spectra of **L12b**

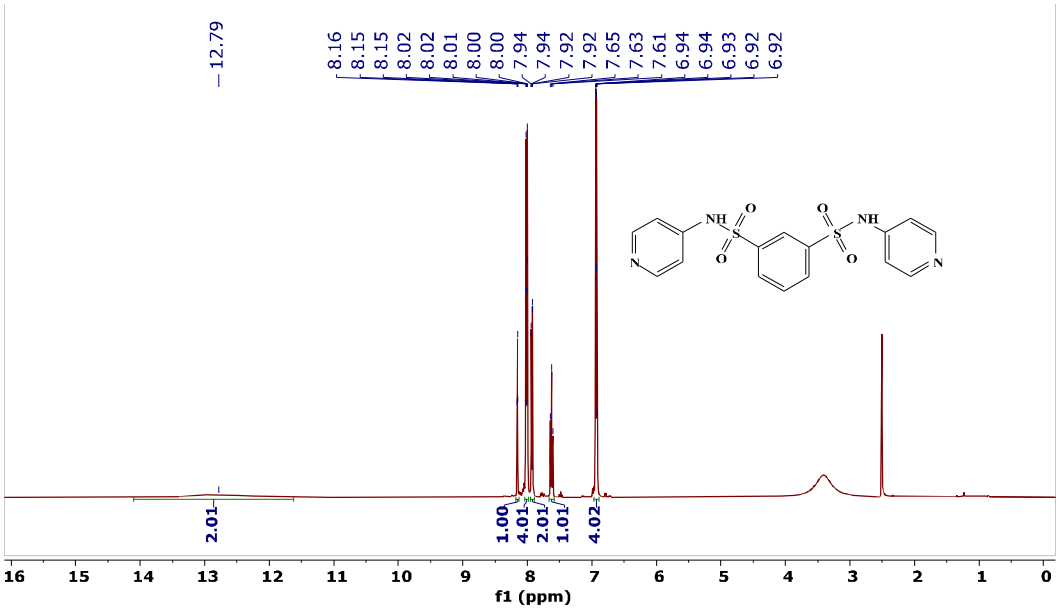

Figure A-58: ^{1}H NMR spectra of **L12b**

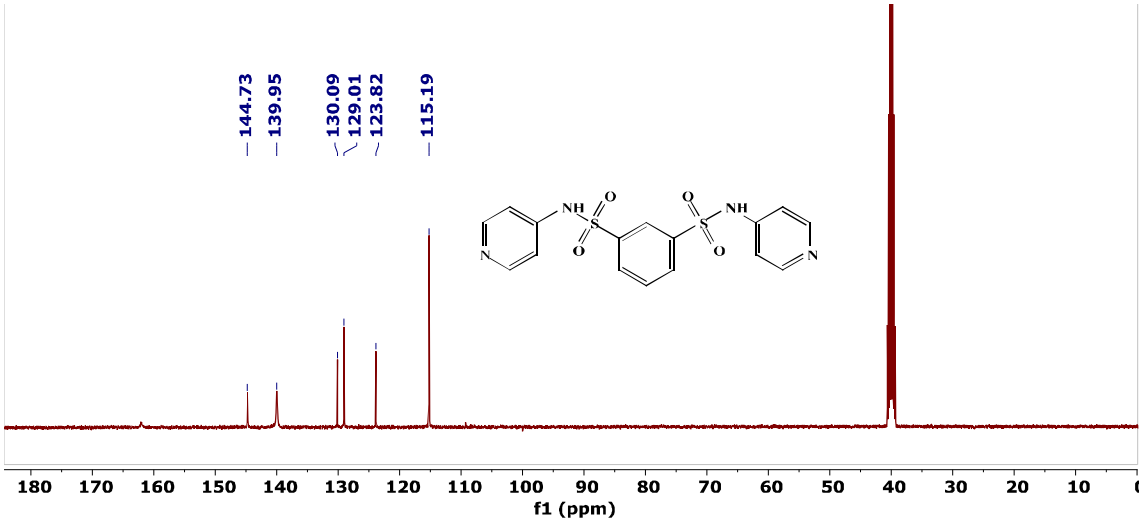

Figure A-59: ^{13}C NMR spectra of **L12b**

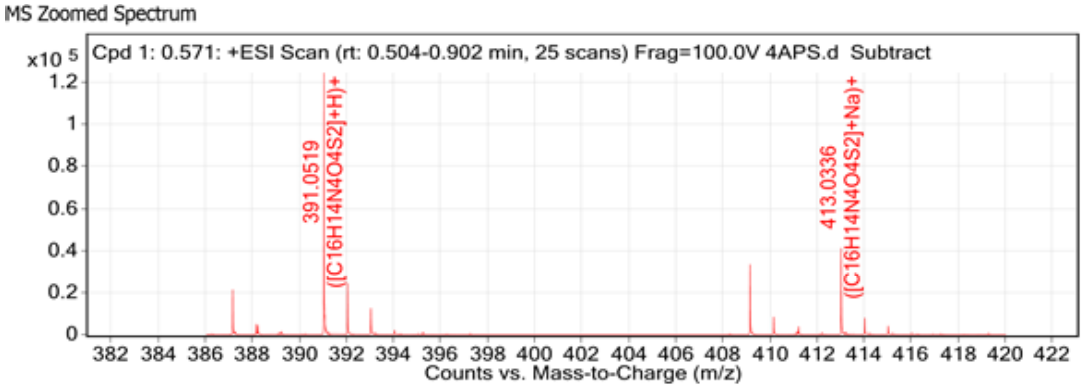

Figure A-60: Mass spectra of **L12b**

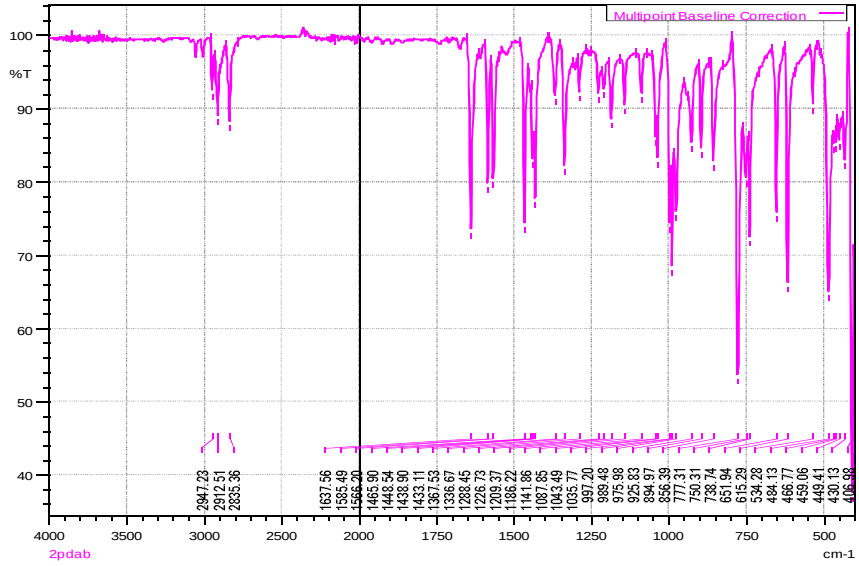

Figure A-61: IR spectra of **L3c**

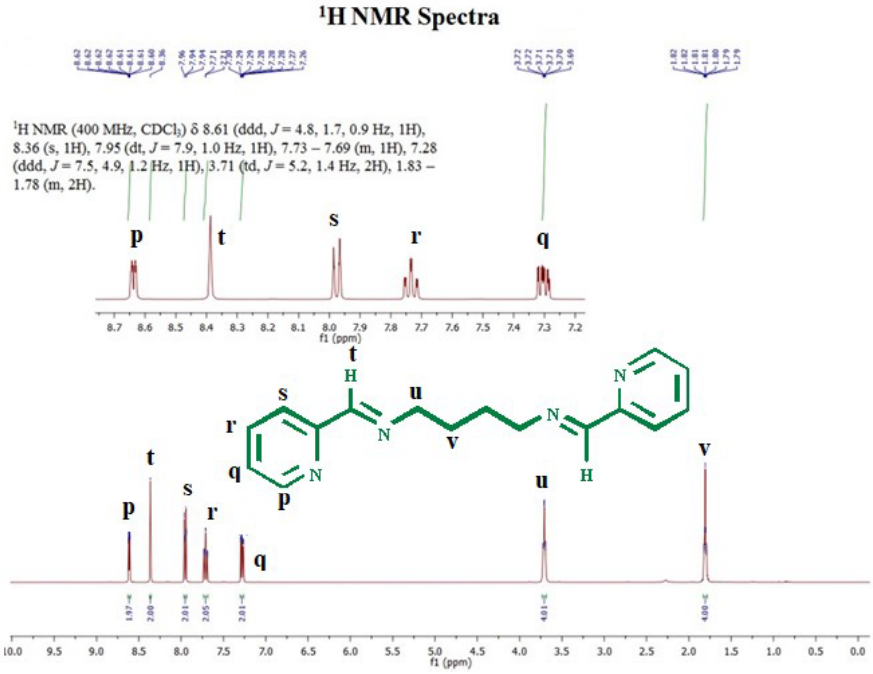

Figure A-62: ^{1}H NMR spectra of **L3c**

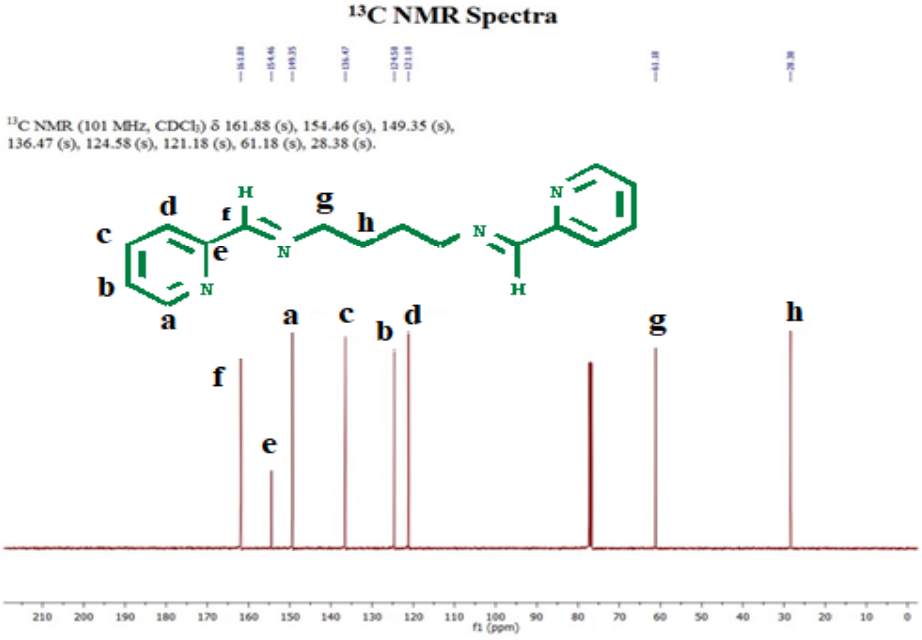

Figure A-63: ^{13}C NMR spectra of **L3c**

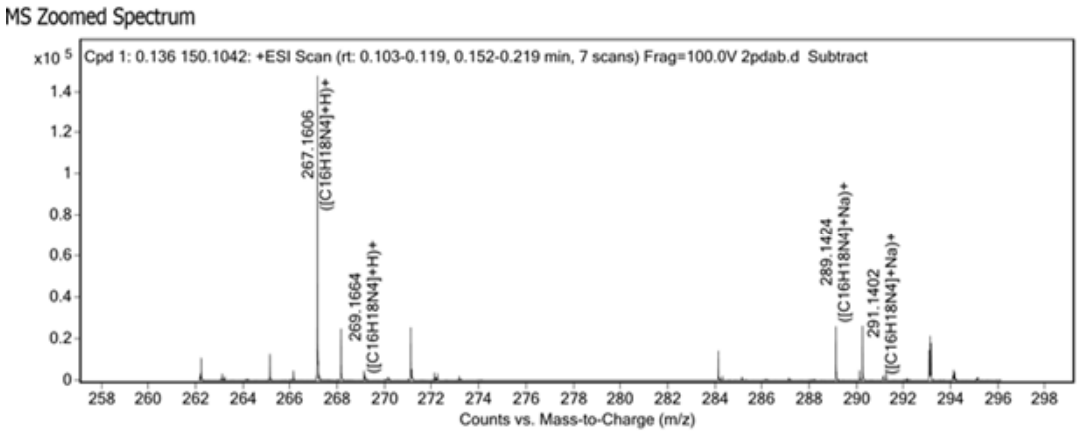

Figure A-64: Mass spectra of **L3c**

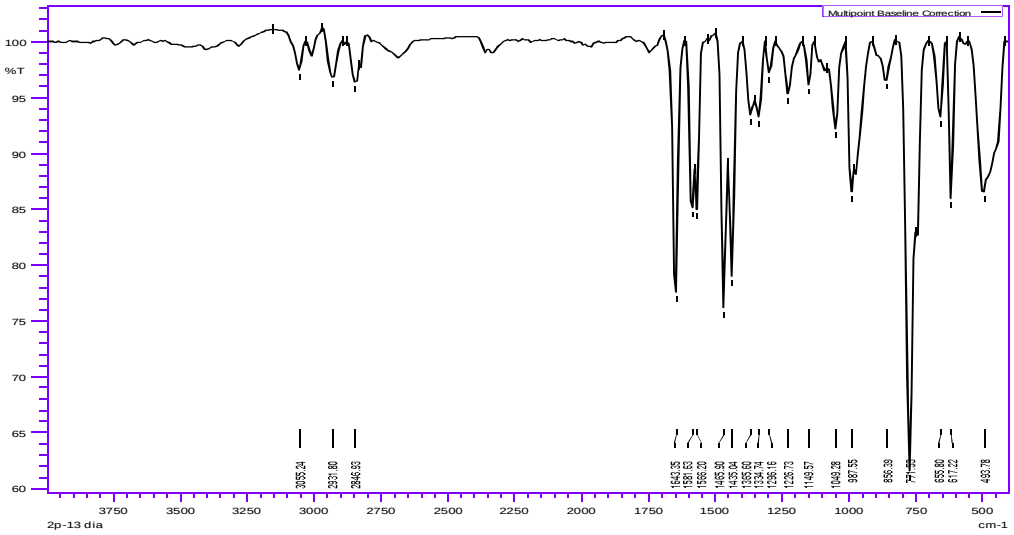

Figure A-65: IR spectra of **L2′c**

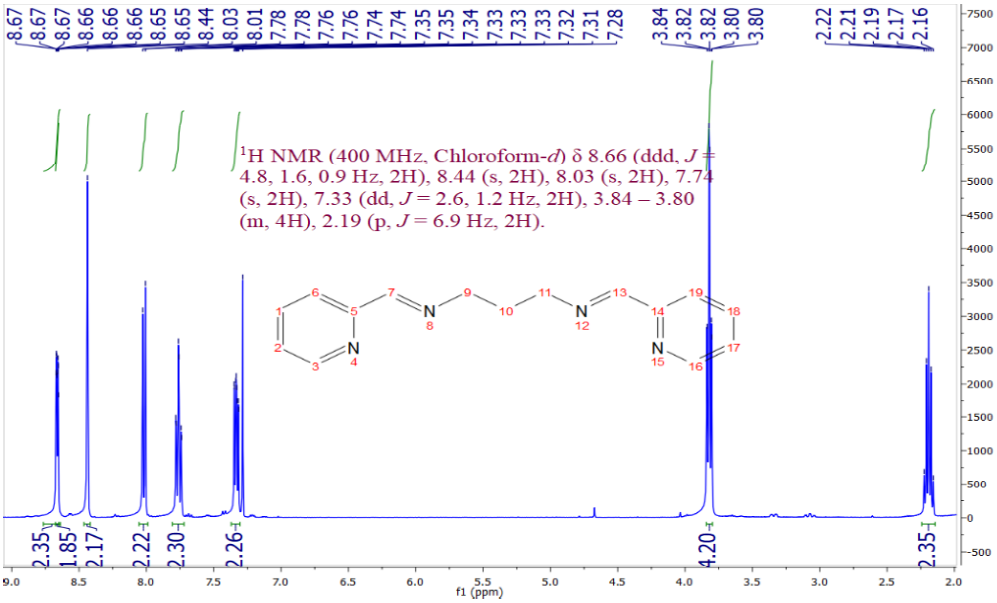

Figure A-66: ^{1}H NMR spectra of **L2′c**

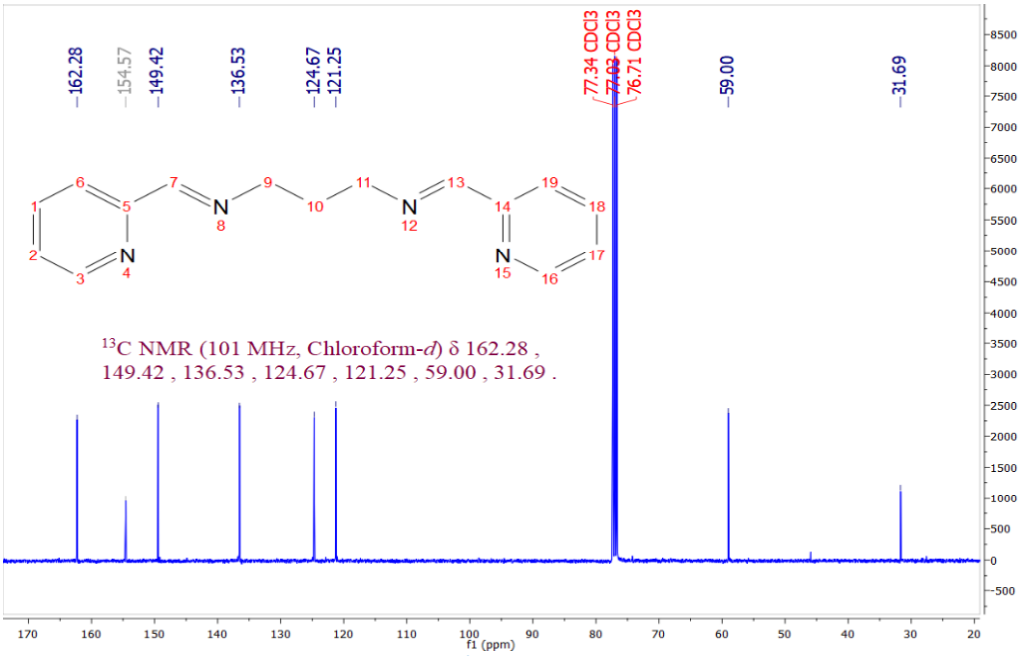

Figure A-67: ^{13}C NMR spectra of **L2′c**

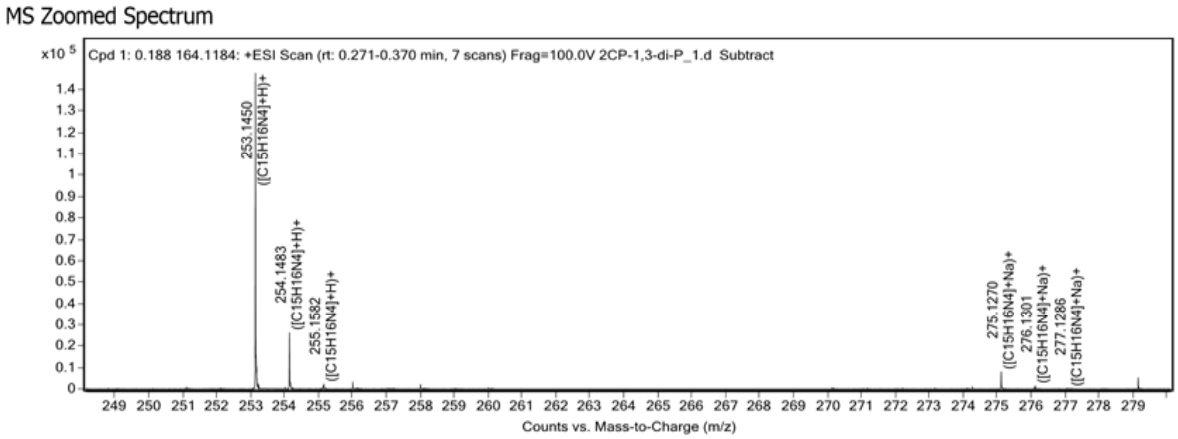

Figure A-68: Mass spectra of **L2′c**

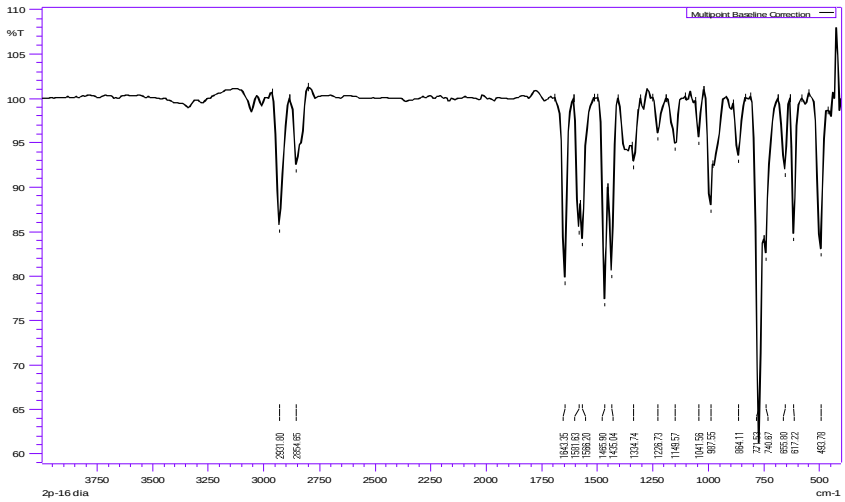

Figure A-69: IR spectra of **L4c**

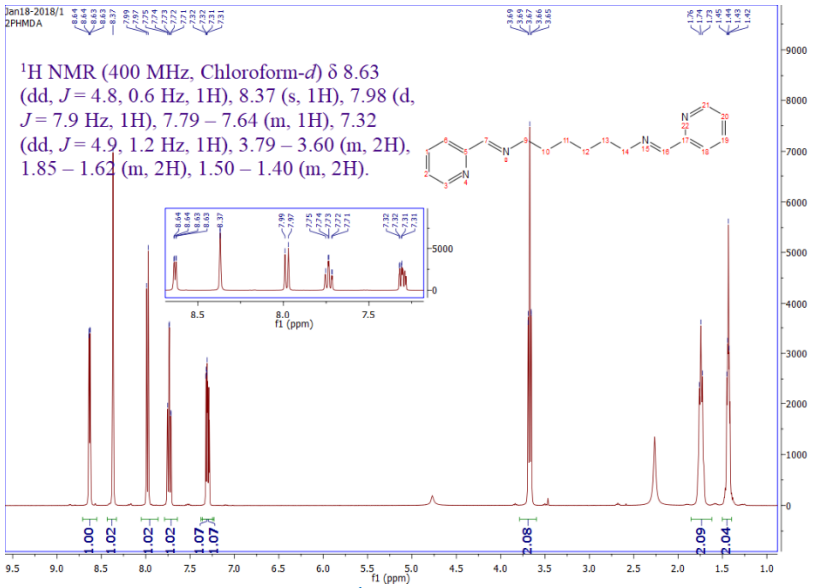

Figure A-70: ^{1}H NMR spectra of **L4c**

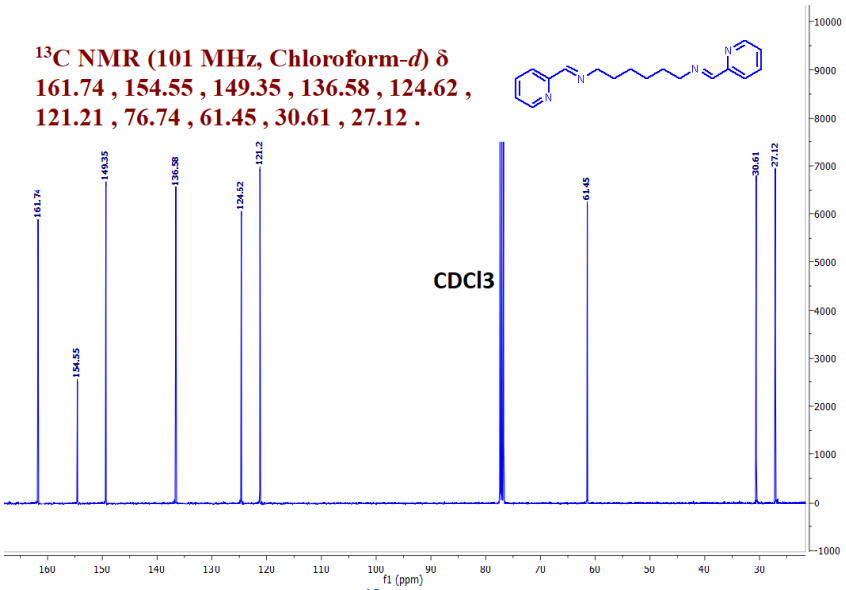

Figure A-71: ^{13}C NMR spectra of **L4c**

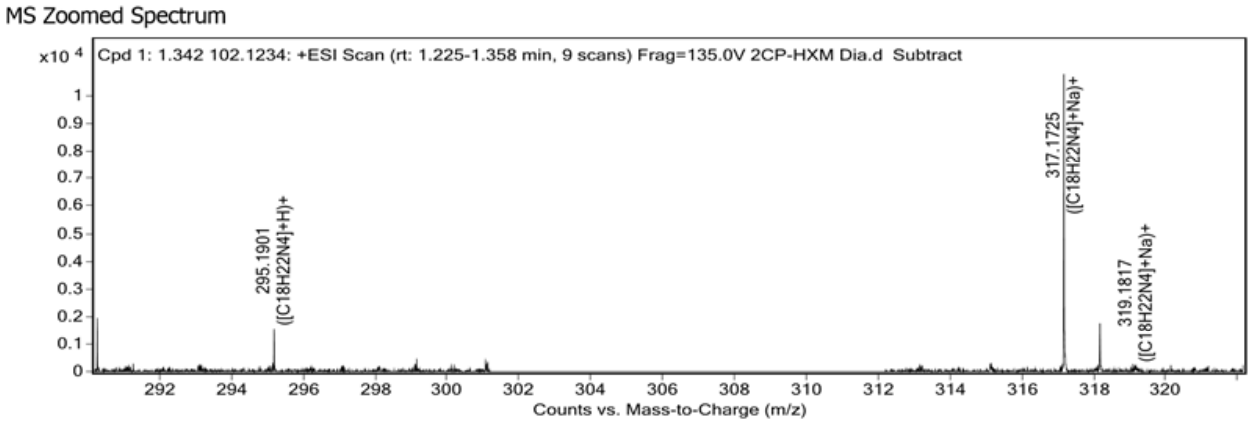

Figure A-72: Mass spectra of **L4c**

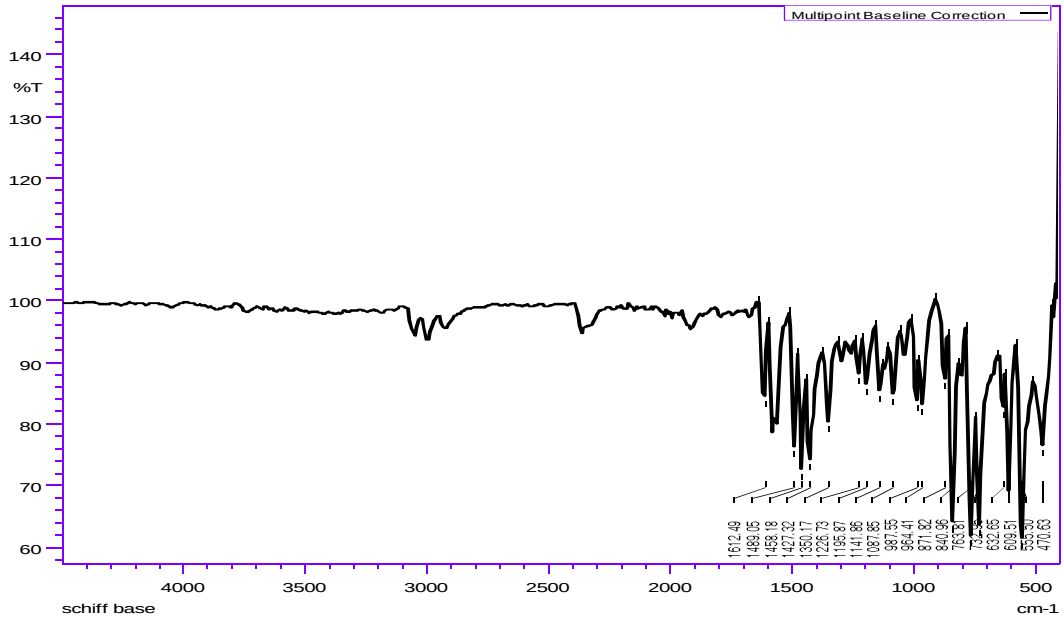

Figure A-73: IR spectra of **L13c**

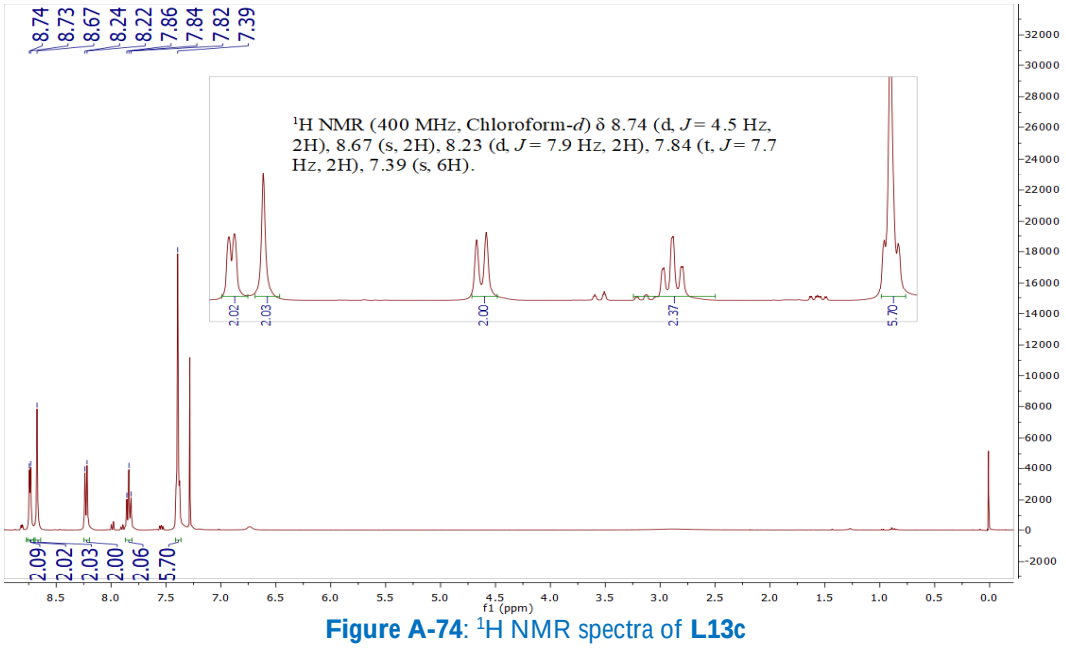

Figure A-74: ^{1}H NMR spectra of **L13c**

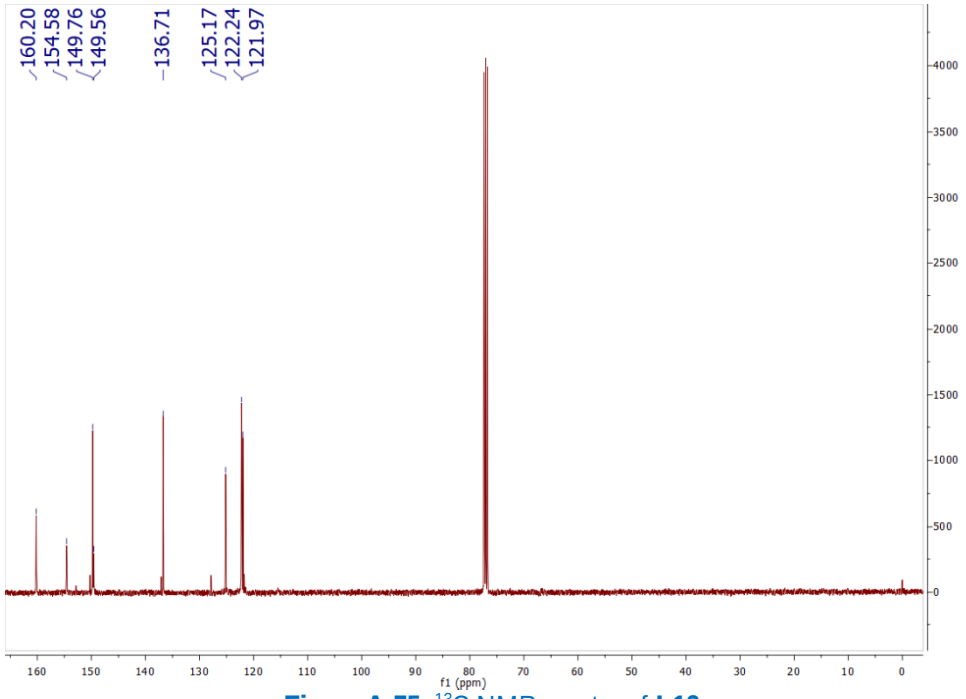

Figure A-75: ^{13}C NMR spectra of **L13c**

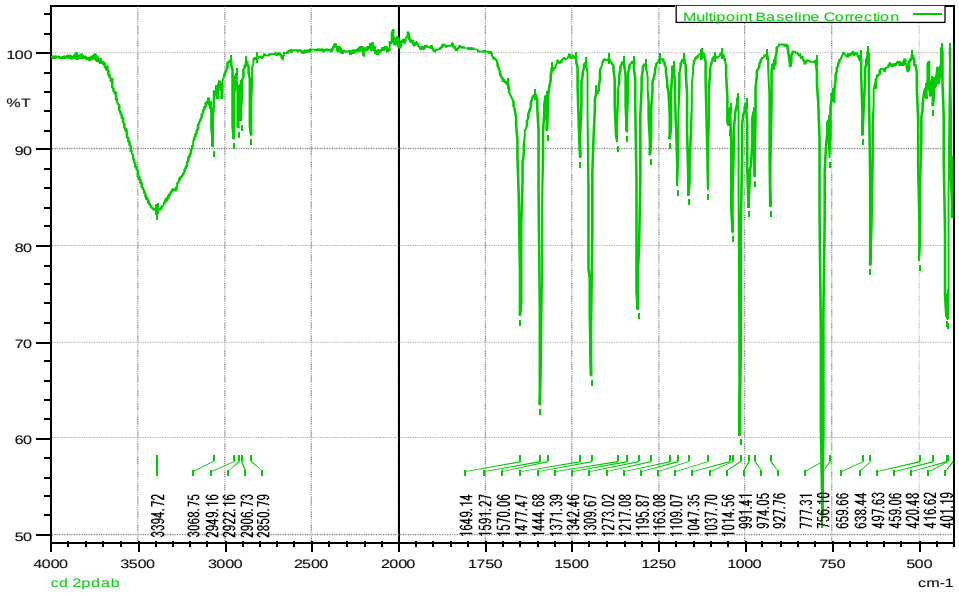

Figure A-76: IR spectra of 1:1 ratio of Cd^{2+} and **L3c**

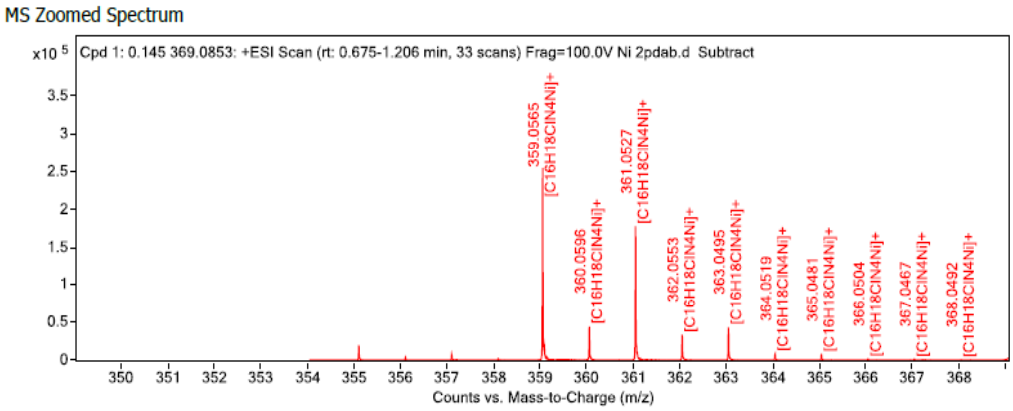

Figure A-77: Mass spectr aof **Cd(II)-L3c**

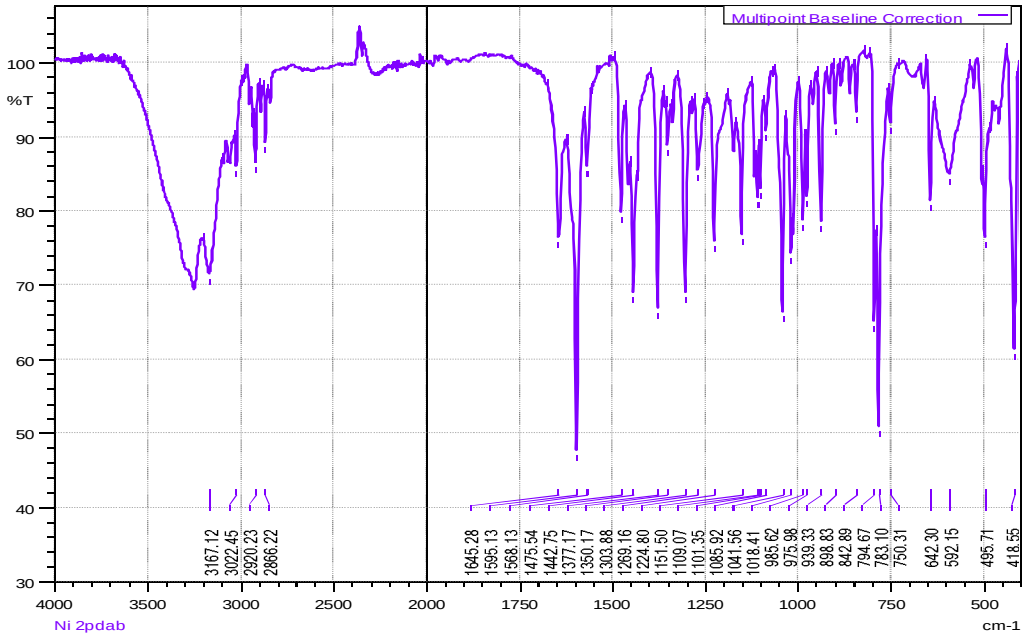

Figure A-78: IR spectrum of 1:1 ratio of Ni^{2+} and **L3c**

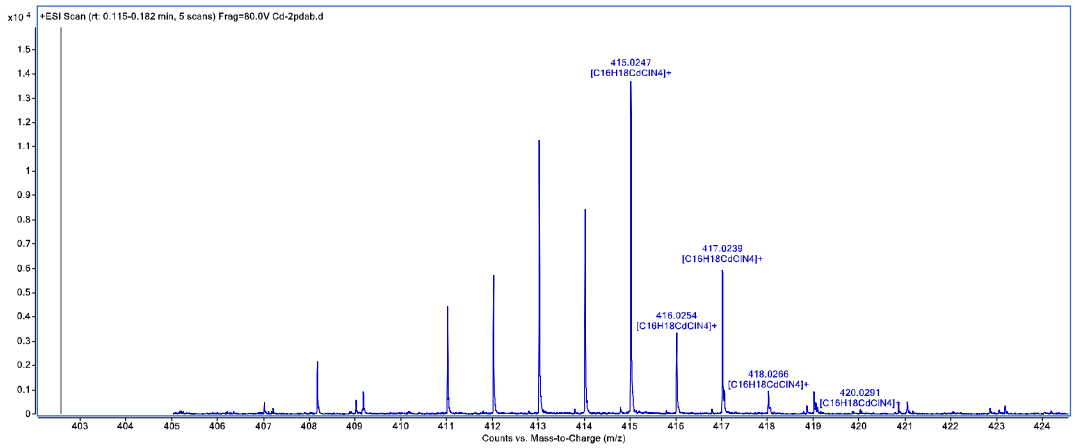

Figure A-79: Mass spectra of 1:1 ratio of Ni^{2+} and **L3c**

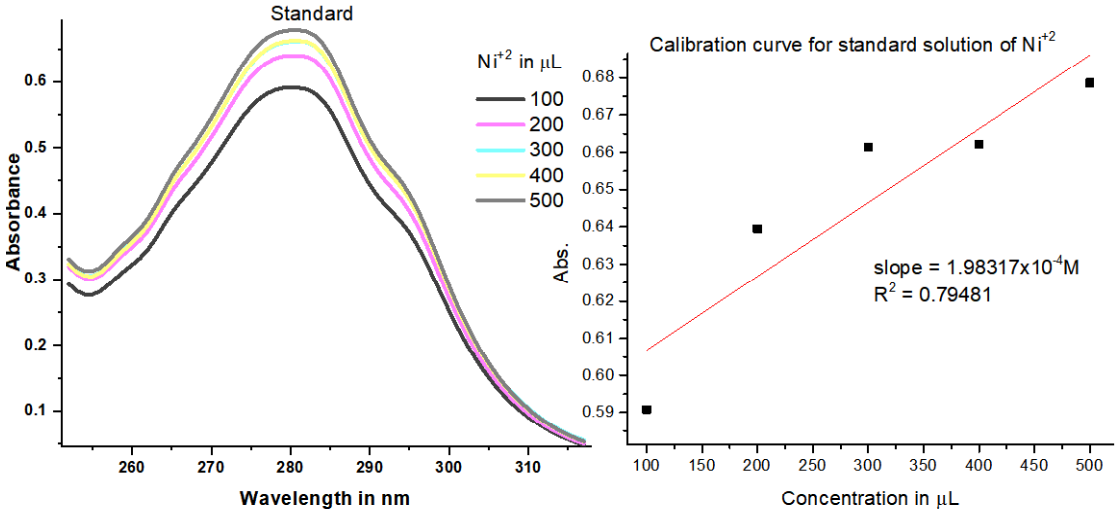

Figure A-80: The curve of different concentration of standard Ni^{+2} solution with sensor **L3c** and their linear calibration plot

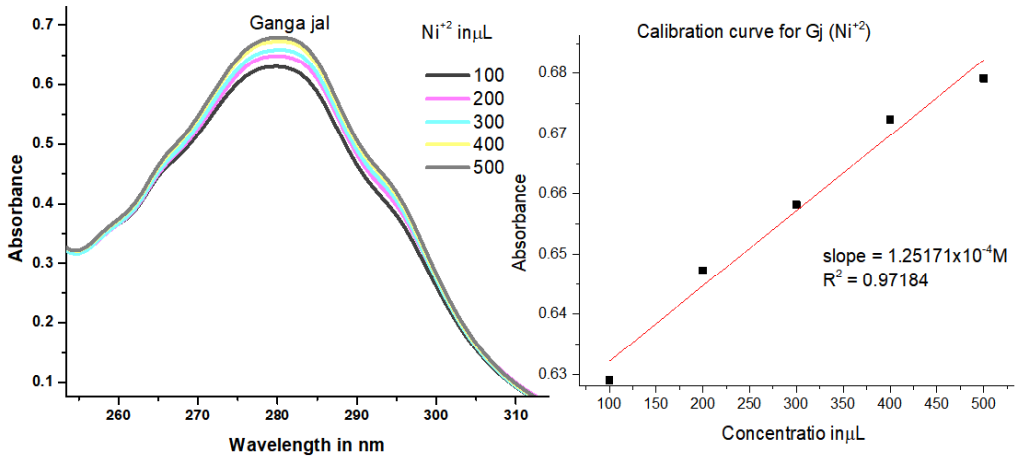

Figure A-81: The curve of different concentration of metal ion spiked into Ni(II) solution and their linear calibration plot

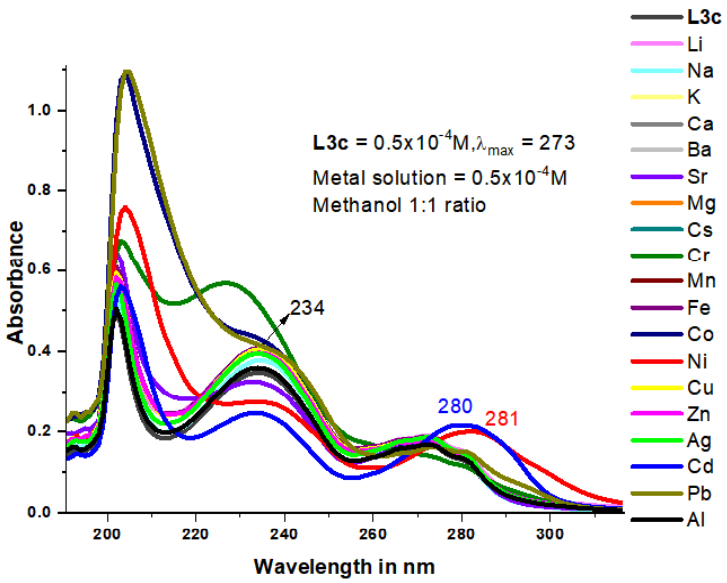

Figure A-82: UV-Visible spectra of **L3c** and different metal ions in 1:1 ratio

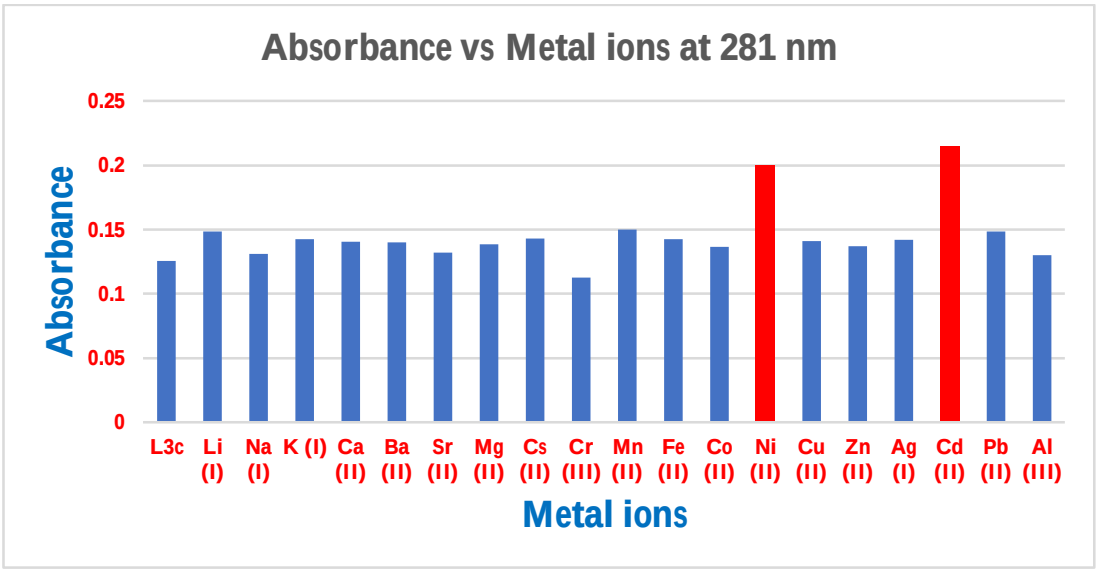

Figure A-83: Absorbance vs metal ions profile shows the comparison of absorbance

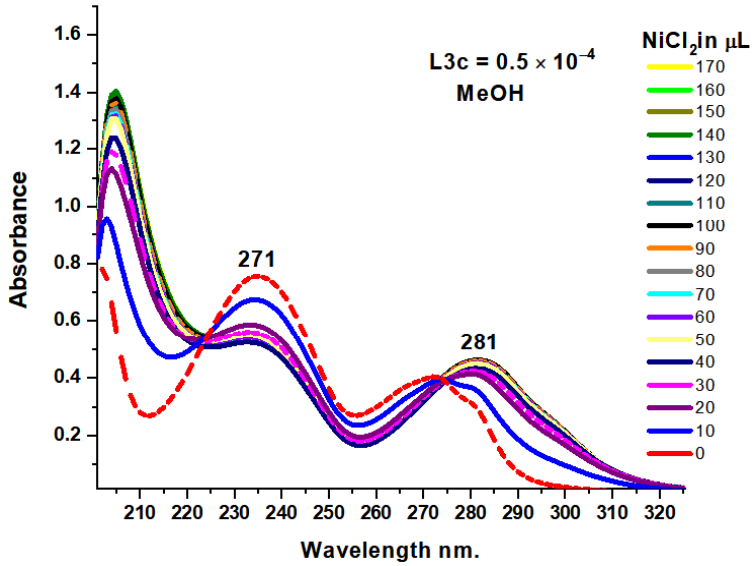

Figure A-84: UV-Visible absorption spectra of 1mL of 0.5x10^{-4} M **L3c** on adding different volume (10-170µL) of 10^{-3}M of Ni(II) of solution (Total solution volume = 2mL)

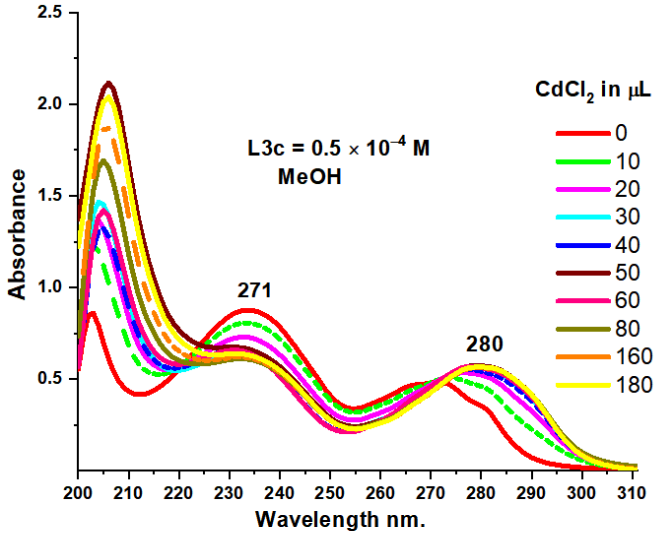

Figure A-85: UV-Visible absorption spectra of 1mL of 0.5×10^{-4} M **L3c** on adding different volume of 10^{-3}M of Cd(II) of solution (Total solution volume = 2mL)

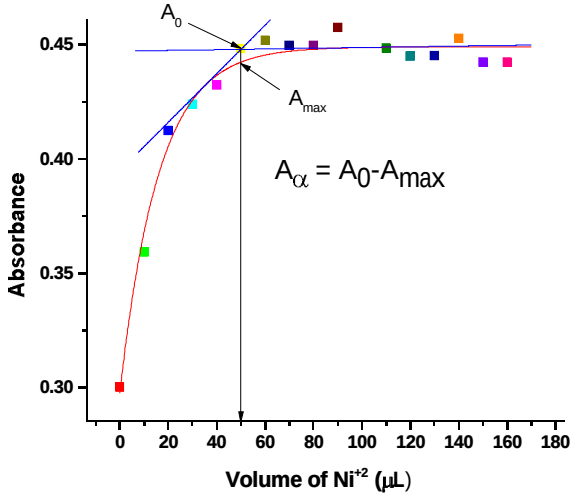

Figure A-86: First order non-linear exponential grow 1 fit with tangent for $NiCl_2$

Table A-4: Determination of Binding Constant of Ni^{2+} and **L3c** (From Figure A-86)

$$MmLn \leftrightarrow mM + nL$$

C	0	0	Initial concentration
$(1-\alpha)C$	$m\alpha C$	$n\alpha C$	Equilibrium concentration

$$K = \frac{(1-\alpha)C}{m(\alpha C)^m (n\alpha C)^n} \quad (1)$$

$$A_\alpha = A_0 - A_{max} \quad (2)$$

$$A_\alpha = 0.4482 - 0.4419$$

$$A_\alpha = 0.0063$$

$$A_\alpha = \epsilon . b(\alpha C) \quad (3)$$

$$\alpha = \frac{A_\alpha}{\epsilon b C} \quad (4)$$

$$\alpha = \frac{0.0063}{0.3304 \times 10^4 \times 1cm \times 10^{-4}}$$

$$\alpha = 0.0191$$

$$K = \frac{(1 - 0.0191) \times 10^{-4}}{(0.0191 \times 10^{-4})(0.0191 \times 10^{-4})}$$

$$K = 26.88 \times 10^6 \, M^{-1}$$

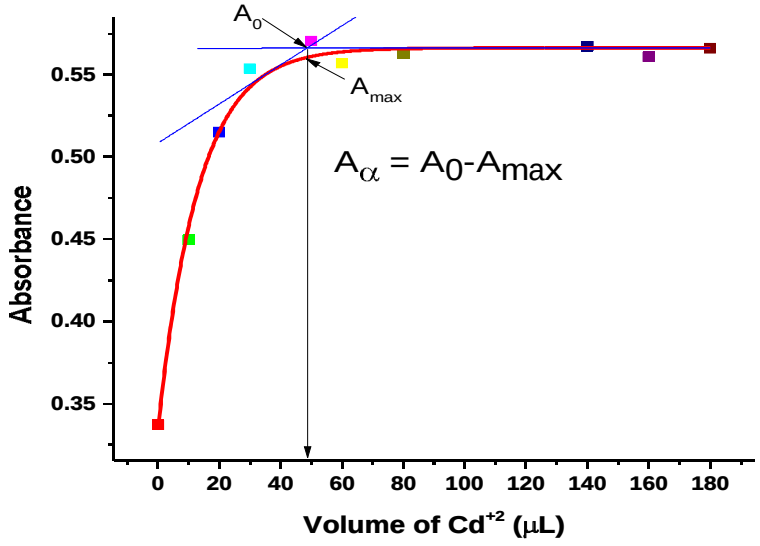

Figure A-87: First order non-linear exponential grow 1 fit with tangent for $CdCl_2$

Table A-5: Binding constant of **Cd(II)-L3c** from figure A-87

$$\alpha = \frac{0.0255}{0.5413 \times 10^4 \times 1cm \times 10^{-4}}$$

$$\alpha = 0.0471$$

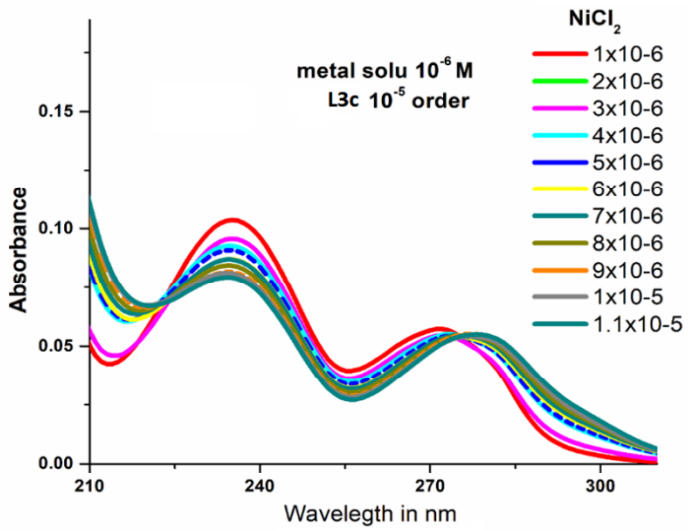

Figure A-88: Absorbance vs wavelength plot of **L3c** (1×10^{-5} M) with Ni^{+2}

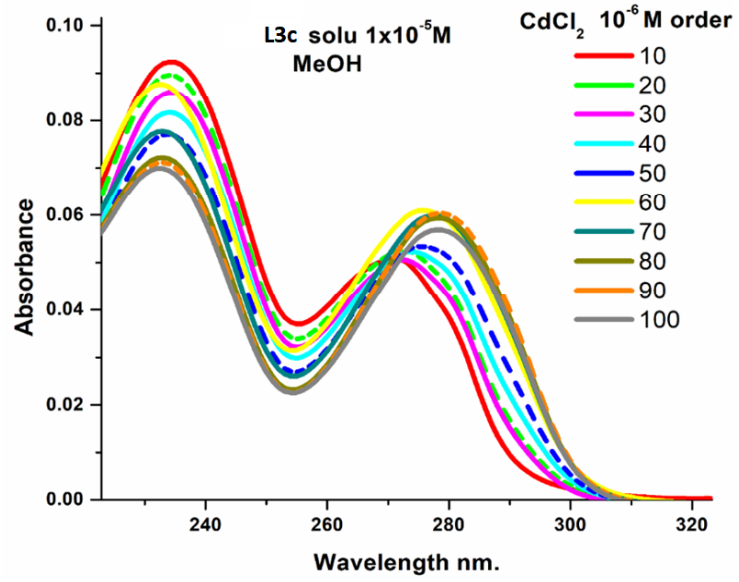

Figure A-89: Absorbance vs wavelength plot of **L3c** (1×10^{-5} M) with Cd^{+2}

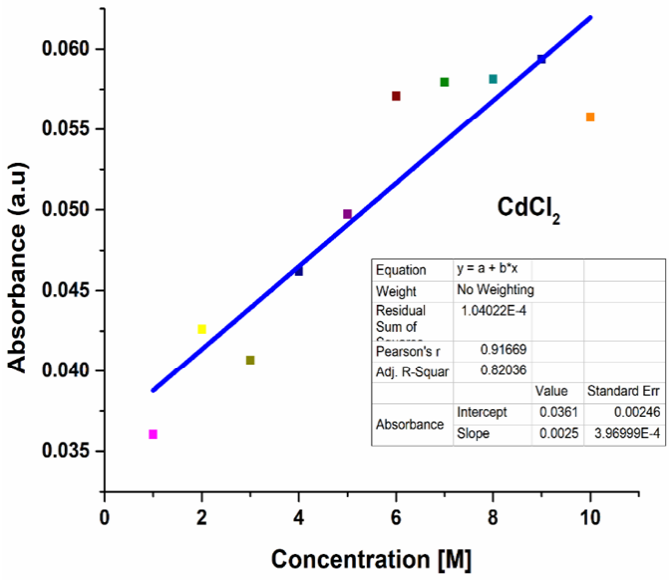

Figure A-90: Linear fit of absorbance vs concentration plot of **L3c** (1×10^{-5} M) with Cd^{+2}.

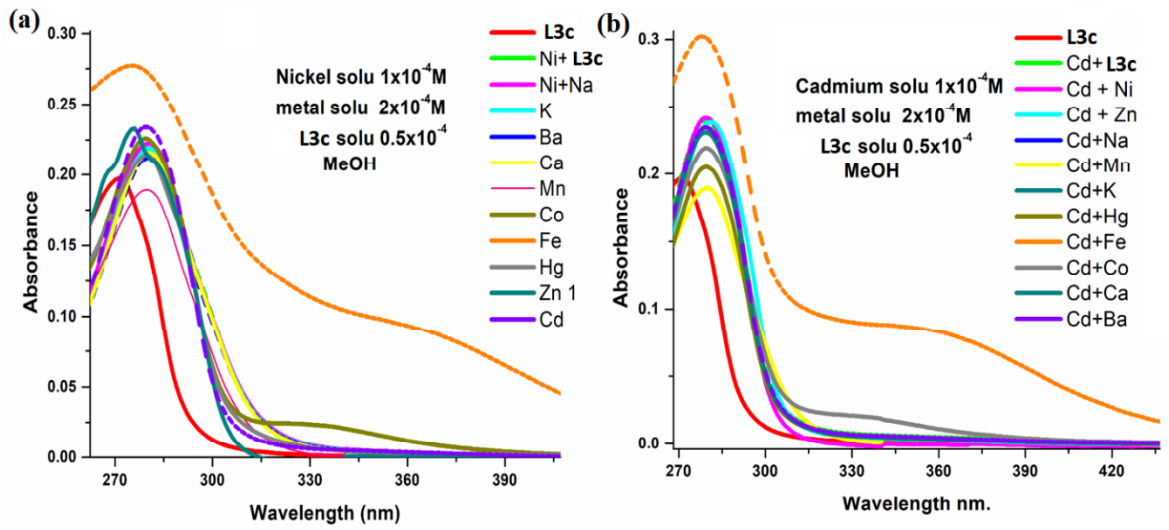

Figure A-91: (a) Selectivity of **L3c** towards Ni^{2+} in presence of other metal ions, (b) Selectivity of **L3c** towards Cd^{2+} in presence of other metal ions

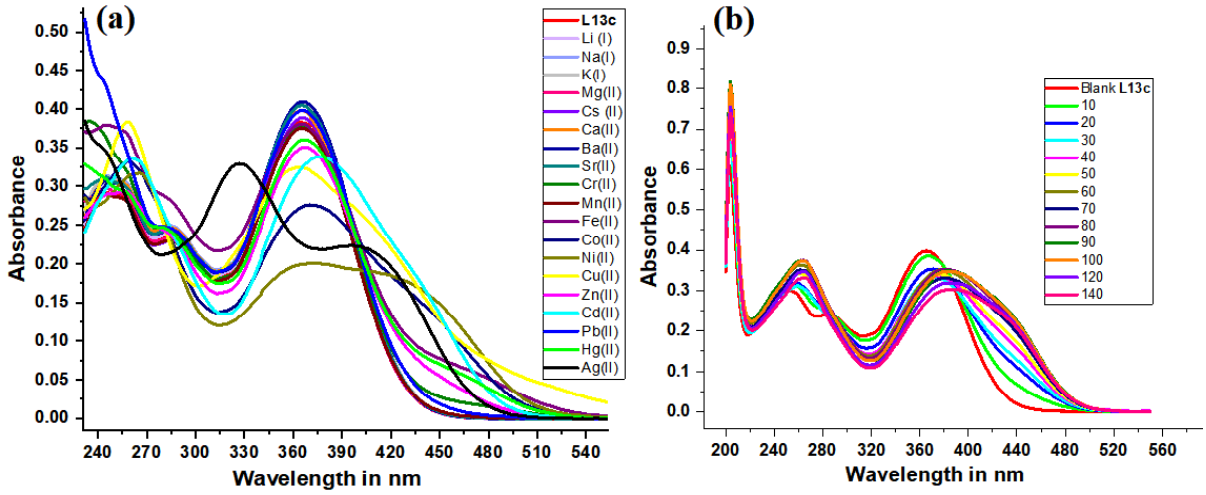

Figure A-92: (a)UV-Visible absorption spectra of **L13c** with different metal ions, (b) the binding ratio **L13c** is 2:1 (Metal:Ligand), (**L13c** = 50µL, Cd^{+2} = 100µL), (observed maximum red shift at 100 µL)

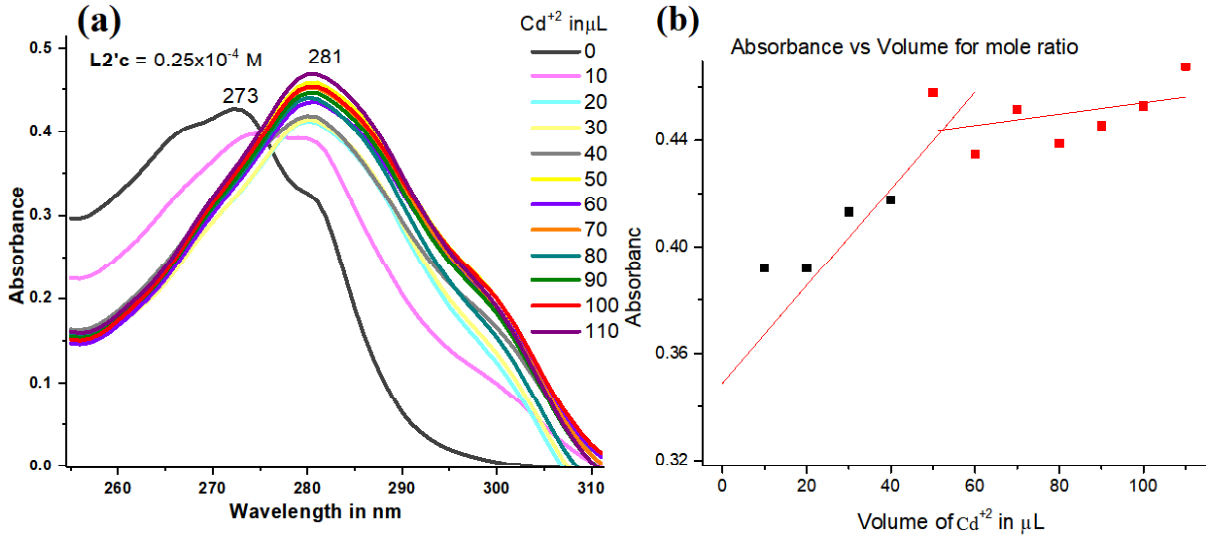

Figure A-93: Using mole ratio method, UV-Visible titration of **L2′c** with Cd(II) ions in 1:1 ratio (**L2′c** = 50µL, Cd^{+2} = 50µL)

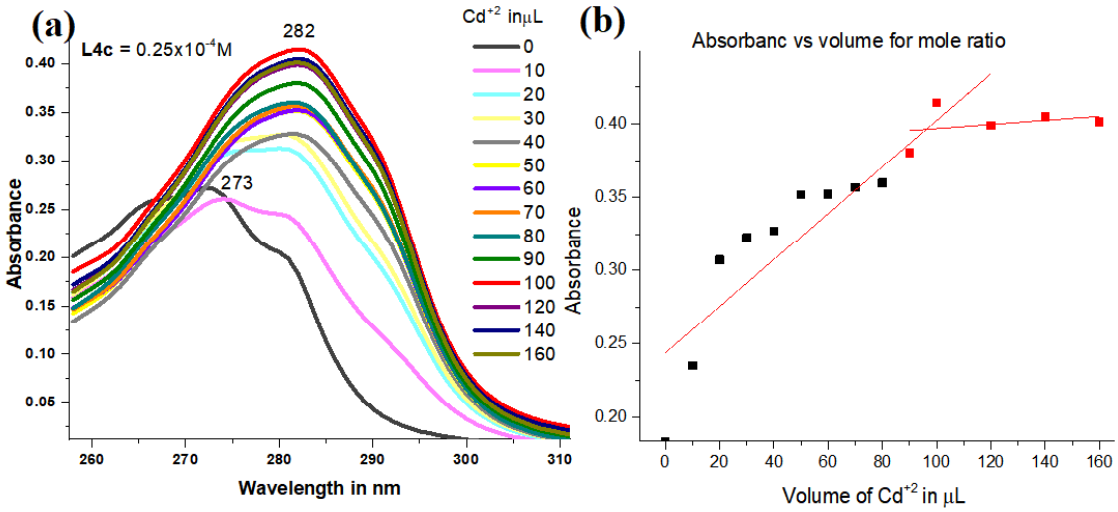

Figure A-94: Using mole ratio method, UV-Visible titration of **L4c** with Cd(II) ions in 1:2 ratio (L4c = 50μL, Cd^{+2} = 100μL

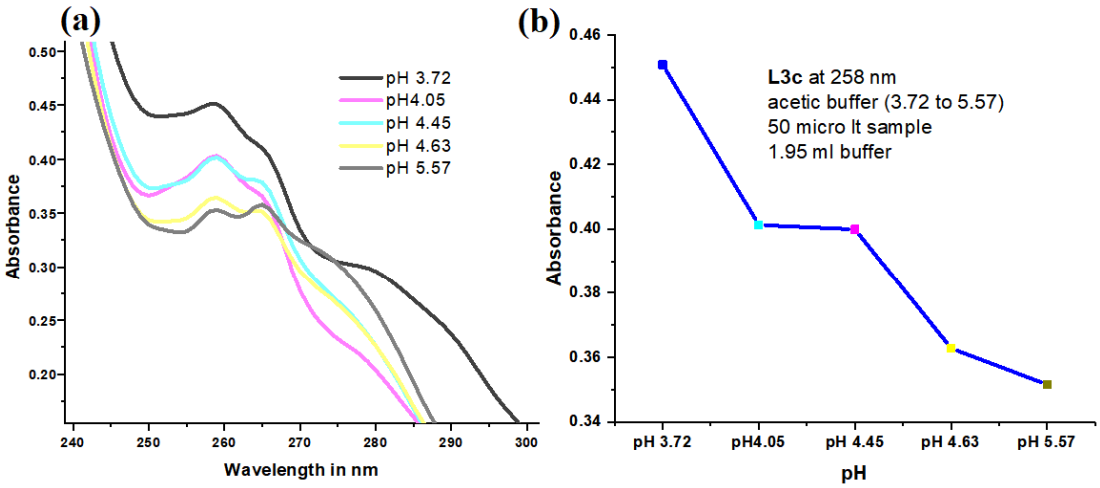

Figure A-95: The pH study of **L3**c

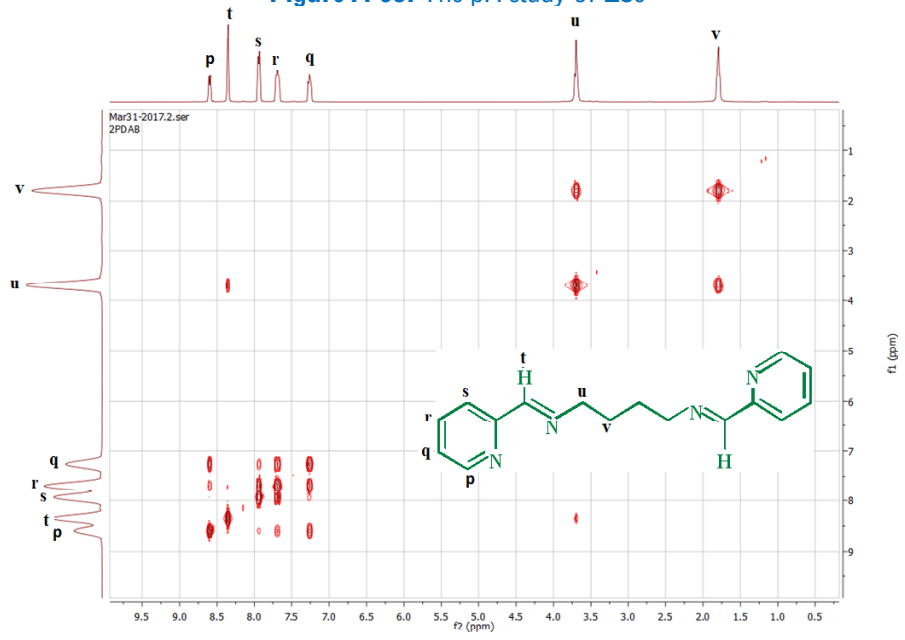

Figure A-96: COSY of **L3c**

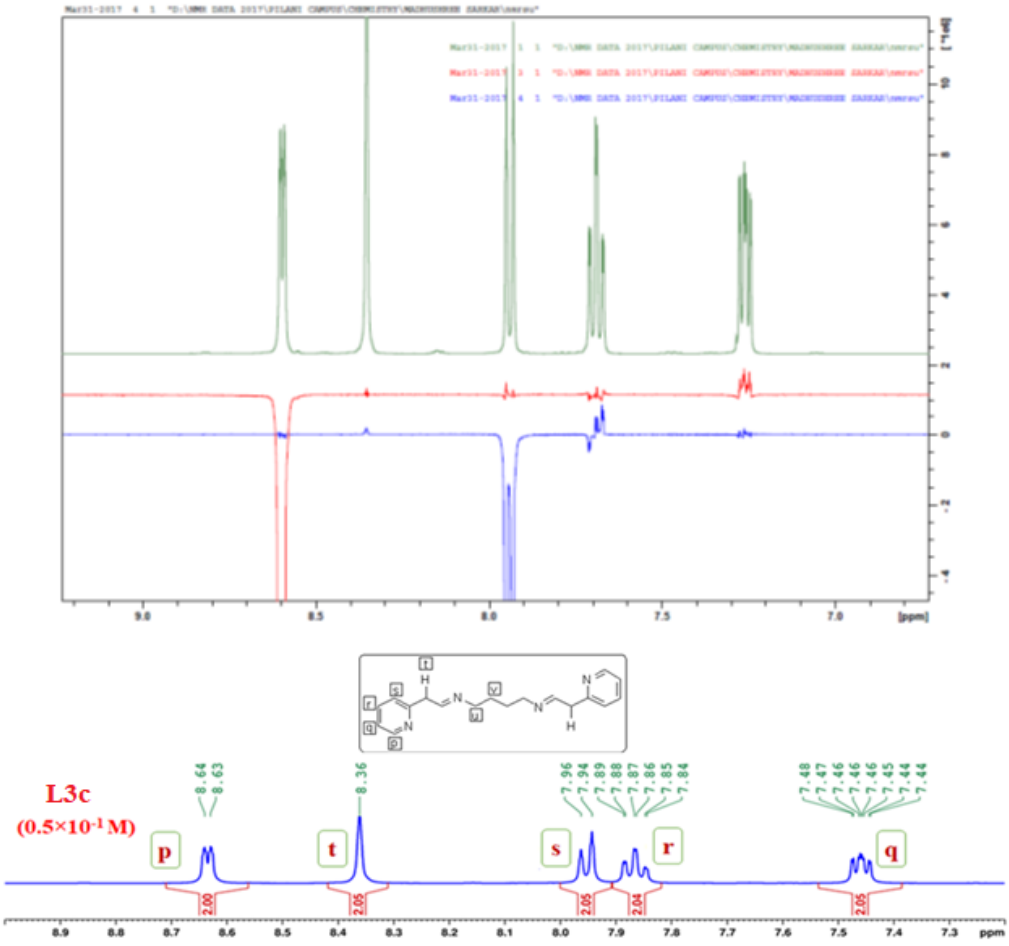

Figure A-97: NOE of **L3c**, irradiated (p) proton and (r) proton (Please refer the ^{1}H-NMR below)

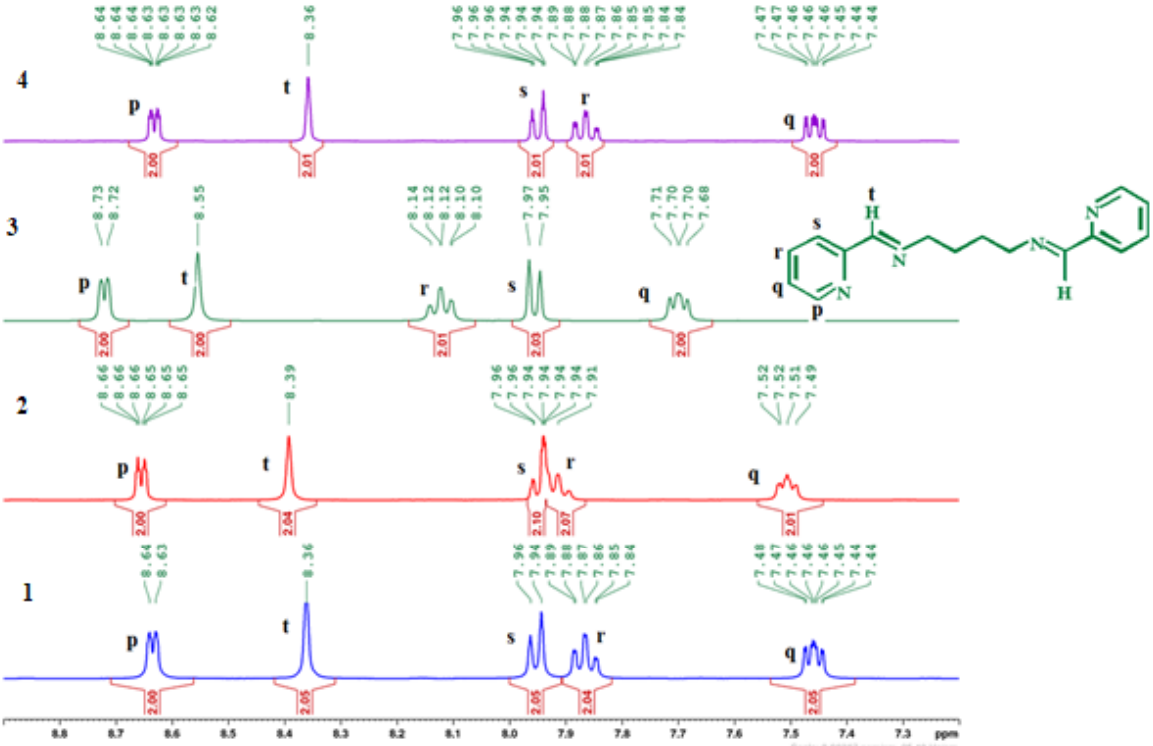

Figure A-98: ^{1}H-NMR of (1) 0.5×10^{-1} M of **L3c** with (2) 0.08×10^{-1} M of $CaCl_2$ (3) 0.5×10^{-1} M $CaCl_2$ at t = 0 hours and (4) at t = 24 hours 0.5×10^{-1} M of $CaCl_2$

Table A-6: Comparison of **L3c** as Ni^{2+} sensor with various other Ni^{2+} sensors reported in Literature

Ni^{+2} Sensor	Binding Constant	Detection limit	Metal Interference	Ref.
Schiff base	$26.88 \times 6\ M^{-1}$	3.08μM	Fe^{+2}	**Our work**
Chalcone based	$1.91 \times 10^5 M^{-2}$	$5.14\mu M$	Ce^{+3} Fe^{+2}	[1]
Schiff base Cinnamaldehyde	$1.29 \times 10^5 M^{-1}$	$1 \times 10^{-7} M$		[2]
Quinoxaline	$1.26 \times 10^5 M^{-1}$	$4.16\mu M$	Co^{+2}	[3]
Quinoxaline	$2.5 \times 10^5 M^{-1}$	$1.47\mu M$	Co^{+2} Fe^{+2}	[4]
Coumarine Schiff base	$2.9 \times 10^4 M^{-1}$			[5]
Coumarine Schiff base	$2.343 \times 10^4 M^{-1}$	$as\ low\ as\ 0.5\mu M$	Hg^{+2} Cu^{+2}	[6]
Perylene tetracarboxylic diimide	$2.7 \times 10^9 M^{-2}$		Zn^{+2} Co^{+2}	[7]
Calix[4]arene	$log\beta = 4.92\ (\pm 0.05)$			[8]
Fluorescent sensor	$193 \pm 5\mu M$	Ca.25 fold		[9]
Benzothiadiazoyl triazoyl	$2.88 \times 10^7 M^{-1}$		Hg^{+2} Cu^{+2} Co^{+2}	[10]
Dipyrrolyl	$11 \times 10^5 K/M^{-1}$			[11]
2-(5-bromo-2-pyridylazo)-5-(diethylamino)phenol		$0.3\mu g\ mL^{-1}$		[12]

Table A-7: Comparison of **L3c** as Cd^{2+} sensor with various other Cd^{2+} sensors reported in Literature

Cd^{+2} Sensor	Binding Constant	Detection limit	Metal Interference	Ref.
Schiff base	$4.29 \times 10^6 M^{-1}$	$1.4688\mu M$	Fe^{+2}	**Our work**
Ferrocenyl Schiff base	$(7.49 \pm 0.18) \times 10^5 M^{-1}$	$0.94\mu M$	Zn^{+2}	[13]
Azo Schiff base	$4.73 \times 10^3 ML^{-1}$	$1.03 \times 10^{-6} ML^{-1}$		[14]
Ferrocene derivative	$log\beta = 4.03$			[15]
Coumarin amide Dipicolylamine	$logK = 15.12$	as regular		[16]
Schiff base of Phenithaizine	$2.6 \times 10^8 L/mol$	$1\mu M/L$	Co^{+2}	[17]
Schiff base		$0.3\ ng\ ML^{-1}$	Hg^{+2}, Cd^{+2}	[18]
Fluorescent sensor	$log\beta = 4.25$		Zn^{+2}	[19]
Quinoxaline	$3.7 \times 10^4 M^{-1}$			[20]
Naphthyridine	$0.75 \times 10^5 M^{-1}$			[21]
Schiff base ionophore		$5 \times 10^{-8} M$		[22]

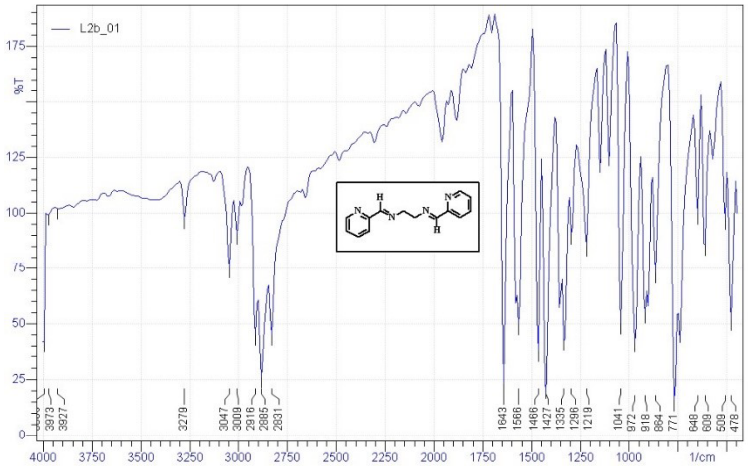

Figure A-99: IR Spectra of **L2c**: (cm^{-1} KBr pellet): 3047(s), 3009(w), 2916(s), 2885(vs), 2831(s), 1643(vs), 1566(vs), 1466(vs), 1427(vs), 1335(vs), 1296(s), 1219(s), 1041(vs), 972(vs), 918(vs), 864(vs), 771(vs).

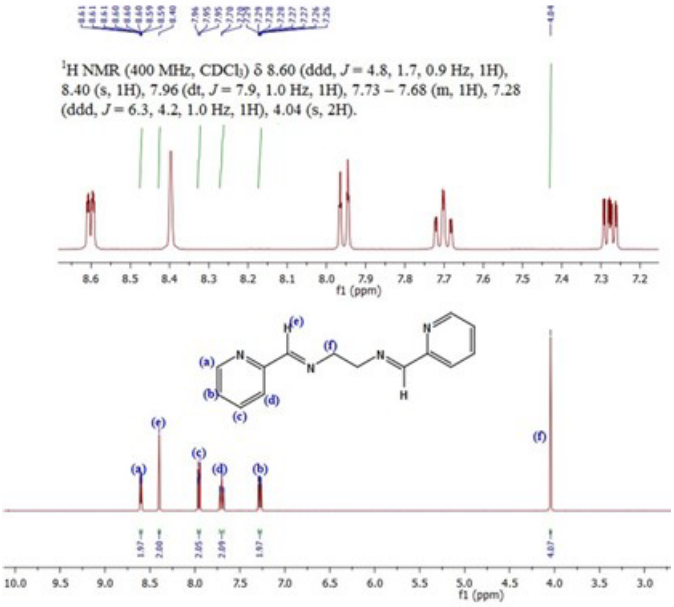

Figure A-100: ^{1}H NMR spectra of **L2c**

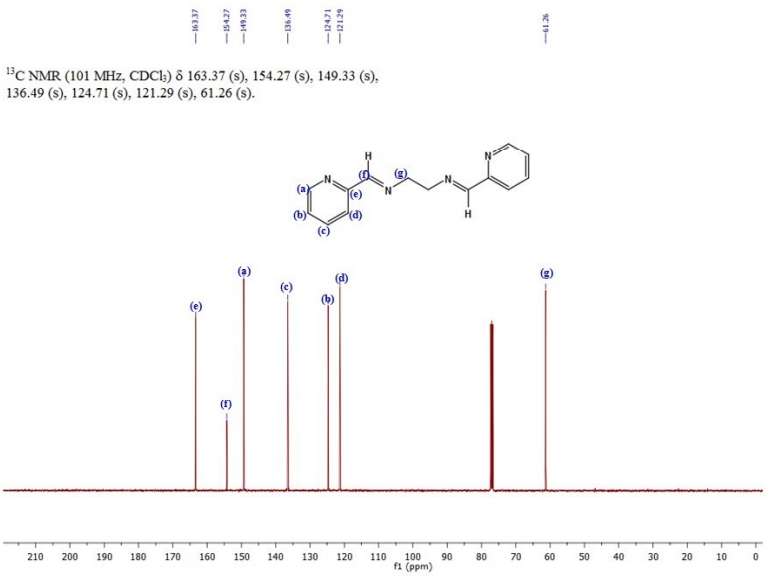

Figure A-101: ^{13C} NMR spectra of **L2c**

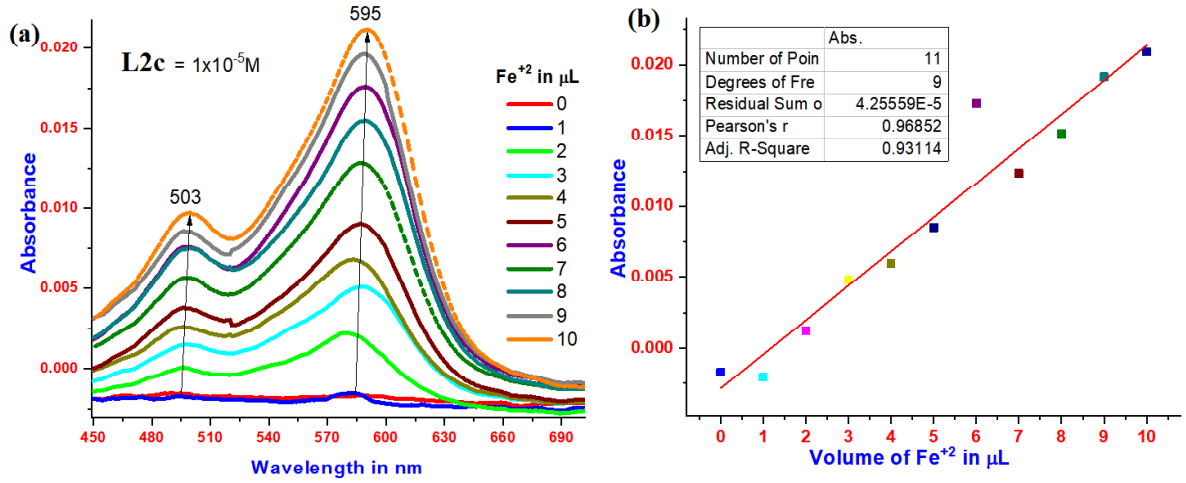

Figure A-102: (a) Titration UV-Visible spectra of Fe^{+2} with **L2c** and (b) Linear fit of Absorbance (~595nm) *Vs* Concentration of Fe (II) in 1×10^{-5} M of **L2c**

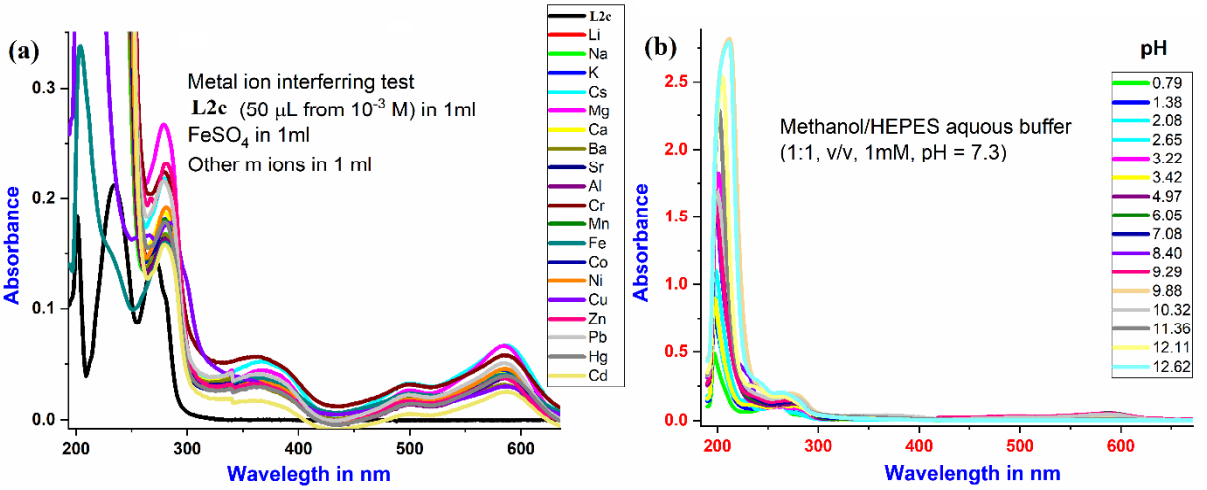

Figure A-103: (a) UV-Visible spectra for interfering metal ion test, (b) UV-Visible spectra of pH study

Table A-8: Theoretical Data Table

Complex	HOMO (Hartees)	HOMO (eV)	LUMO (Hartees)	LUMO (eV)	Eg (eV)
Fe-**L2c**6	-0.47602	-12.953163	-0.61936	-16.85364278	3.8923
Fe- **L2c**7	-0.46737	-12.71778453	-0.60052	-16.3409803	3.6232
Fe- **L2c**10	-0.46746	-12.72023355	-0.60109	-16.35649079	3.6362
Fe- **L2c**12	-0.48083	-13.08404975	-0.62573	-17.02697929	3.9429
L2c2	-0.06258	-1.702888409	-0.24999	-6.802573879	5.09968
L2c2ccdc2	-0.06573	-1.788604268	-0.25714	-6.997135274	5.2085
L2c2ccdc2ml	-0.07207	-1.961124443	-0.26251	-7.143260406	5.1821
L2cccdc2ml UV again	-0.08234	-2.240585356	-0.24810	-6.75114436	4.5105

Table A-8a: Comparison with other reported sensors							
Receptor	**Ions**	**Type of sensor**	**Limit of detection**	**Binding constant *(K)***	**Interfering Metal ions/Journal**	**Year**	**Ref.**
1)Phenonthroimidazole-Coumarine S.B	Fe^{+3}	Turn off Fluorescence	4.28 μM 0.83 μM	1.52×10^5 M^{-1} 7.69×10^4 M^{-1}	Tetrahedran letters	2016	Qigang Deng
2)Rhodamine Based S.B	Fe^{+3} Zn^{+2}, Cu^{+2}	Fluorescence (Naked eye)	0.08 μM		Spectrochimica Acta Part A: Molecular and Biomolecular Spectroscopy	2016	Liang Ni, Juan Han
3)Pyrene SB	Fe^{+3}, Fe^{+2} F^-	Fluorescence	Fe^{+2} 0.3 ppm		Journal of FLuorescence	2016	An-Tai Wu
4) Anionic mesoporous silica nano particles S.B	Fe^{+3}	Fluorescence			Dalton	2016	Fangyuan Gai and Farid Akhta
5) 2,3-dihydroxybenzaldehyde S.B	Fe^{+3}	Colorimetric	0.19 μM		Sensors and Acuutators B Chemical	2015	Cheal Kim
6) Salen type S.B	Mn+2, Fe+2, Zn+2	Colorimetric/ Fluorescence			Spectrochimica Acta Part A: Molecular and Biomolecular Spectroscopy	2015	Philip Anthony
7)Rhodamine S.B	Cu(II) Al(III) Fe(III)	Fluorometric	Fe (III) 1.9×10^{-8}M		Sensors and Acuutators B Chemical	2015	Vinod Kumar Gupta
8)Silica cross-linked nanoparticles encapsulating a phenothiazine-derived S.B	Fe^{+3}	Luminoscent chemosensor			Journal of Materials Chemistry B	2014	Qisheng Huo
9) Juloidine Imidazole S.B	Zn and Al FeII FeIII	Fluorescence Fluorescence Colorimetric Colorimetric	FeII 7.4 μM FeIII 6.8 μM	FeII 3.3×10^5 FeIII 3.3×10	Sensors and Acuutators B Chemical	2014	Cheal Kim
10) Schiff base	Fe^{+2}	Colo/Fluo-chemosensor	7.4 μM		Fe^{+3},Al^{+3}, Zn^{+2}	2014	7
11) Schiff base	Fe^{+2}	Fluorescent	3 ppm	$3.04 \times 10^9 M^{-1}$	F^- and Fe^{+3}	2016	3

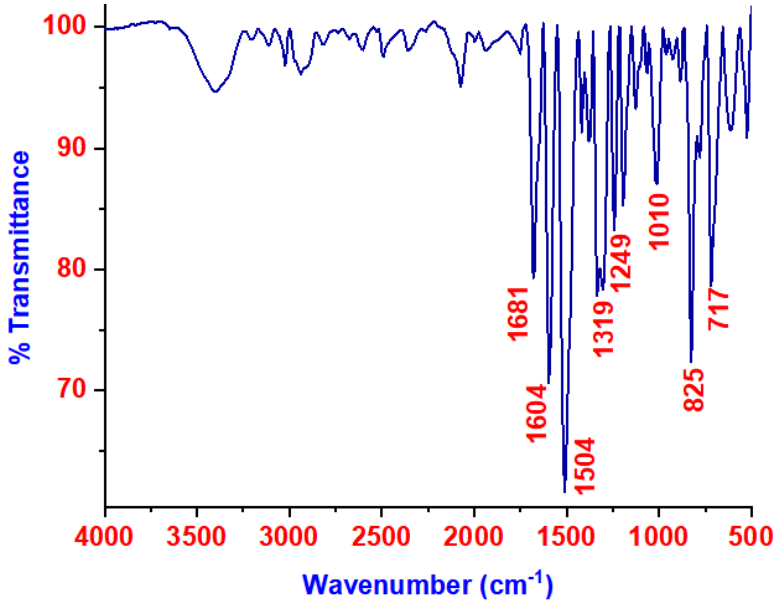

Figure A-104: IR spectra of **L15b**

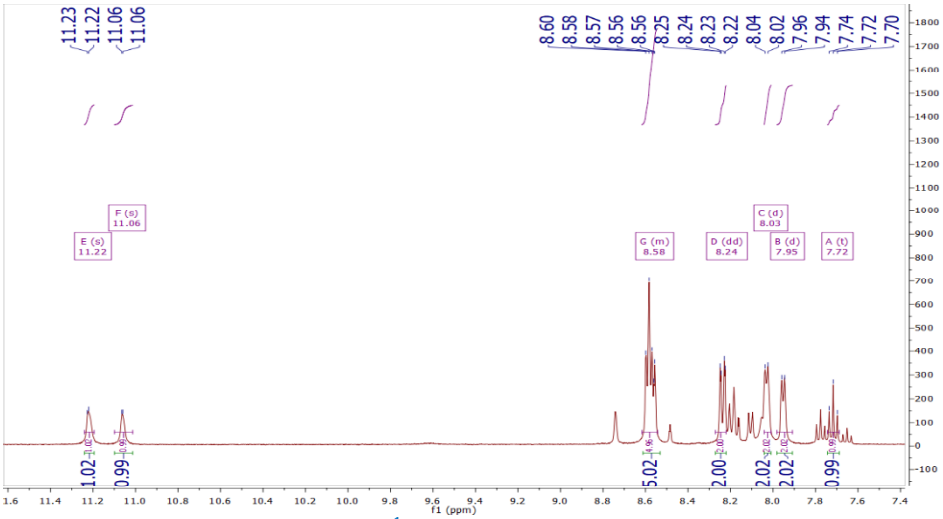

Figure A-105: ^{1}H-NMR spectra of **L15b**

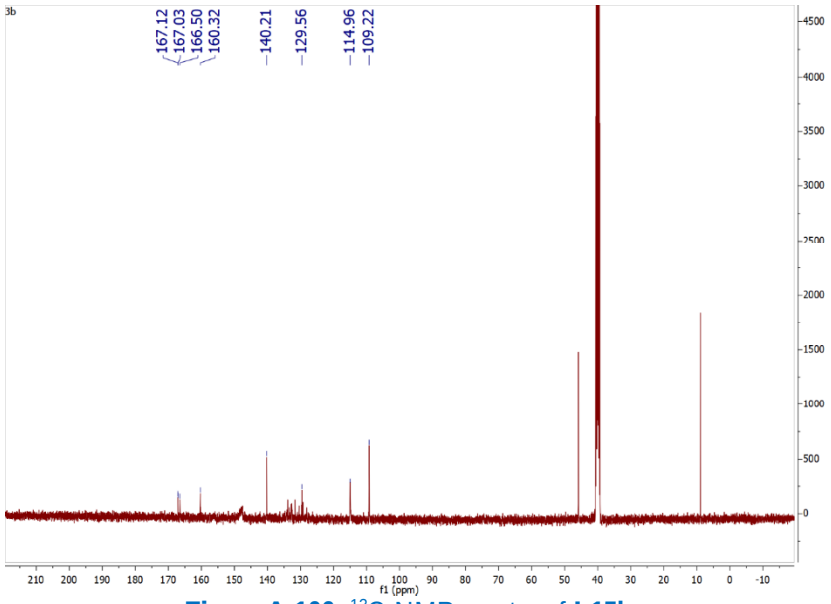

Figure A-106: ^{13}C-NMR spectra of **L15b**

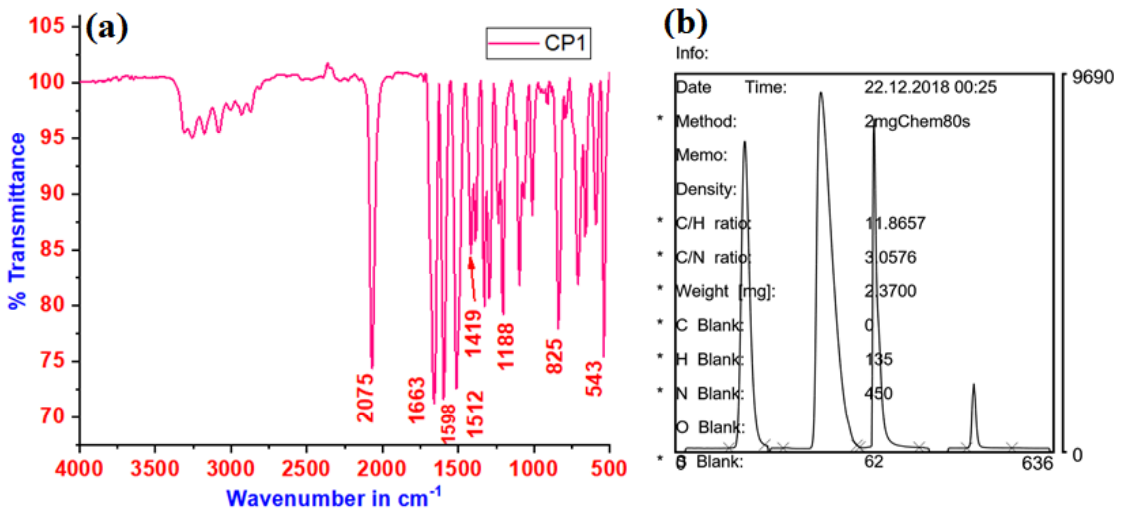

Figure A-107: (a) IR spectra of **CP1**, (b) CHN analysis of **CP1**

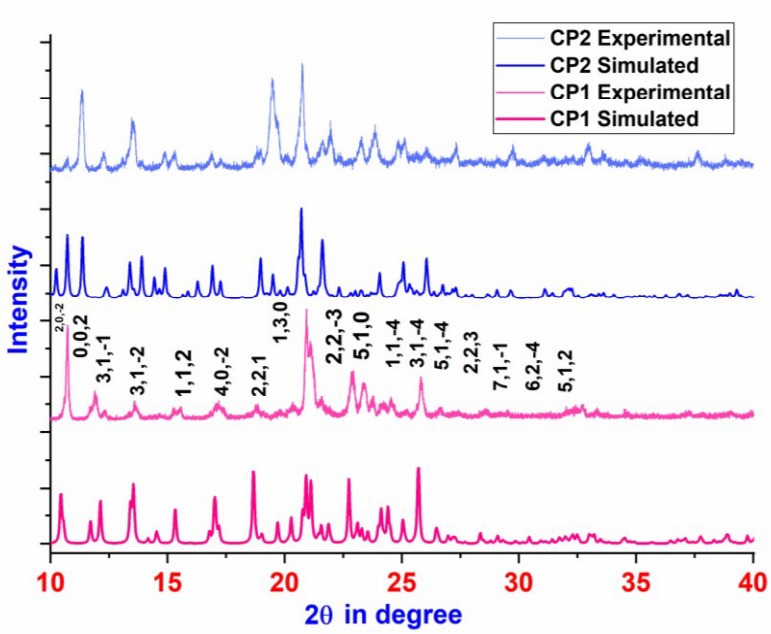

Figure A-108: PXRD of **CP1** and **CP2**

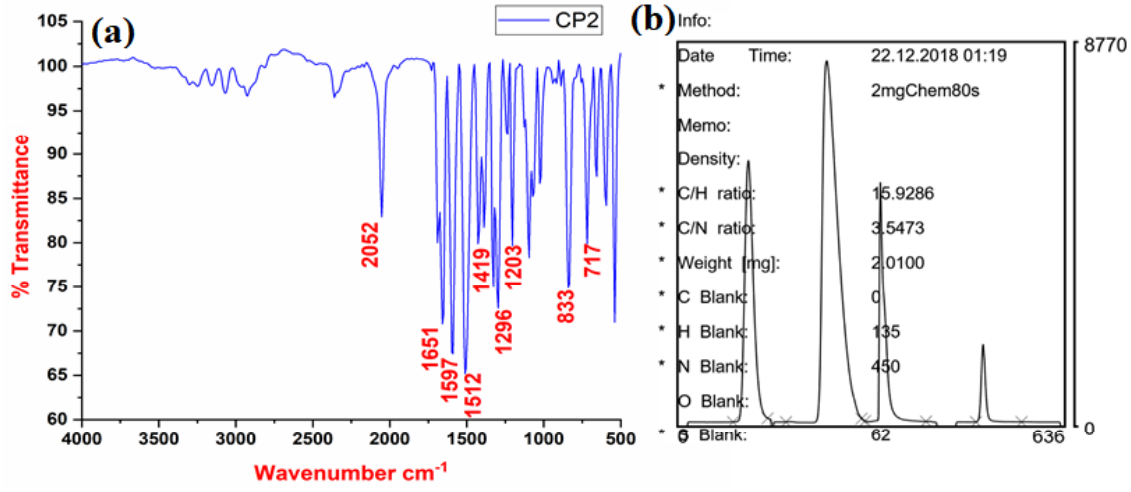

Figure A-109: (a) IR spectra of **CP2**, (b) CHN analysis of **CP2**

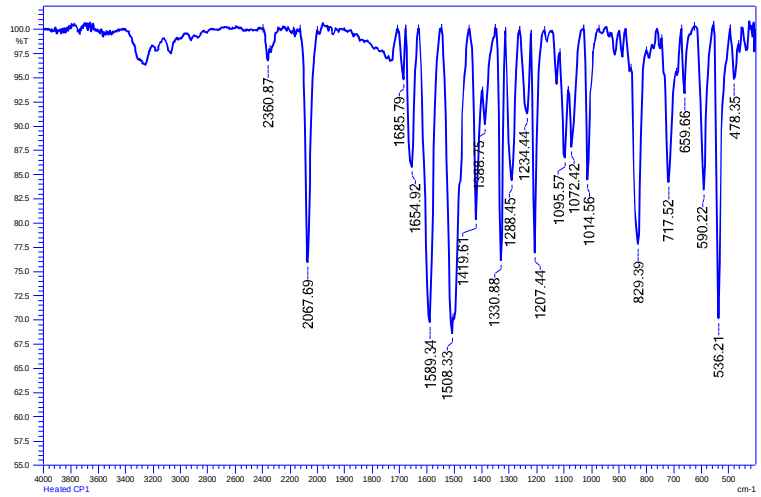

Figure A-110: (a) IR spectra of **CP1***

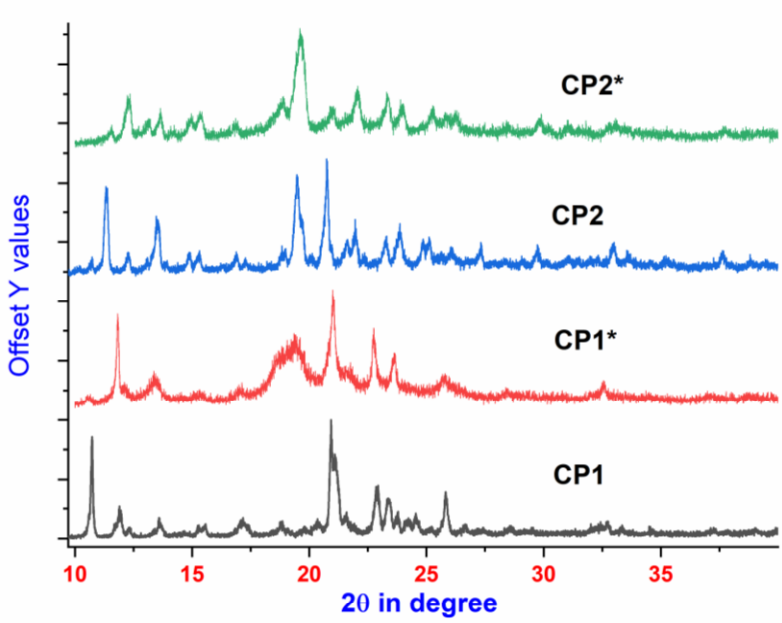

Figure A-111: PXRD of **CP1*** and **CP2***

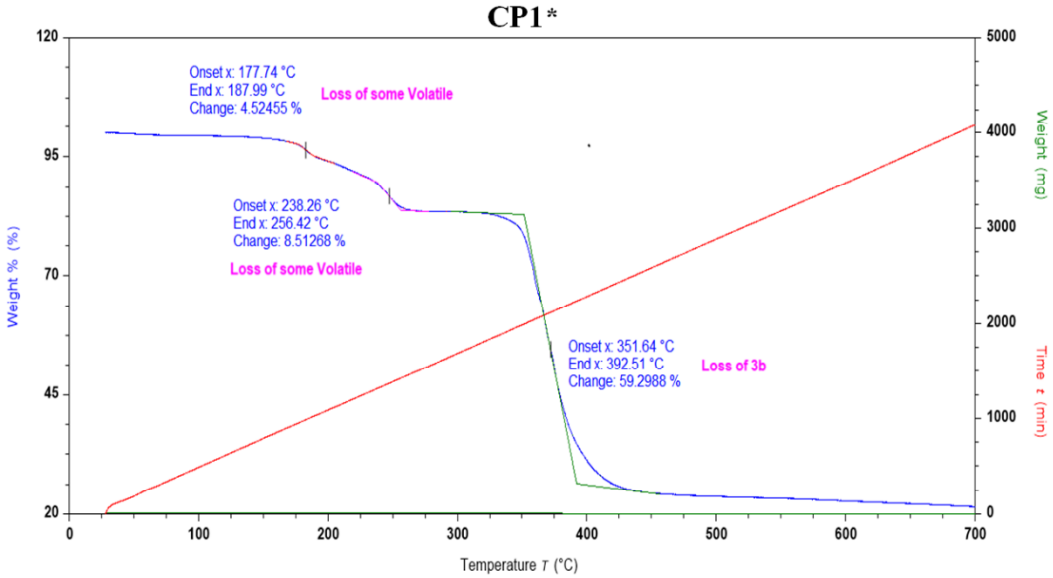

Figure A-112: TGA analysis of **CP1***

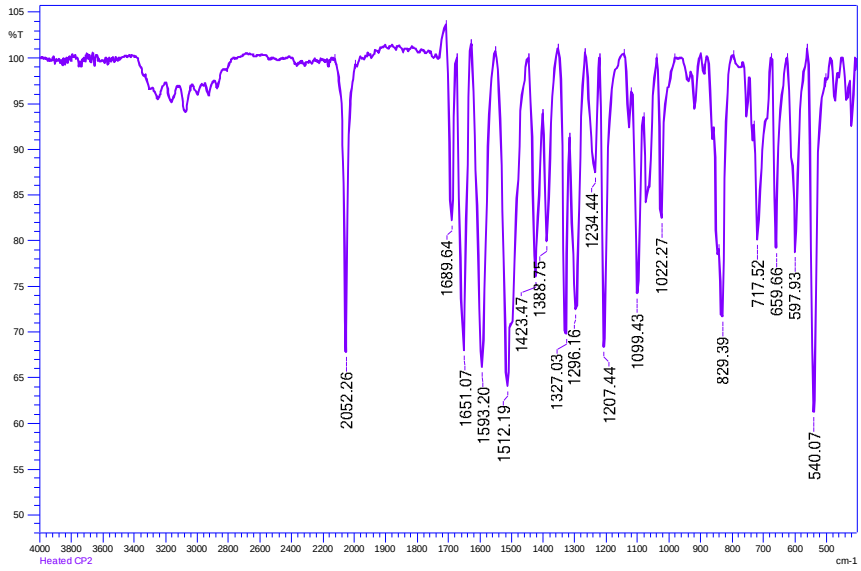

Figure A-113: (a) IR spectra of **CP2***

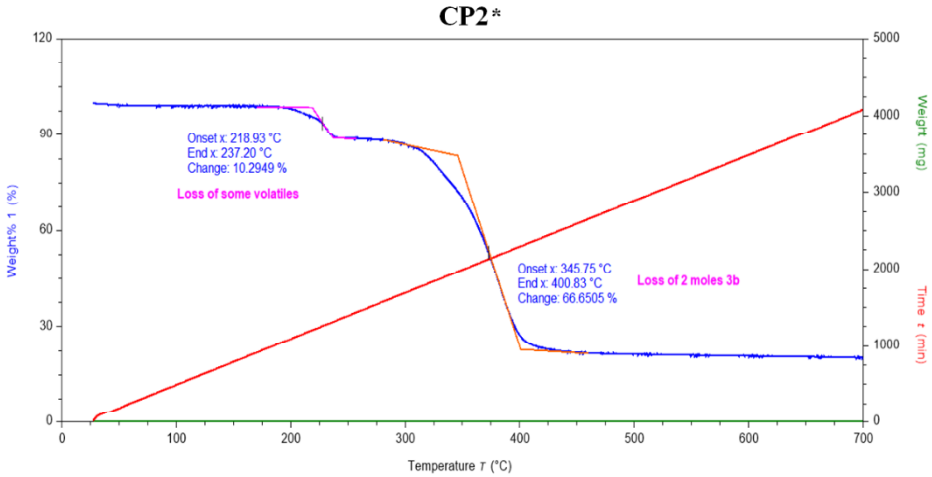

Figure A-114: TGA analysis of **CP2***

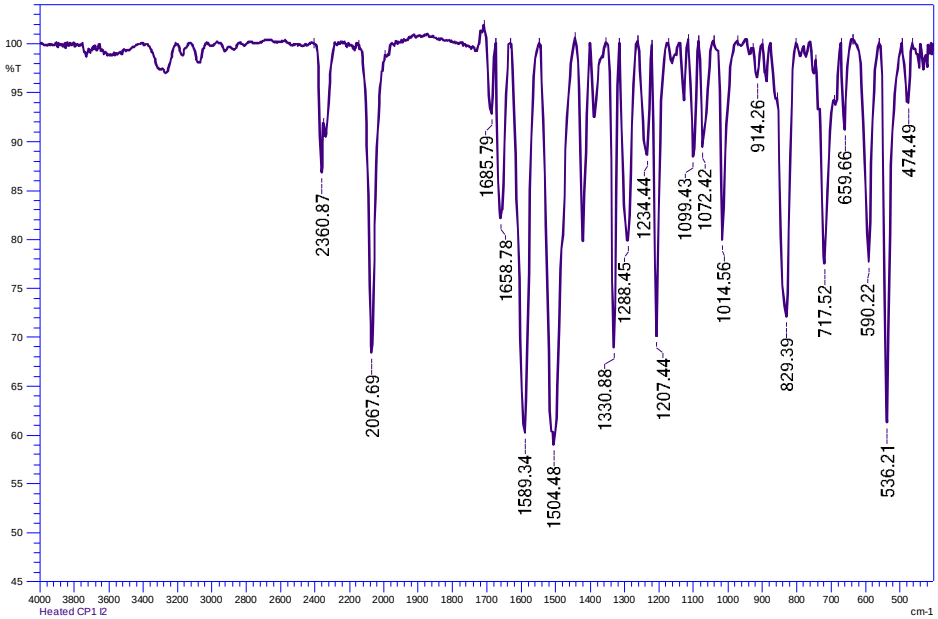

Figure A-115: (a) IR spectra of **I_2@CP1**

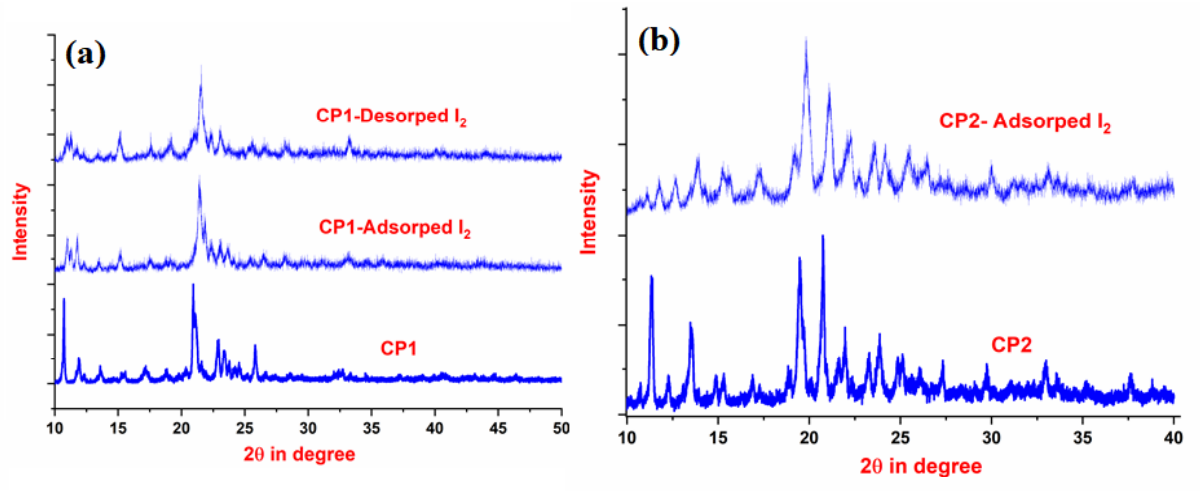

Figure A-116: PXRD of **I_2@CP1** and **I_2@CP2**

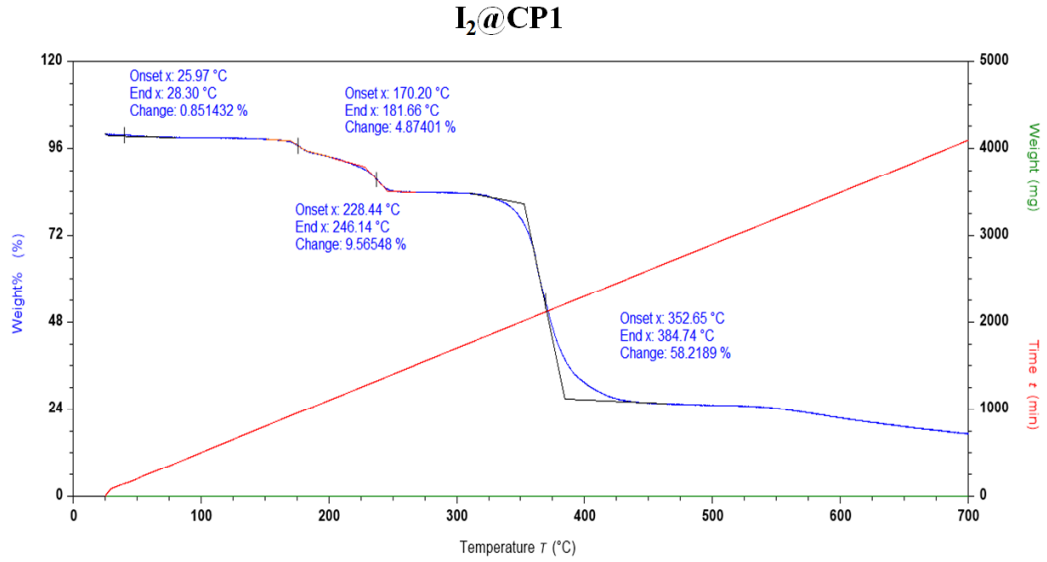

Figure A-117: TGA analysis of **I_2@CP1**

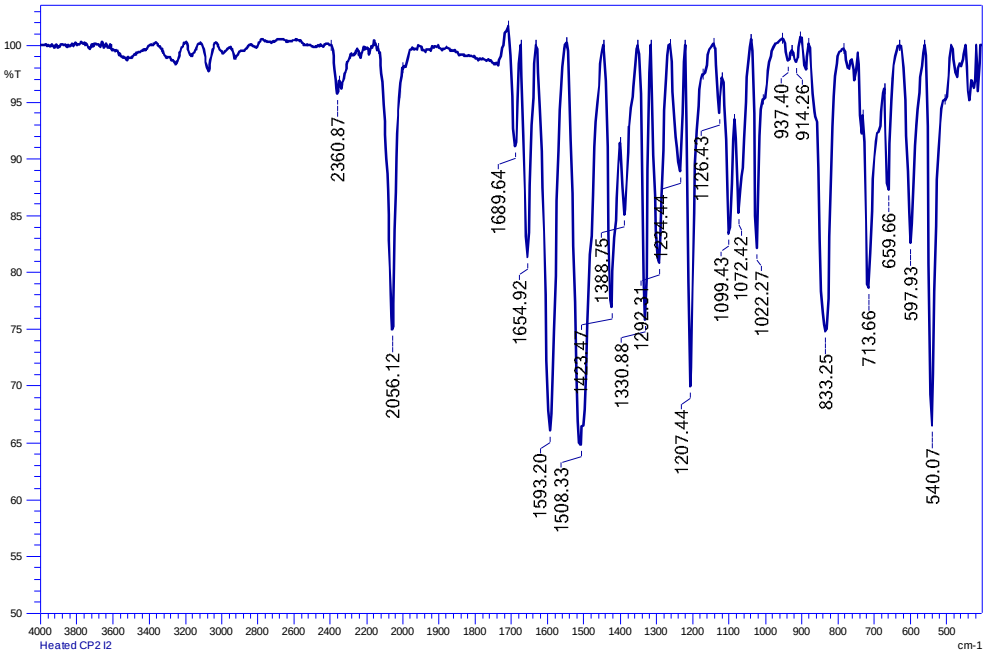

Figure A-118: IR spectra of **I_2@CP2**

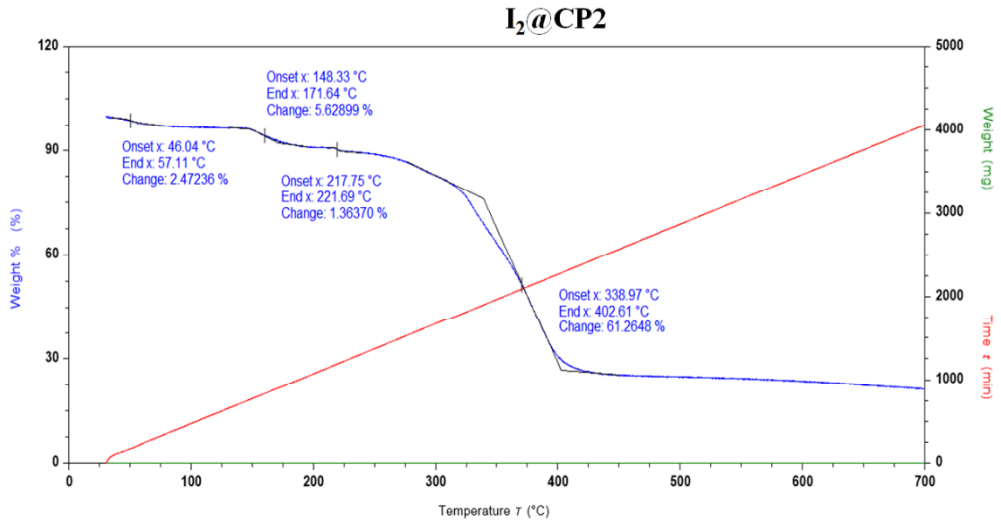

Figure A-119: TGA analysis of **I_2@CP2**

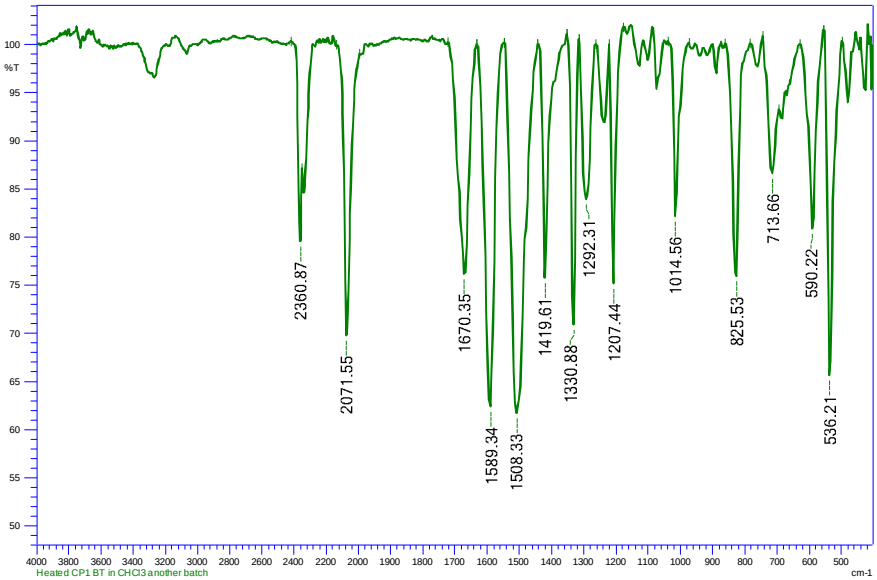

Figure A-120: IR spectra of **CP1-BT**

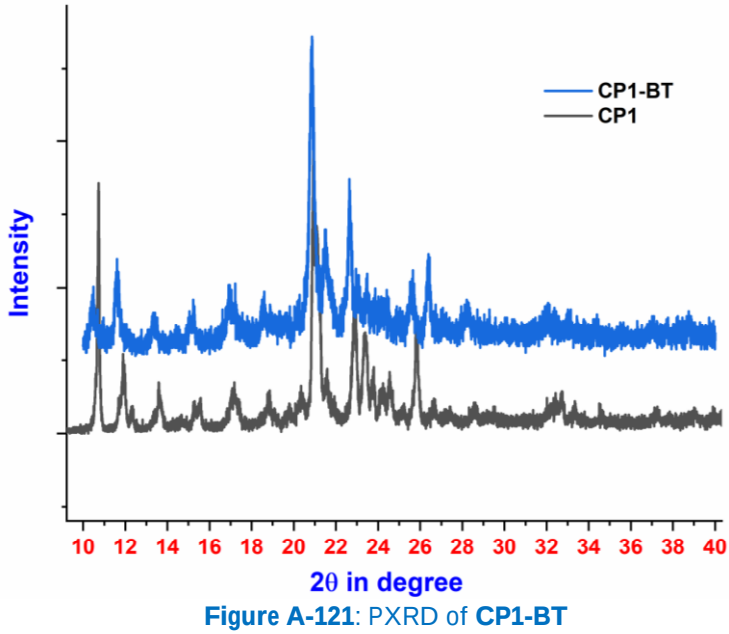

Figure A-121: PXRD of **CP1-BT**

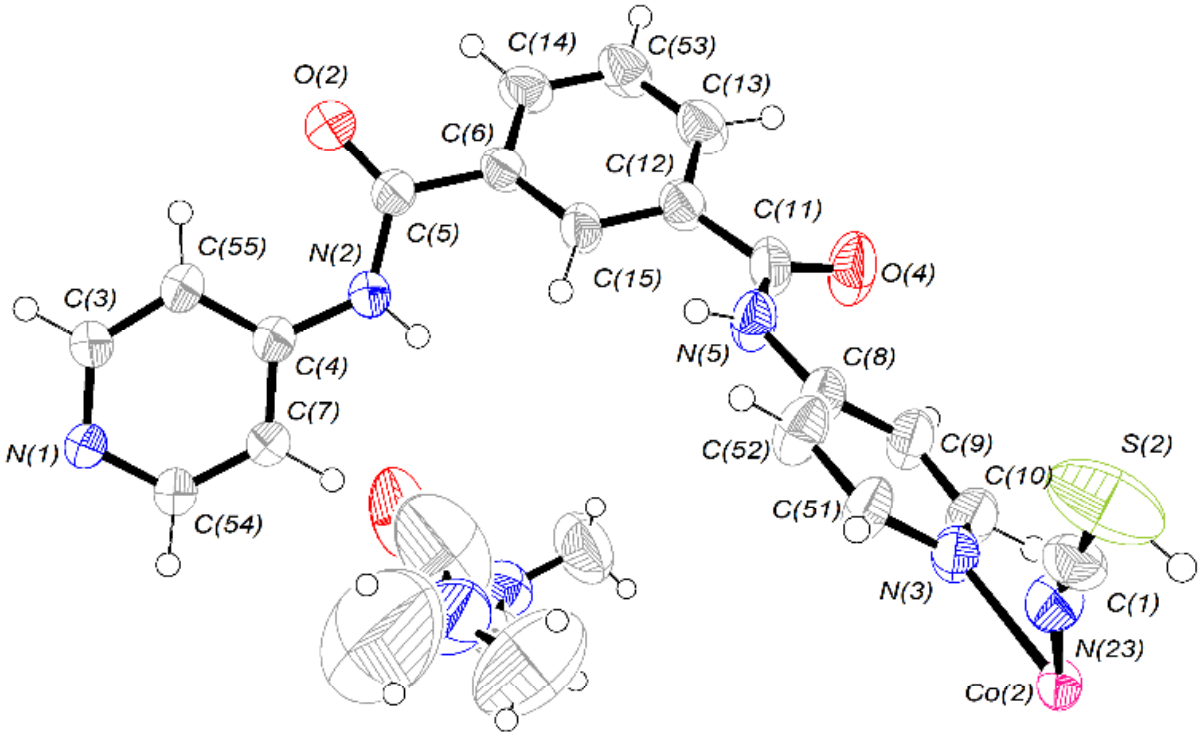

Figure A-122: ORTEP plot of **CP1** drawn at ***50***% probability level

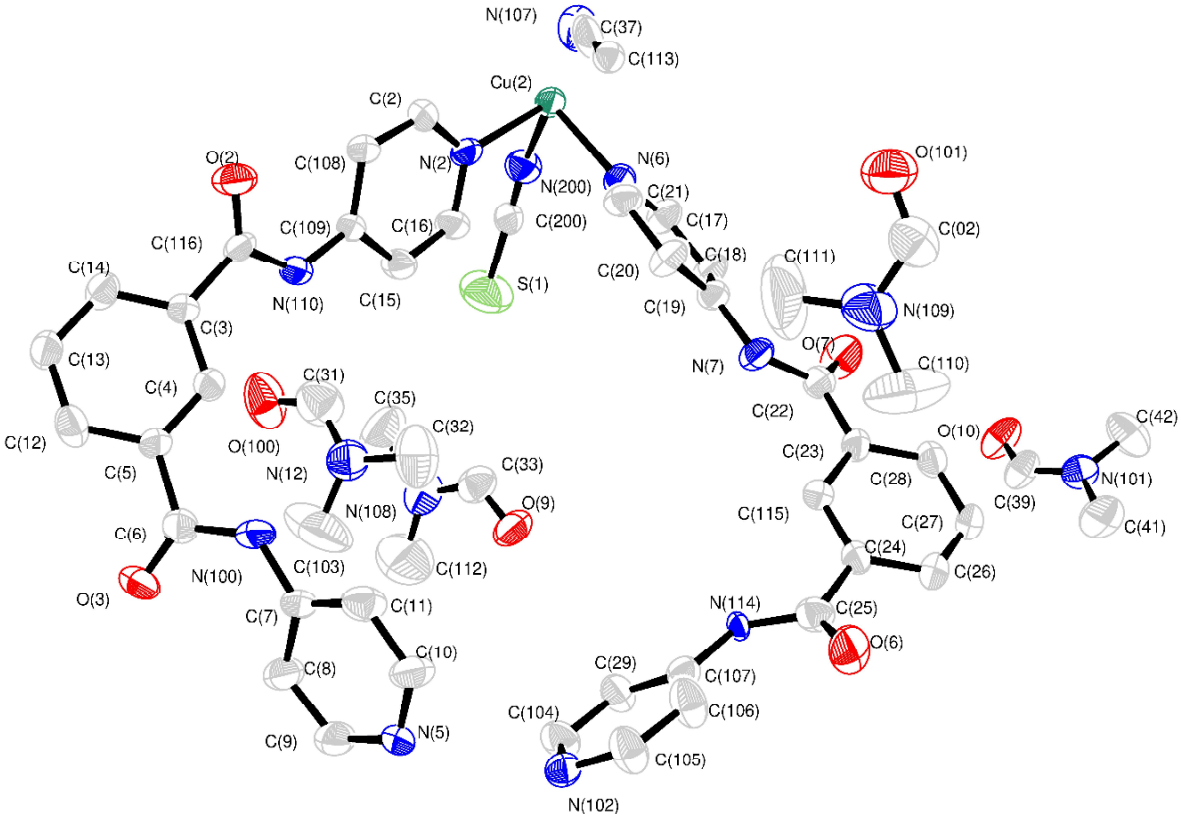

Figure A-123: ORTEP plot of **CP2** drawn at ***50***% probability level

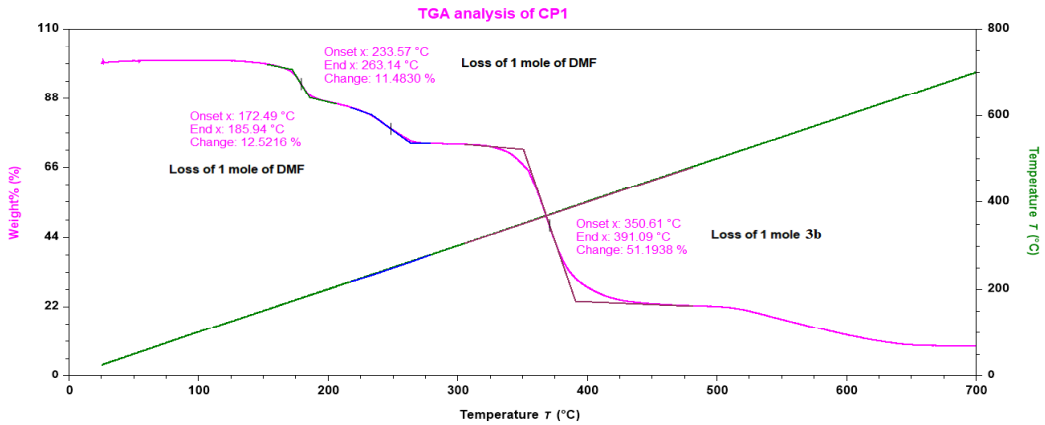

Figure A-124: TGA Analysis of **CP1**

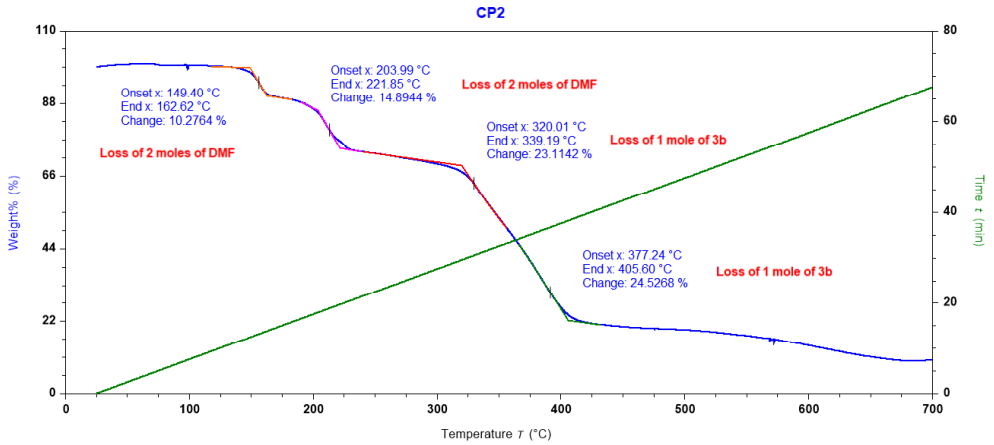

Figure A-125: TGA Analysis of **CP2**

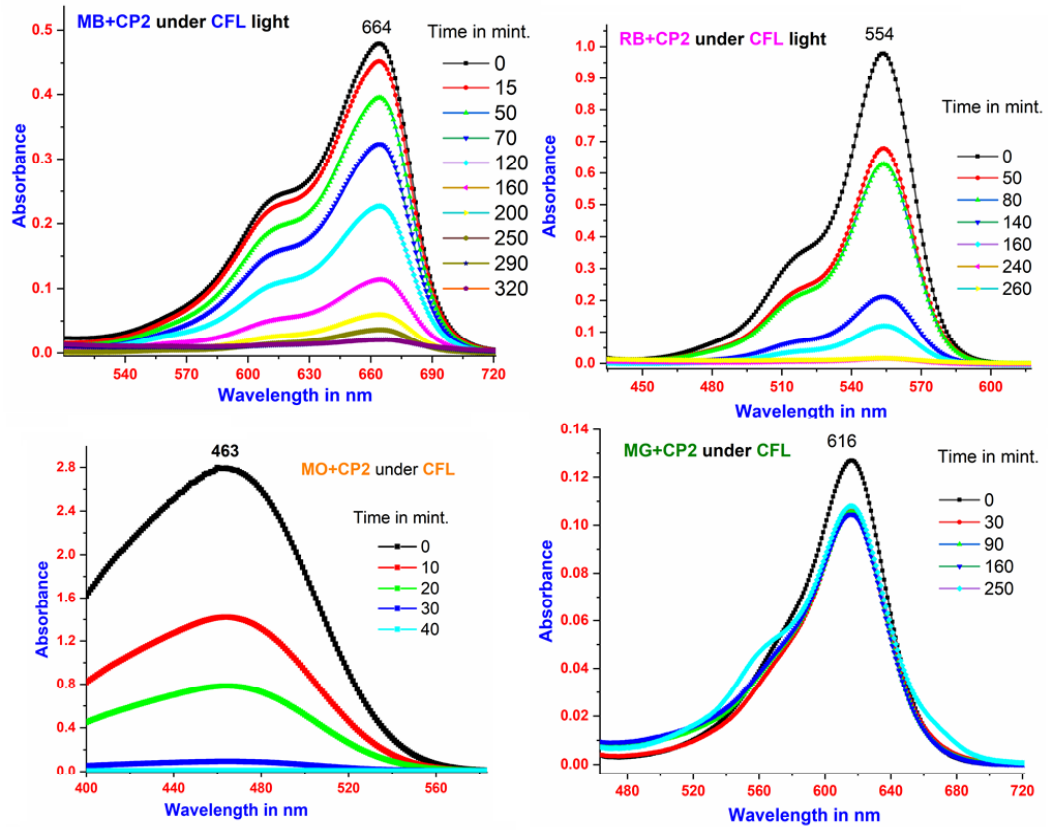

Figure A-126: Degradation of Dyes by **CP2** under CFL light

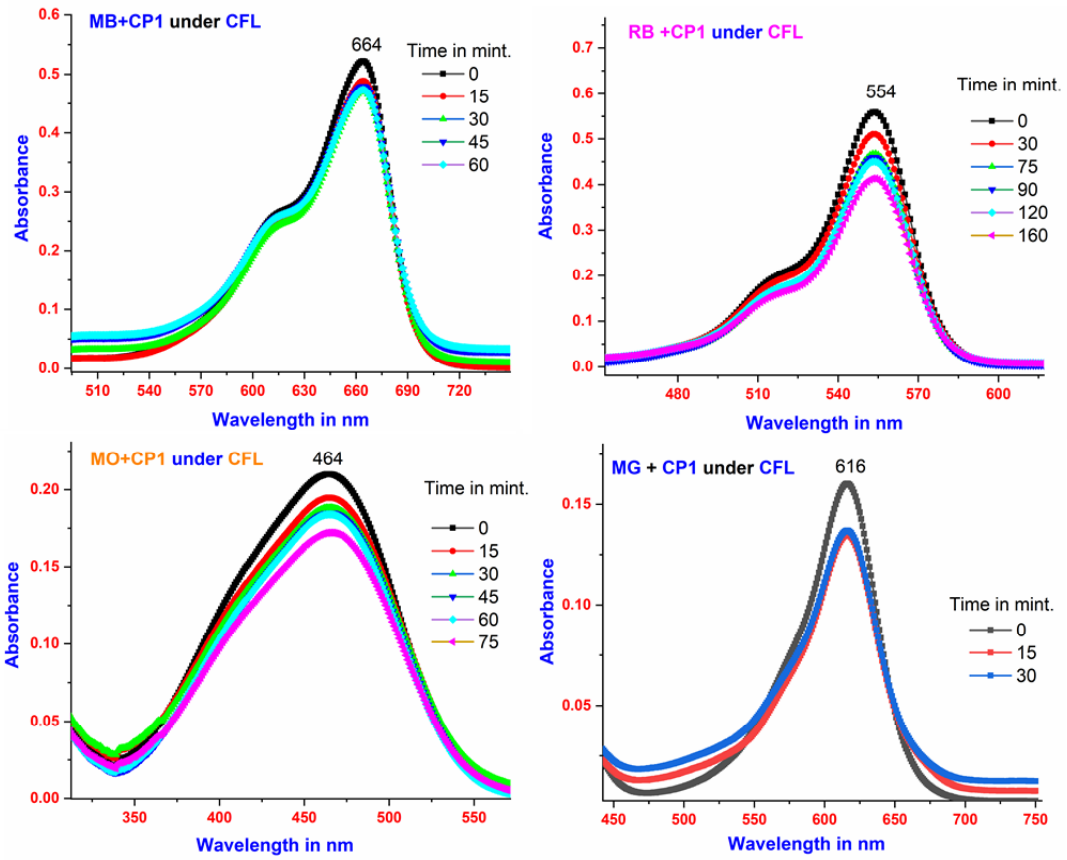

Figure A-127: Degradation of Dyes by **CP1** under CFL light

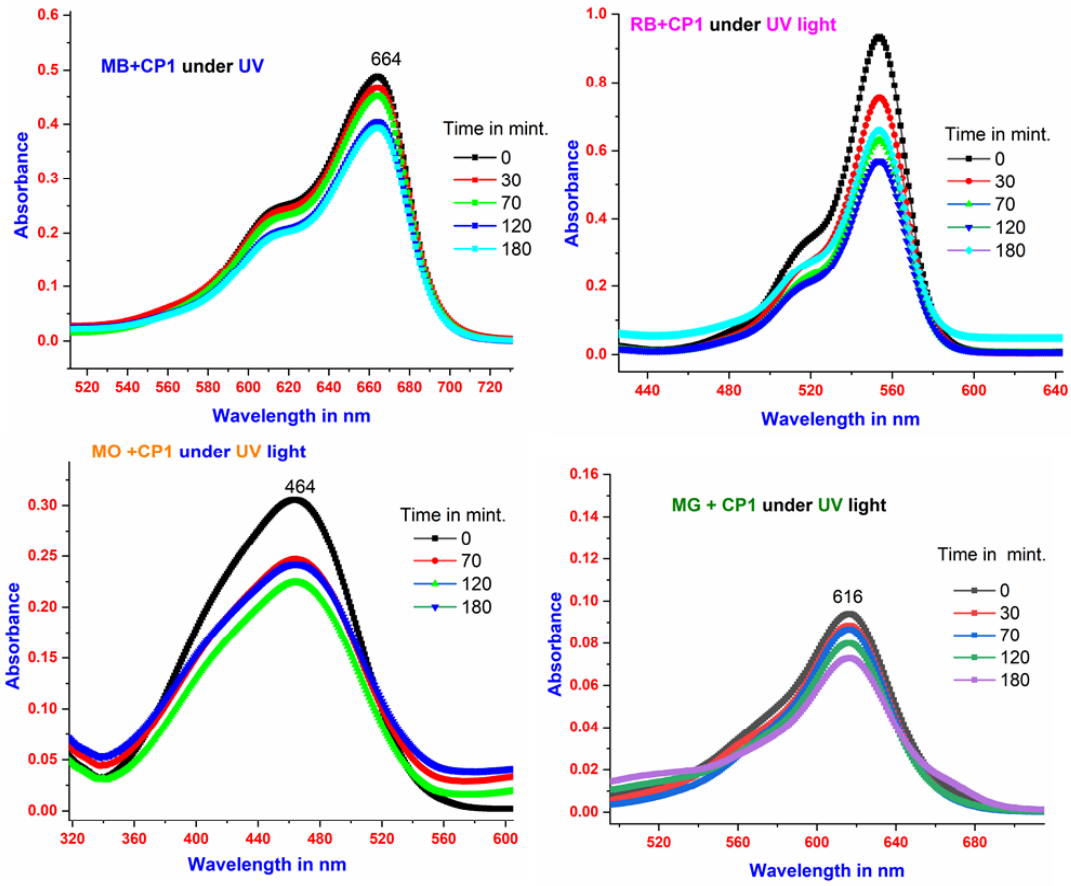

Figure A-128: Degradation of Dyes by **CP2** under UV light

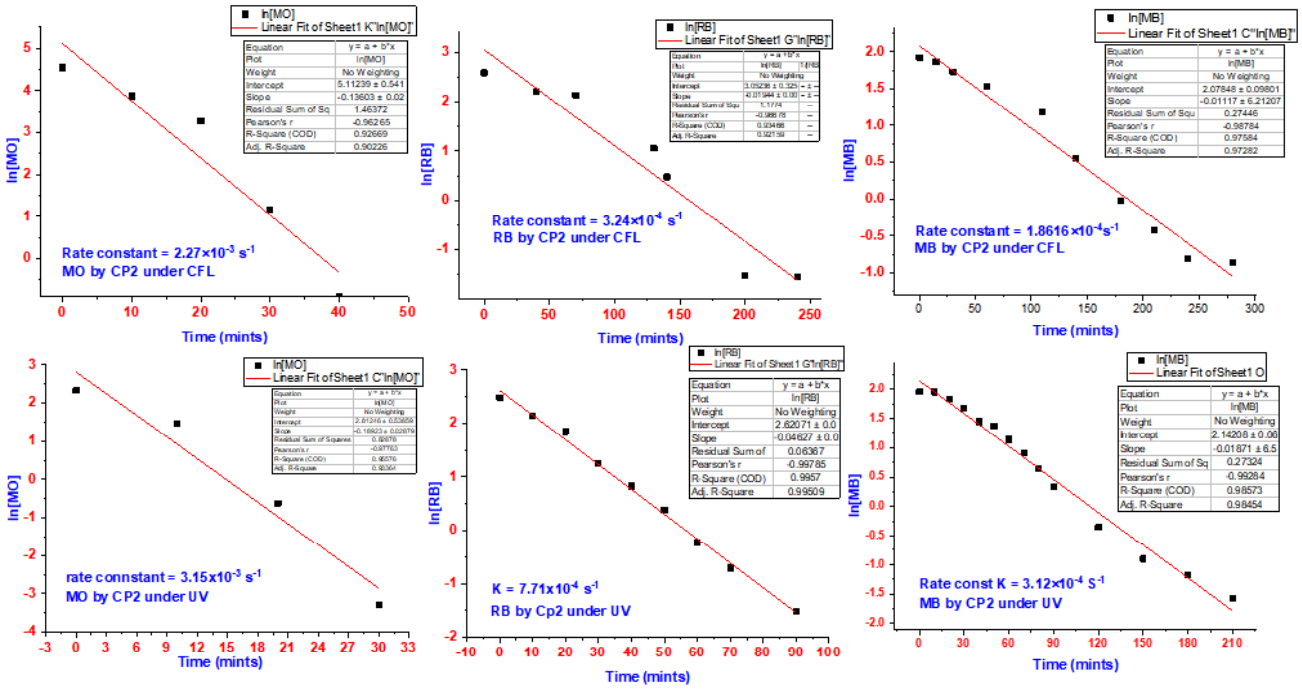

Figure A-129: Rate constants for the photodegradation of MO, RB and MB in presence of **CP2** under UV light

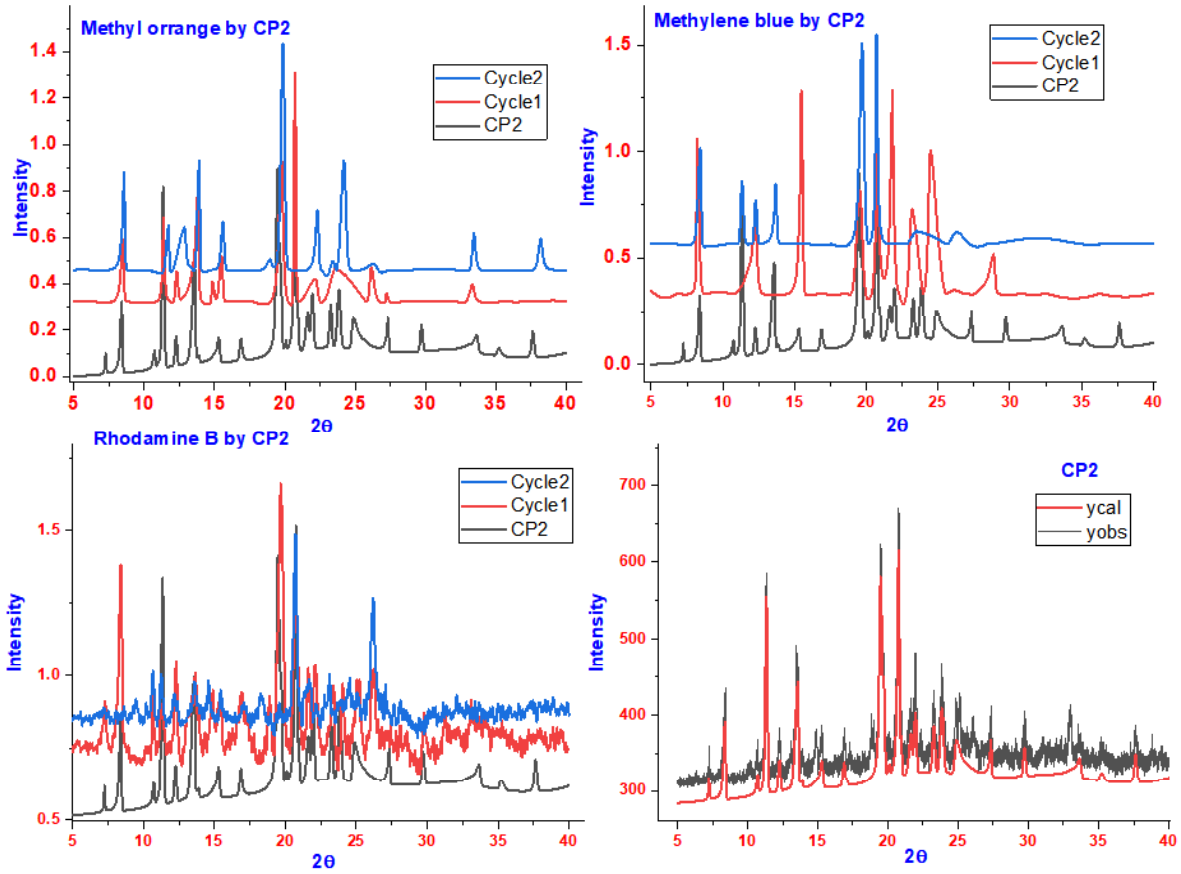

Figure: A-130: PXRD of recovered samples after photocatalysis (under UV light)

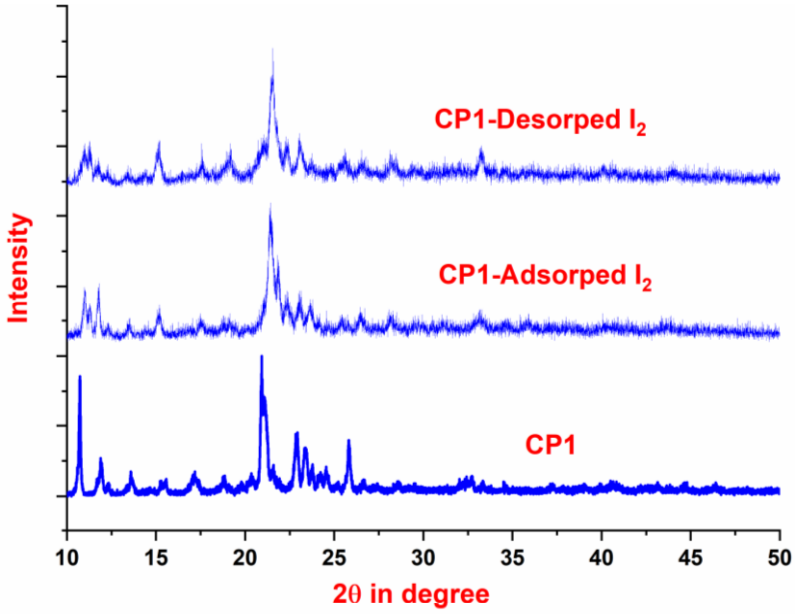

Figure A-131: PXRD of **I_2@CP1**

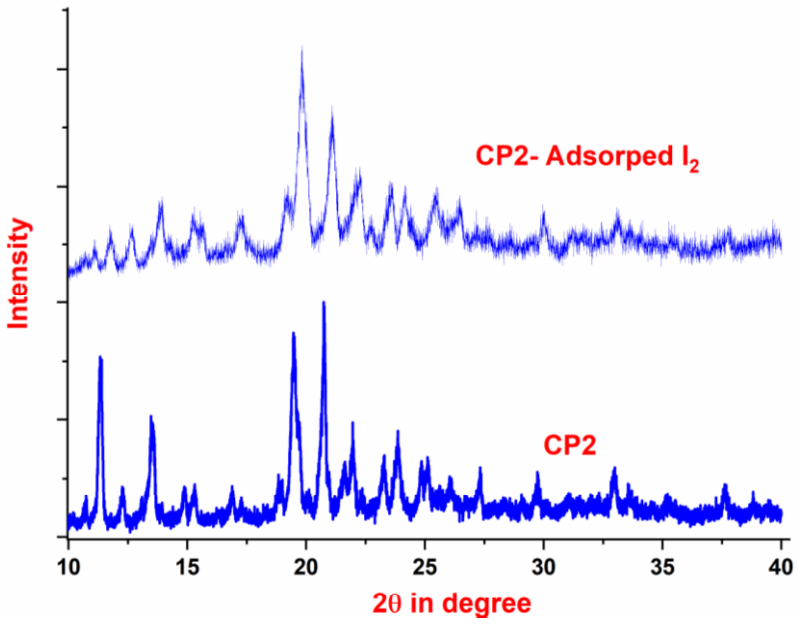

Figure A-132: PXRD of **I_2@CP2**

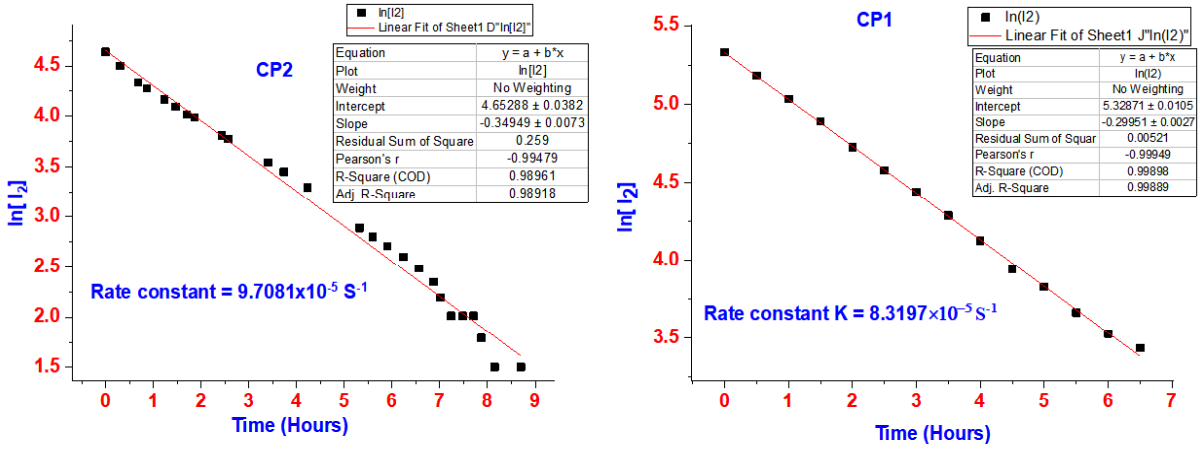

Figure A-133: Plot of *ln[I_2]* Vs. Time to study the kinetics of Iodine adsorption

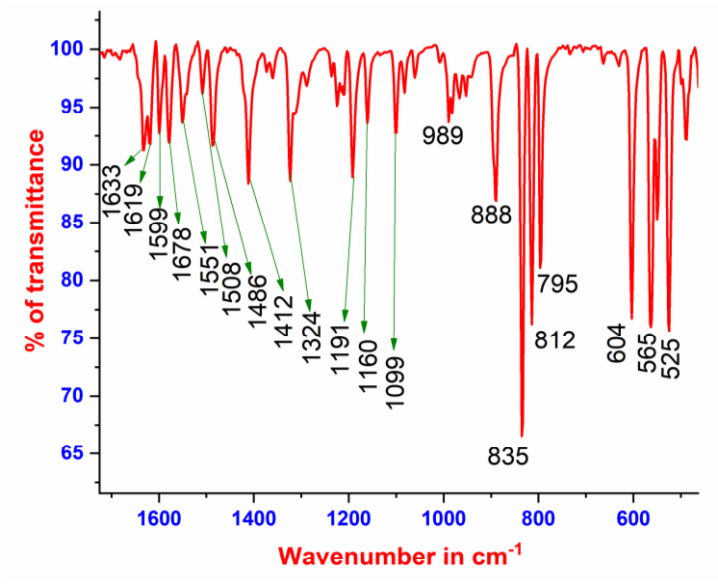

Figure A-134: IR spectra of **L14c**

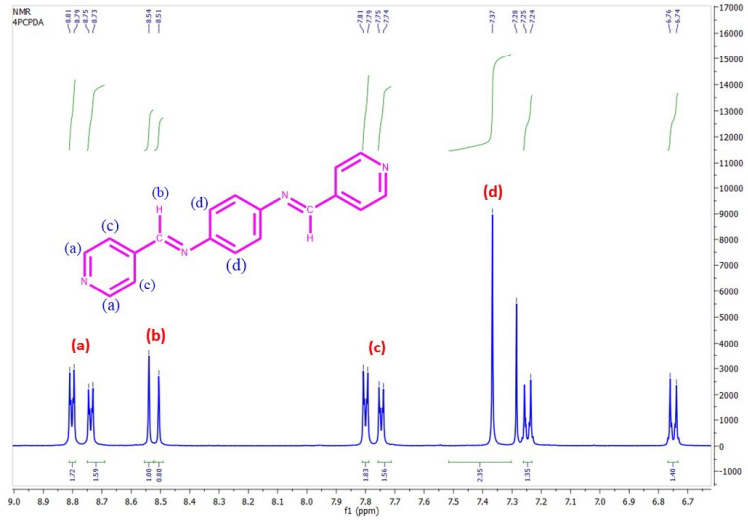

Figure A-135: ^{1}H-NMR spectra of **L14c**

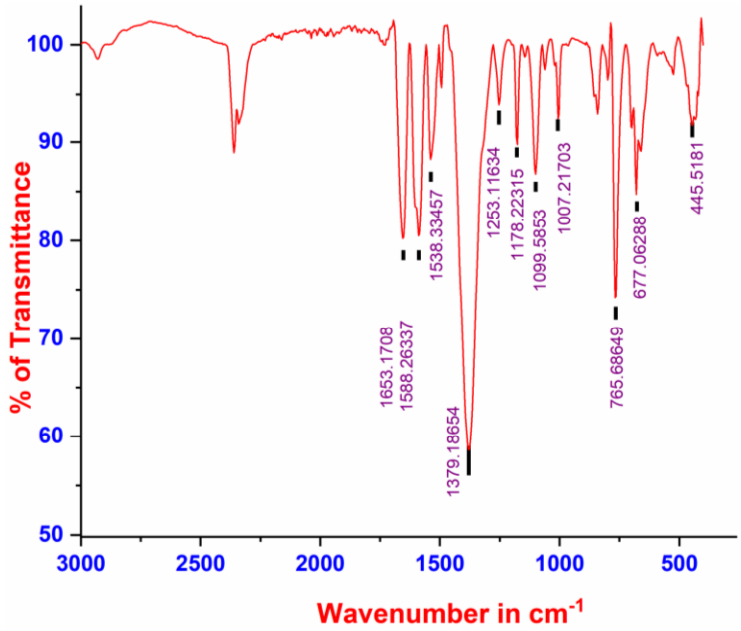

Figure A-136: IR spectra of **Zn-MOF**

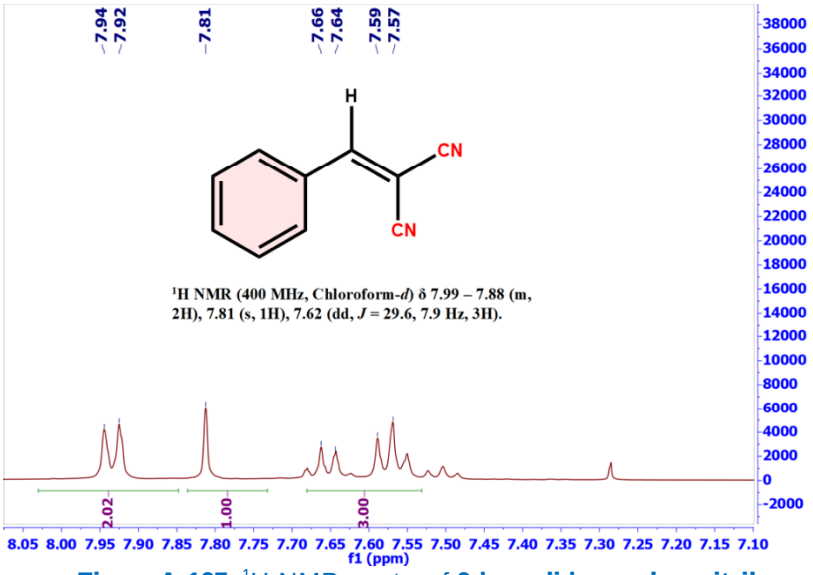

Figure A-137: ^{1}H-NMR spectra of **2-benzylidenemalononitrile**

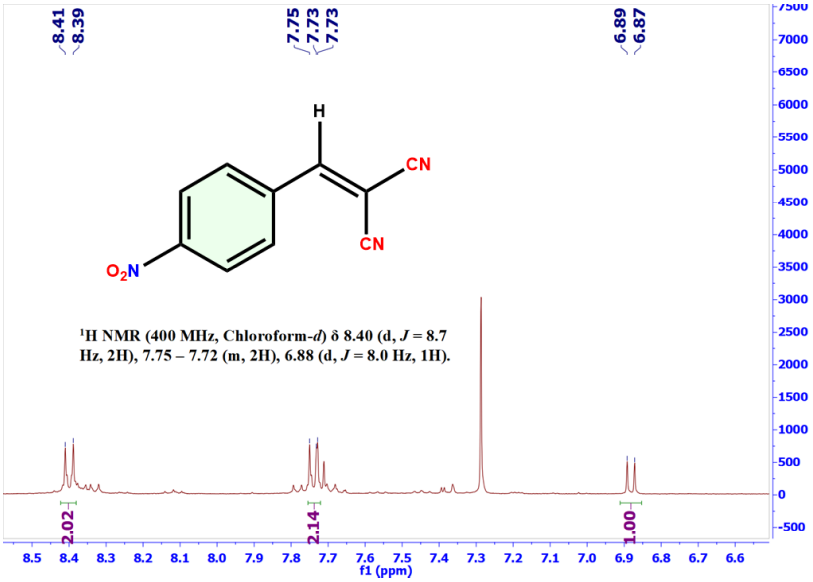

Figure A-138: ^{1}H-NMR spectra of **2-(4-nitrobenzylidene)malononitrile**

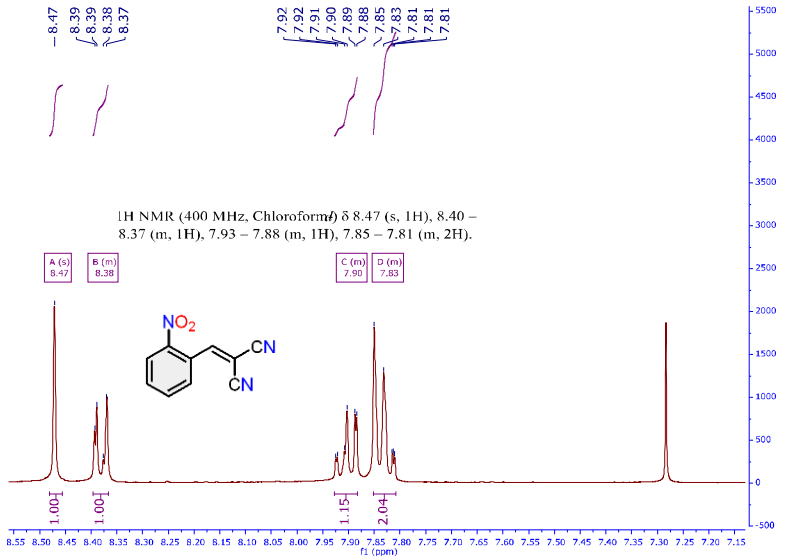

Figure A-139: ^{1}H-NMR spectra of **2-(2-nitrobenzylidene)malononitrile**

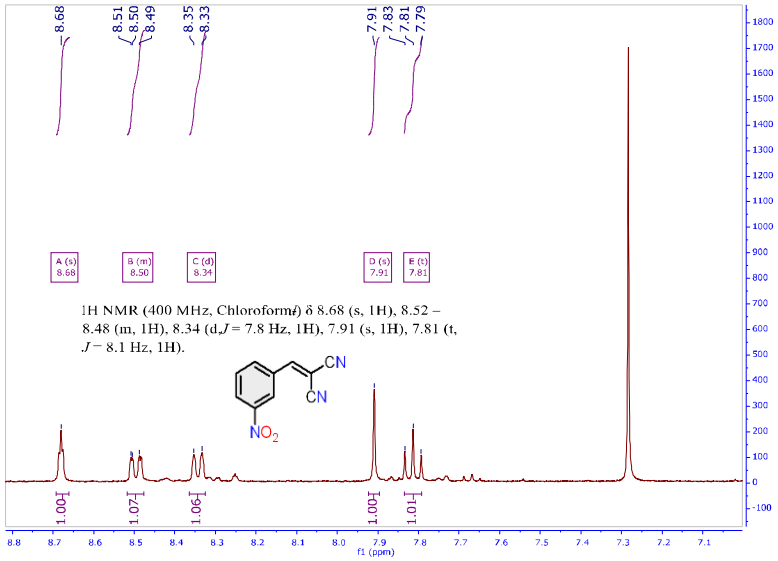

Figure A-140: ^{1}H-NMR spectra of **2-(3-nitrobenzylidene)malononitrile**

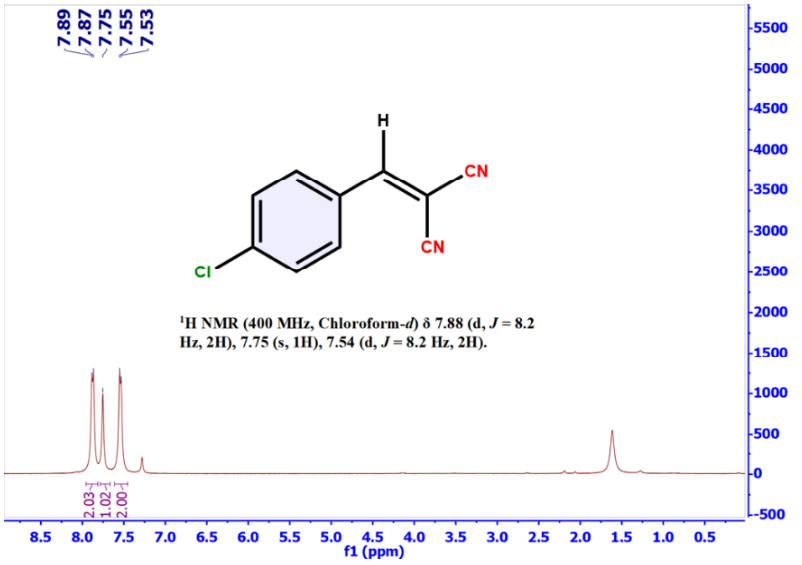

Figure A-141: ^{1}H-NMR spectra of **2-(4-chlorobenzylidene)malononitrile**

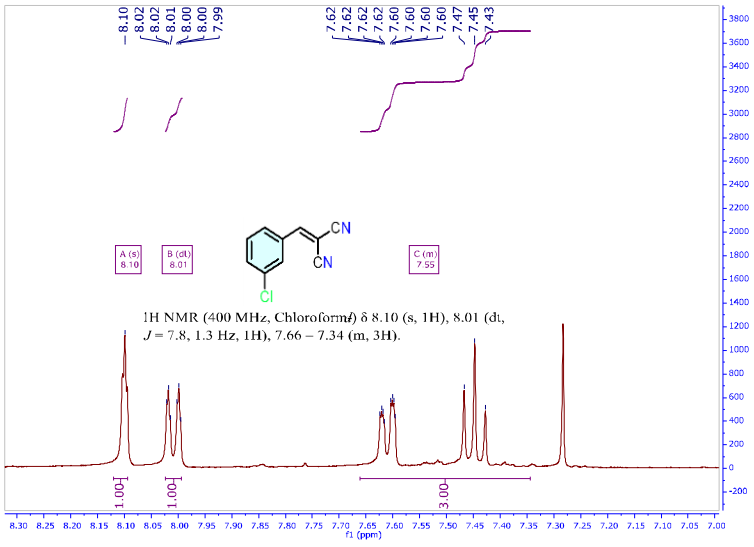

Figure A-142: ^{1}H-NMR spectra of **2-(3-chlorobenzylidene)malononitrile**

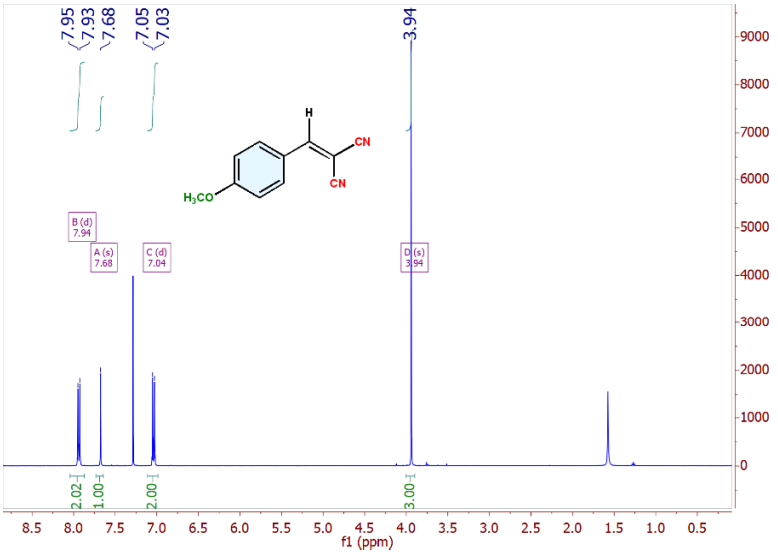

Figure A-143: ^{1}H-NMR spectra of **2-(4-methoxybenzylidene)malononitrile**

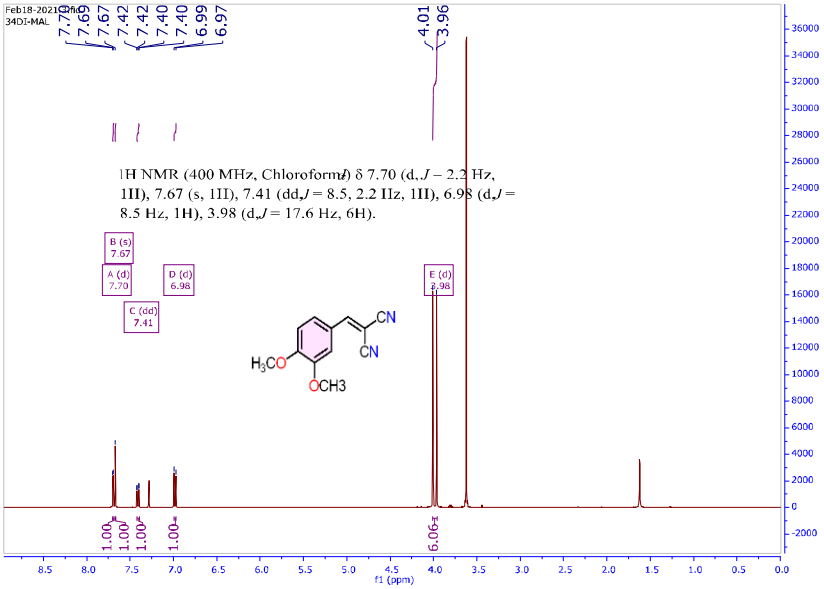

Figure A-144: ^{1}H-NMR spectra of **2-(3,4-dimethoxybenzylidene)malononitrile**

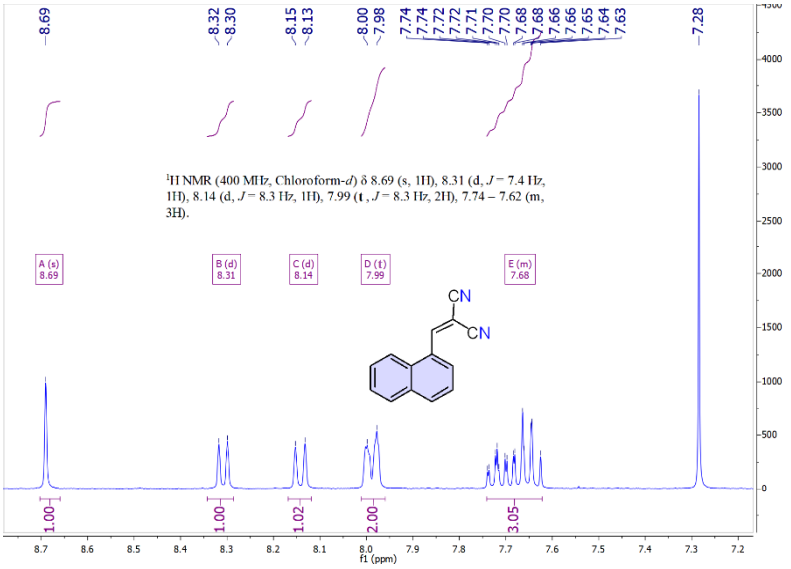

Figure A-145: ^{1}H-NMR spectra of **2-(naphthalen-1-ylmethylene)malononitrile**

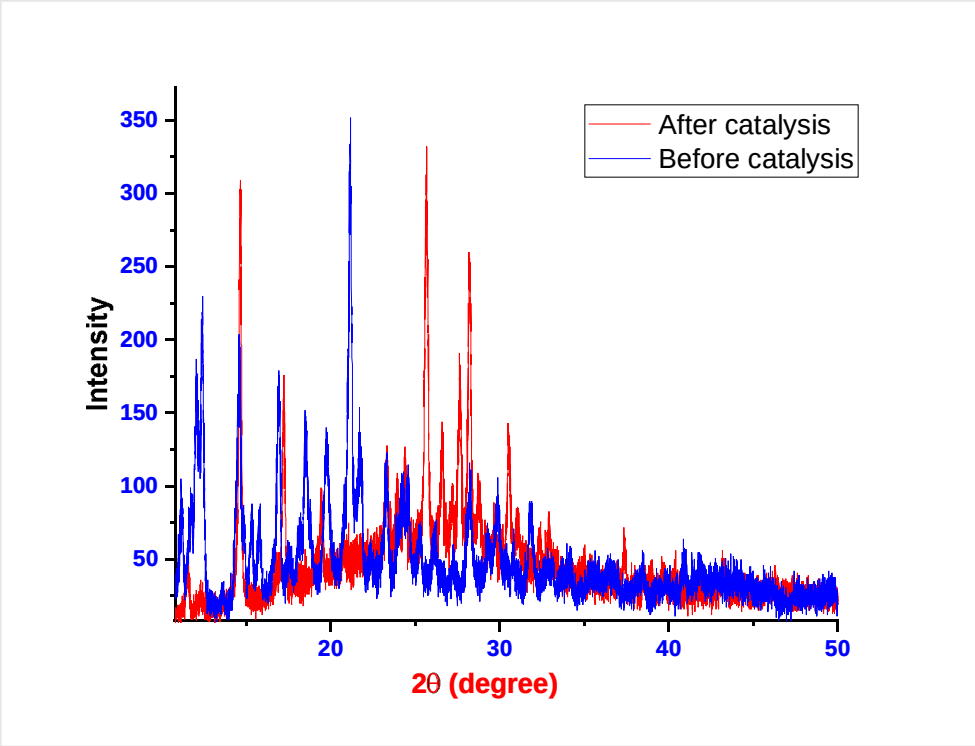

Figure A-146: PXRD spectra of Zn(II)-MOF before and after catalysis